Enhancing Superconductivity in Low Dimensional

$TlBa_2Ca_2Cu_3O_{10-\delta}$ System

By

Sajjad Hussain

Department of physics
Quaid-i-Azam University
Islamabad، Pakistan
2012

Enhancing Superconductivity in Low Dimensional

$TlBa_2Ca_2Cu_3O_{10-\delta}$ System

This work is submitted as a dissertation in partial fulfillment of the requirement for the degree of

MASTER OF PHILOSOPHY
IN
PHYSICS
By

Sajjad Hussain

Department of physics
Quaid-i-Azam University
Islamabad، Pakistan
2012

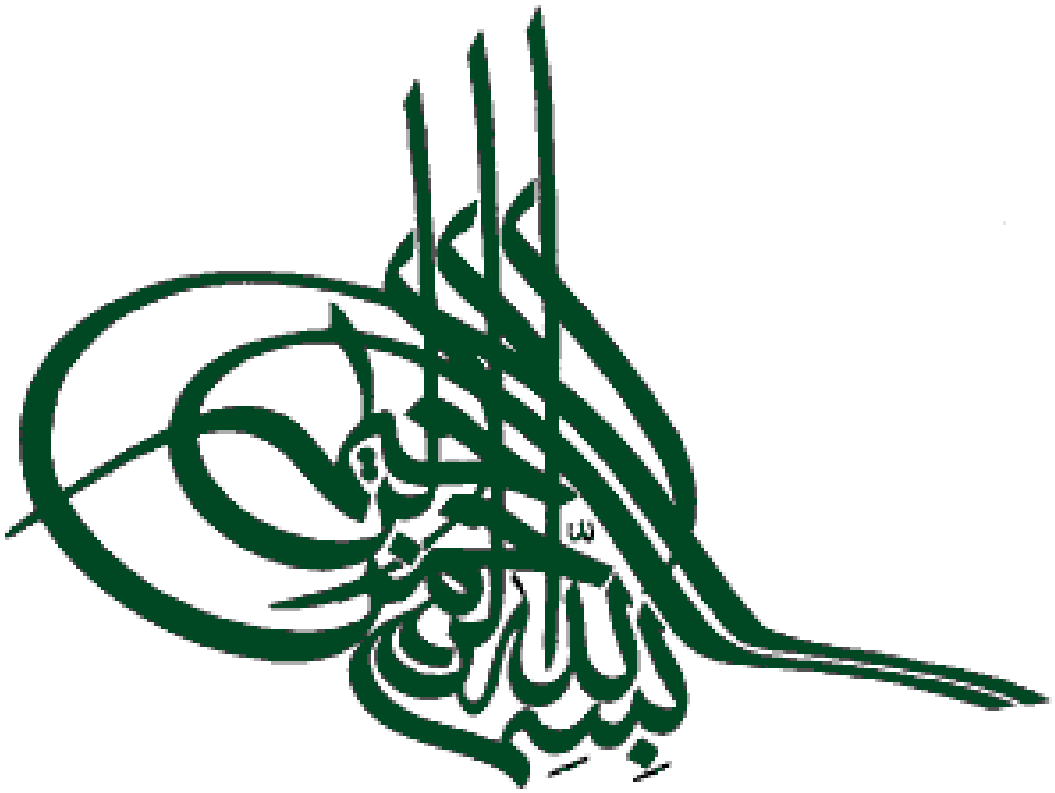

READ, in the name of thy Lord!
Who created man from congealed blood!
Read, for thy Lord is most generous!
Who taught the pen!
Taught man what he did not know!
(Sura “ALLAK”, aayat 1 to 5)

Certificate

This is to certify that **Mr. Sajjad Hussain** S/O **Abdul Aziz** has carried out the experimental work in this dissertation under my supervision in Materials Science Laboratory, Department of Physics, Quaid-i -Azam University, Islamabad.

Supervisor

Dr. Nawazish Ali Khan
Department of Physics
Quaid-i-Azam University
Islamabad, Pakistan

Submitted through

Prof. Dr. S. K. Hasanain
Chairman
Department of Physics
Quaid-i-Azam University
Islamabad, Pakistan.

DEDICATED

TO

MY LOVING
PARENTS

ACKONWLEDGEMENT

All praises to Allah Almighty alone the most merciful who helped me in every step and difficulty of my life. I also offer my greatest and heartiest feelings to our last **Holly Prophet Muhammad (P.B.U.H)** who is torch of guidance and knowledge for humanity as a whole. He is the one who showed us the path of knowledge and right direction.

The work presented in this manuscript was accomplished under the supervision of ***Dr. Nawazish Ali Khan.*** I feel honor to express my gratitude to him for his guidance, generous assistance and support from initial to final level enabled me to develop an understanding of the subject. Throughout my project, he provided me encouragement, sound advice, and lots of good ideas. I am really impressed by his new ideas and ways of thinking. I thank him for his inspiring and encouraging way to guide me to a deeper understanding of scientific work, and his invaluable comments during the formation of this dissertation.

I am also heartedly thankful to Chairman Department of Physics ***Dr. S.K Hasanain*** for providing me opportunity to learn and grow in such an impressing environment.

I am really gratefull to my lab fellows M. Rahim, Shakeel Ahmed, Annie, M. Arif, Sadaf Aziz, Saleem Abbas, Mubarra and Javeria, for their worthy contributions to my research work. Thanks to all my friends for their help and support.

Lastly, and most importantly, I wish to thank my parents. They, raised me, supported me, taught me, and loved me. Due to their affection I always feel comfortable in difficult circumstances and it is because of their prayers that I am here at this point.

Sajjad Hussain

Abstract

Mg doped $Tl(Ba_{2-x}Mg_x)(Ca_{2-y}Be_y)Cu_3O_{10-\delta}$ (y=0; x=0, 0.25, 0.50, 0.75, 1.0, 1.25,1.5) and $Tl(Ba_{2-x}Mg_x)(Ca_1Be_1)Cu_3O_{10-\delta}$ (x=0, 0.25, 0.5, 0.75, 1.0, 1.25, 1.50, 1.75) superconductors are synthesized at the normal pressure and the possible mechanism of superconductivity in these compounds is studied. $Tl(Ba_{2-x}Mg_x)(Ca_{2-y}Be_y)Cu_3O_{10-\delta}$ (y=0) samples have shown an orthorhombic crystal structure and their c-axes length decreases up to Mg-doping of x=0.75 and then increases up to Mg-doping of x=1.50. The c-axes length in $Tl(Ba_{2-x}Mg_x)(Ca_1Be_1)Cu_3O_{10-\delta}$ samples, however, decreases up to a Mg-doping of x=1.25 and then increases for Mg-doping of x=1.5. 1.75. In these studies we have investigated the role of decreased thickness of charge reservoir layer on the mechanism of superconductivity. The $T_c(R=0)$ in as-prepared $Tl(Ba_{2-x}Mg_x)(Ca_{2-y}Be_y)Cu_3O_{10-\delta}$ (y=0; x=0, 0.25, 0.5, 0.75, 1.0, 1.25) samples was 100, 98, 101, 102, 100, 96K and in the oxygen post-annealed $T_c(R=0)$ is observed around 99, 98, 108, 127, 109, 97K, respectively. However, in as-prepared $Tl(Ba_{2-x}Mg_x)(Ca_1Be_1)Cu_3O_{10-\delta}$ (x=0.25, 0.5, 0.75, 1.0, 1.25, 1.50) samples the $T_c(R=0)$ is observed around 97, 99, 100, 94, 92, 93, 91K and in oxygen post-annealed samples the $T_c(R=0)$ is observed at 100, 98, 103, 101, 100, 99, 99K, respectively. The magnitude of the superconductivity after Mg-doping is improved in $Tl(Ba_{2-x}Mg_x)(Ca_{2-y}Be_y)Cu_3O_{10-\delta}$ (y=0; x=0.25, 0.5, 0.75, 1.0, 1.25) and $Tl(Ba_{2-x}Mg_x)(Ca_1Be_1)Cu_3O_{10-\delta}$ (x=0.25, 0.5, 0.75, 1.0, 1.25, 1.50) samples. It was observed from the FTIR absorption measurements that the phonon modes related to CuO_2 planar oxygen atoms are hardened with the doping of Mg in the charge reservoir layer. These studies have shown that the thickness of charge reservoir layers decreases with Mg-doping which most likely makes charge transfer mechanism more efficient that increases in the magnitude of superconductivity in the final compound.

TABLE OF CONTENT

List of Figures

List of Tables

Chapter 1

Introduction and Historical Review

1. Introduction

Superconductivity is a fascinating and challenging field of physics. Scientists and engineers throughout the world have been striving to develop an understanding of this remarkable phenomenon for many years. This chapter starts with the brief description of beautiful phenomenon of superconductivity, its brief history and classification of superconductor and then explores the simplest theoretical model, the London equation and some of its consequences, in particular the existence of vortices in superconductors and the difference between type I and type II superconductors, and then BCS theory of superconductors.

1.1. Superconductivity

An element, inter-metallic alloy or a compound that will conduct electricity without resistance below a certain temperature is known as superconductor. Once set in motion, electrical current will flow forever in a closed loop of superconducting material making it the closest thing to perpetual motion in nature. Scientists refer to superconductivity as a "macroscopic quantum phenomenon". A superconductor can be distinguished by following two properties:

(1) Vanishing of resistivity below critical temperature (T_c)

(2) Expulsion of magnetic flux below a critical field (H_c)

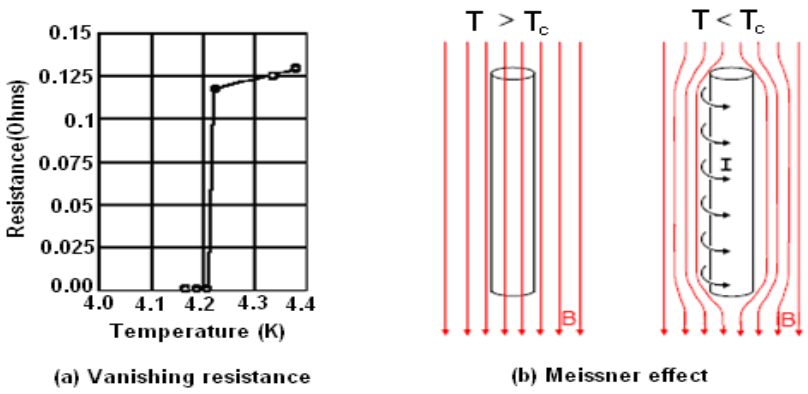

Fig. 1.1: (a) Vanishing resistance **(b)** Meissner effect

1.1.1. Explanation

Electrical resistance in metals arises because electrons moving through the metal are scattered due to deviations from translational symmetry. These are produced either by impurities, giving rise to a temperature independent contribution to the resistance, or by the vibrations of the lattice in the metal.

In a superconductor below its critical temperature, there is no resistance because these scattering mechanisms are unable to impede the motion of the current carriers. As a negatively-charged electron moves through the space between two rows of positively-charged atoms, it pulls inward on the atoms of the lattice. This distortion attracts a second electron to move in behind it. Suppose an electron approaches a positive ion core. It suffers attractive coulomb interaction. Due to this attraction, ion core is set into motion and consequently distorts the lattice. Smaller the mass of ion core greater will be the distortion. Suppose towards that side another electron comes and sees this distortion lattice. Thus the interaction between the two, the electron and the distorted lattice occurs which in its effect lowers the energy of second electron. Thus we can see that two electrons interact via the lattice distortion or the phonon field (also called acoustic quanta phonons in acoustics are analogous to photons in electromagnetic. The energy of a phonon is usually less than 0.1eV and thus is one or two orders of magnitude less than that of a photon) resulting in the lowering of energy for the electrons. This lowering of electron energy implies that force between the electrons is attractive. Two such electrons which interact attractively in the phonon field are called cooper pairs [1].

Briefly we can say that an electron comes and emits a virtual phonon which interacts with another electron lowers its energy which implies that force between the electrons is attractive. This phenomenon is depicted in the Fig.1.2.

The two electrons travel together in a pair and encounter less resistance overall. In a superconductor, electron pairs are constantly forming, breaking and reforming, but the overall effect is that electrons flow with little or no resistance. The current is carried then by “Cooper pairs”.

Any real specimen of metal cannot be perfectly pure and will contain some impurities. Therefore the electrons, in addition to being scattered by thermal vibrations of

the lattice atoms, are scattered by the impurities and this impurity scattering is more or less independent of temperature. As a result there will be a certain residual resistivity which remains even at the lowest temperature. The more impure the metal, the larger will be its residual resistivity. The transformation to the superconducting state may occur even if the metal is so impure that it would otherwise have a large residual resistivity.

Below the critical temperature these superconducting materials have no electrical resistance and so they can carry large amount of electrical current for long periods of time without losing energy as Ohmic heat. For example, loops of superconducting wire have been shown to carry electrical currents for several years with no measurable loss. This property offers tremendous challenges and opportunities in the modern world. [2]

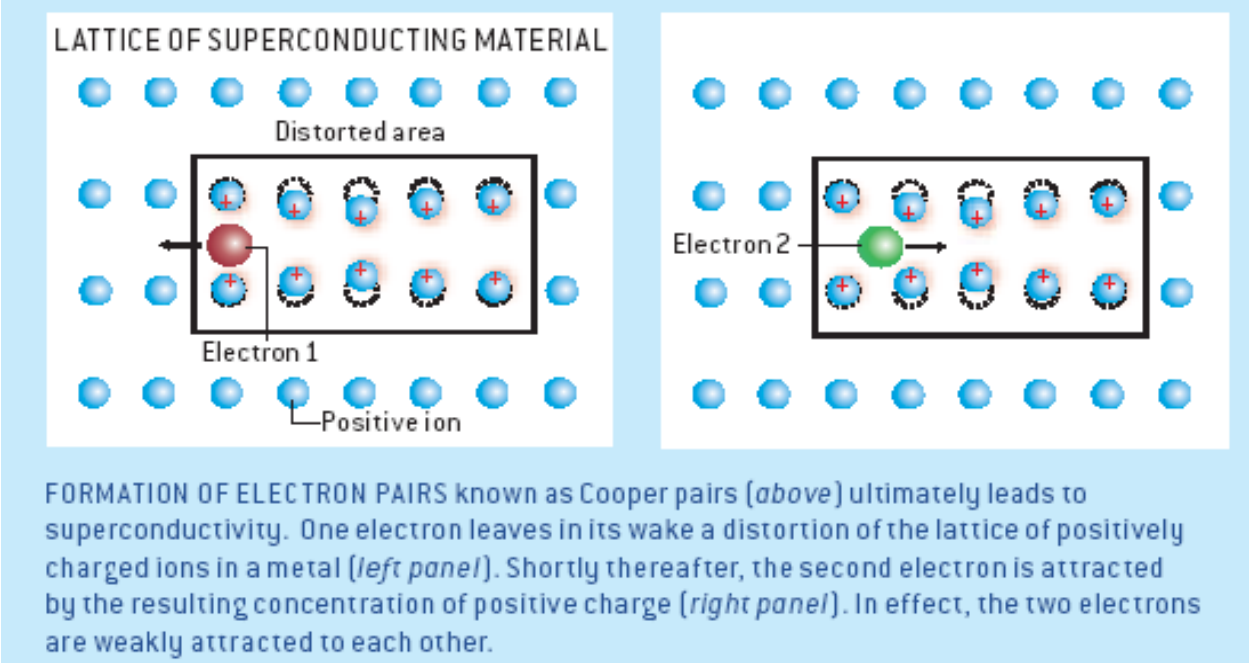

Fig. 1.2: Formation of Cooper pairs

1.2. History of Superconductivity

The phenomenon of superconductivity was a complete surprise when it was first observed by H. Kammerling Onnes in 1911. He was testing the validity of Drude theory by measuring the resistivity at the lowest temperature possible. Turning his attention to mercury, because of its especially high purity, he expected a very small perhaps even

zero residual resistivity in exceptionally pure substances. Surprisingly he discovered that all signs of resistance appeared to vanish suddenly below 4K. This was quite unexpected and was in fact the discovery of a new state of matter: Superconductivity.

In subsequent decades, superconductivity was found in several other materials. In 1913, lead was found to super-conduct at 7K, and in 1941 niobium nitride was found to super-conduct at 16K [3]. He also observed that in the vicinity of 4K, resistance of mercury was dropped to zero. As the temperature was decreased, the resistance disappeared instantly rather than gradually. It was obvious that the sample had undergone a transformation into a novel, as yet unknown state, characterized by zero electrical resistance. The phenomenon was named as “Superconductivity” [4].

The next important step in understanding superconductivity occurred in 1933, was taken by Meissner and Ochsenfeld. They demonstrated that when a superconducting material is placed in a uniform magnetic field the magnetic lines of forces which pass through the material when the temperature is above T_c (i.e. when material is in normal state) get completely expelled out of the bulk material, when it is cooled through the superconducting transition. This effect is termed as "Meissner effect"[3]. The first theory which could account for the existence of the Meissner effect was developed by two brothers, F. London and H. London, in 1935. Their theory was originally motivated by the two fluid model of super-fluid He. They assumed that some electrons in the solid become super fluid and rest remain normal. F. and H. London showed that the Meissner effect was a consequence of the minimization of the electromagnetic free energy carried by superconducting current [5].

In 1950, the phenomenological Ginzburg-Landau theory of superconductivity was devised by Landau and Ginzburg. This theory describes the superconducting phase transition from thermodynamic point of view. It was originally introduced as a phenomenological theory, but later Gorkov showed that it can be derived from full microscopic Bardeen Cooper Schrieffer (BCS) theory in suitable limit [6]. In particular, Abrikosov showed that Ginzburg-Landau theory predicts the division of superconductors into the two categories now referred to as Type-I and Type-II. Abrikosov and Ginzburg were awarded the Nobel Prize for their work in 2003.

Also in 1950, Maxwell and Reynolds et al found that the critical temperature of a superconductor depends on the isotopic mass of the constituent elements. This important discovery pointed to the electron-phonon interaction as the microscopic mechanism responsible for superconductivity [7].

The complete microscopic theory of superconductivity was finally proposed in 1957 by Bardeen, Cooper, and Schrieffer. An important contribution was also made by N.N. Bogolyubov in1958 who developed a mathematical method now widely used in studies of superconductivity. This BCS theory explained the superconducting current as a super-fluid of Cooper pairs, pairs of electrons interacting through the exchange of phonons. For this work, the authors were awarded the Nobel Prize in 1972.

The BCS theory was set on a firmer footing by L.P. Gorkov in1958. Who developed a method to solve the model BCS problem using Green's functions [4]. In 1959, Lev Gor'kov showed that the BCS theory reduced to the Ginzburg-Landau theory close to the critical temperature.

In 1962, the first commercial superconducting wire, a niobium-titanium alloy, was developed by researchers at Westinghouse, allowing the construction of the first practical superconducting magnet. In the same year, Josephson made the important theoretical prediction that a super-current can flow between two pieces of superconductor separated by a thin layer of insulator. This phenomenon, now called the Josephson Effect, is exploited by superconducting devices such as SQUIDs. Josephson was awarded the Nobel Prize for this work in 1973.

In 2008 it was discovered by Valerie Vinokur and Tatyana Baturina that the same mechanism that produces superconductivity could produce a super-insulator state in some materials, with almost infinite electrical resistance.

1.3. High temperature superconductors

For obvious technological reasons, the search continued for materials which could super-conduct at higher temperatures. Despite much work, for decades the highest T_c's belonged to Nb_3Sn (18K) then Nb_3Ge (23K), and the field was considered by many to be at a dead end. A history of the increase in record T_c is shown in Fig.1.3. Three decades after BCS, in 1986, a startling discovery reopened the field of superconductivity

research. Bednorz and Muller, working at IBM in Switzerland, discovered a new class of superconducting materials starting with LaBaCuO, which is superconducting up to 30 K [8]. The following year, the liquid nitrogen temperature barrier (77K) was broken with the discovery of $YBa_2Cu_3O_{7-\delta}$, superconducting at 90K [9]. Soon a whole host of related materials were found. Since the common component in all these new high temperature superconductors is a CuO_2 plane, these materials are referred to as the "cuprates."

The discovery of superconductivity in the cuprates was surprising for several reasons. No previous oxide superconductors had ever been found. Furthermore, in their stoichiometric form (with no additional oxygen or other dopant atoms added) these materials are anti-ferromagnetic Mott insulators. It is conventional wisdom that magnetism cannot coexist with superconductivity. For example, Abrikosov and Gor'kov showed that magnetic impurities disrupt superconductivity and suppress the T_c [10]. The obvious differences between these new high-temperature superconductors (HTSCs) and the old conventional superconductors created a great deal of excitement. Rapidly, all the old experiments which had lead to the unifying theory of conventional superconductors were repeated. But the results were often confusing or contradictory.

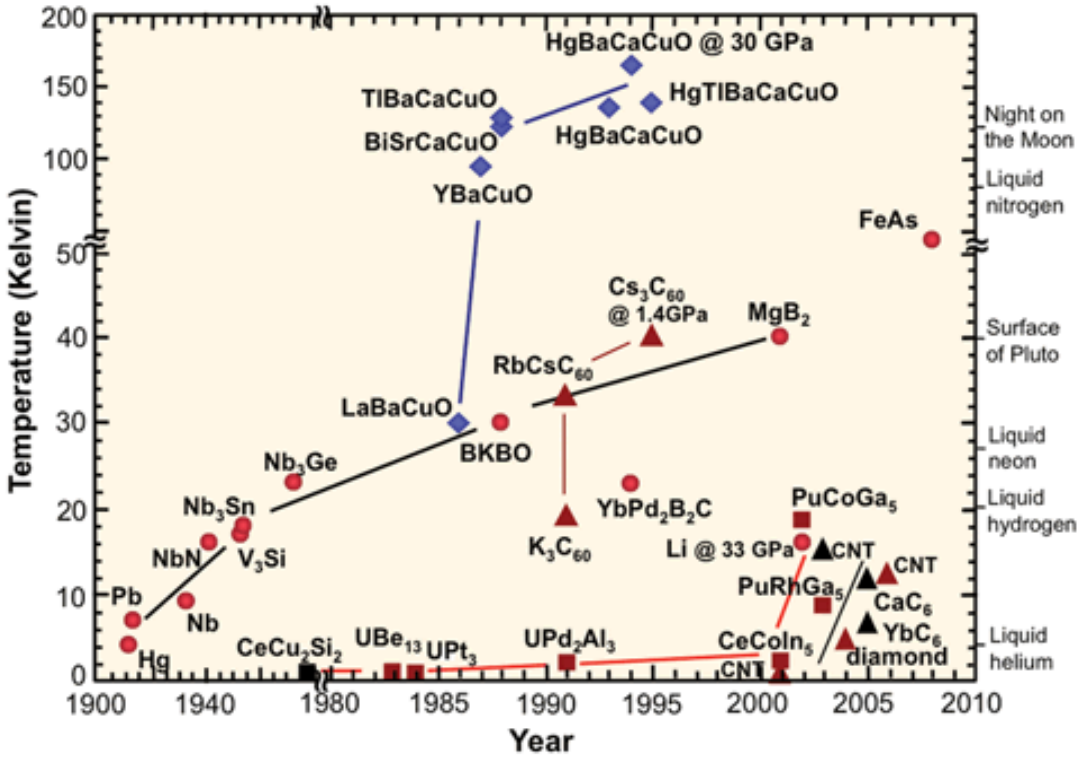

Fig. 1.3: Evolution of T_c with time.

1.4. Cuprate Superconductors Phases

Illustrative of the complexity of the high-temperature superconductor materials is this phase diagram which applies to the cuprate materials. At very low doping, they show the long range order of an anti-ferromagnetic. Fig.1.4 shows that how the phase changes with doping concentration. Doping breaks up the antiferromagnetic order and they become insulators. Only with doping fraction between about 0.1 and 0.2 they become superconductors**.**

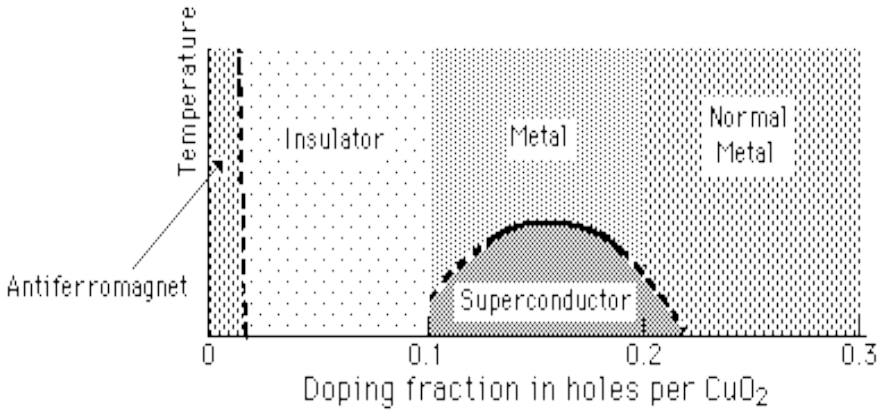

Fig. 1.4: Phase changes with doping concentration.

1.5. Types of Superconductors

Based on the magnetization behavior, superconductors may be classified into two types: Type-1 and Type-2 superconductors.

1.5.1. Type-I Superconductors

Superconductors which show a M verses B curve with an abrupt transition from perfect diamagnetic state to paramagnetic state at B_c are called Type-1 superconductors. Most elemental superconductors exhibit this behavior. The value of critical field B_c is quiet low for these superconductors, not being greater than 0.2 Tesla. These superconductors are also called soft superconductors as shown in Fig.1.5.

1.5.2. Type-2 superconductors

In Type-2 superconductors, the transition from a perfect diamagnetic state to the paramagnetic state is not abrupt as in Type-1 superconductors. The negative magnetization increases linearly up to a certain value of magnetic field B_{c1} and beyond this, magnetization falls gradually, becoming positive at a much higher magnetic field B_{c2}. Upto B_{c1} material is a perfect diamagnet and between B_{c1} and B_{c2} the material is partly diamagnetic, i.e. there is some flux penetration into the material. At Bc_2 material becomes paramagnetic with a small positive magnetization as shown in Fig 1.5. These are also called hard superconductors [3].

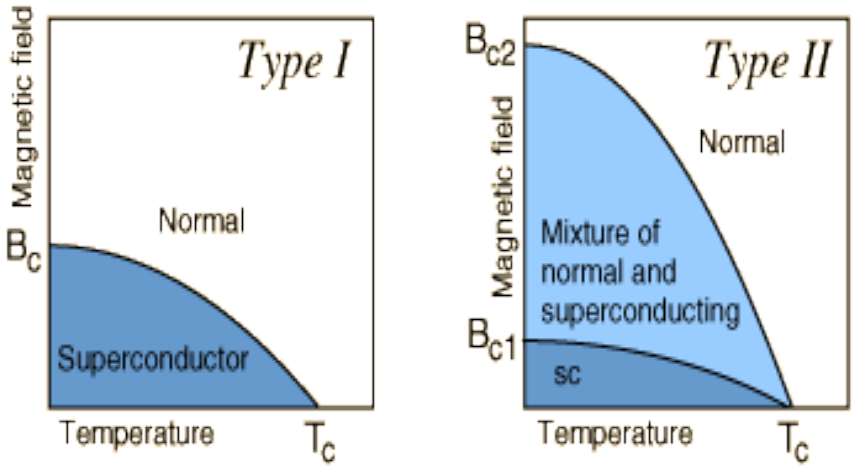

Fig. 1.5: Type 1 and Type 2 Superconductors.

1.6. Important Terms Related To Superconductivity

1.6.1. Zero resistivity

The typical signature of superconductivity is the vanishing of the electrical resistance below some critical temperature. The superconducting state is a thermodynamically distinct state of matter. [11] Classically, the electrical conductivity σ is defined as

$$\sigma \equiv ne^2\tau/m$$
$$\rho \equiv 1/\sigma$$
$$\rho \equiv m/ne^2\tau \qquad (1.1)$$

Where m, n, e and τ is the mass of electron, number of electrons, charge on electron and mean free time, respectively. As the temperature decreases, the lattice vibration begins to

freeze; therefore, the scattering of electrons from lattice vibrations diminishes. This in-turn results into the enhancement of τ (the mean free time of the carriers between collisions) and decreases resistivity. For infinite τ, at sufficiently low temperature the resistivity vanishes entirely which is observed in superconductors [12].

1.6.2. Critical Temperature for Superconductors

"The critical temperature for superconductors is the temperature at which the electrical resistivity drops to zero".

The transition is so sudden and complete that it appears to be a transition to a different phase of matter; this superconducting phase is described by the BCS theory. Several materials exhibit superconducting phase transitions at low temperatures. The highest critical temperature was about 23 K until the discovery in 1986 of some high temperature superconductors.

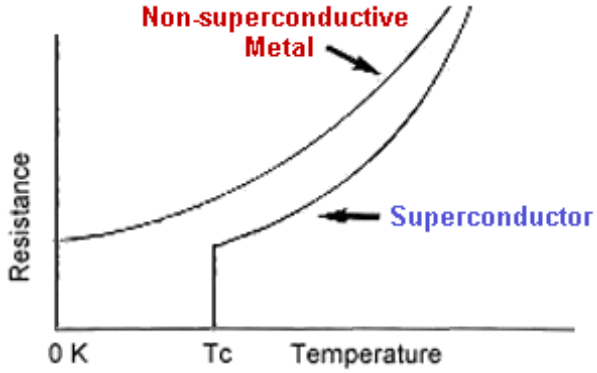

Fig. 1.6: Vanishing of resistance at critical temperature

Materials with critical temperatures in the range 120 K have received a great deal of attention because they can be maintained in the superconducting state with liquid nitrogen (77 K). The T_c of some superconductors is shown in the following table.

Table 1.1 Critical Temperature of some superconductors**.**

Material	Gallium	Aluminum	Indium	Tin	Mercury	Lead	Niobium	Niobium-Tin	La-Ba-Cu-oxide	Y-Ba-Cu-oxide	Tl-Ba-Cu-oxide
T_c(K)	1.1	1.2	3.4	3.7	4.2	7.2	9.3	17.9	30	92	125

1.6.3. BCS Theory of Superconductivity

The properties of Type-I superconductors were modeled successfully by the efforts of John Bardeen, Leon Cooper, and Robert Schrieffer in what is commonly called the BCS theory. A key conceptual element in this theory is the pairing of electrons close to the Fermi level into Cooper pairs through interaction with the crystal lattice. These pairing results from a slight attraction between the electrons related to lattice vibrations; the coupling to the lattice is called a phonon interaction. The decisive step in understanding the microscopic mechanism of superconductivity is due to L.Cooper (1956). The essence of his work can be outlined as follows:

Consider a normal metal in the ground state in k space; all states for non interacting electrons inside the Fermi sphere are occupied, while those outside it are empty. Then an extra pair of electrons is brought in and placed in the state (k↑) and (-k↓), in the vicinity of Fermi surface. It turned out that if two electrons become attracted to each other, they form a bound state regardless of how weak the interaction is. In real space, these electrons form a bound pair called a cooper pair.

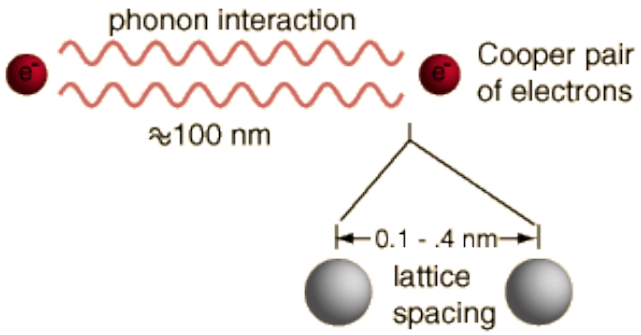

Fig. 1.7: Phonon-electron interaction

BCS theory demonstrated that interaction between electron and phonon can lead to electron- electron attraction. As a result electrons form cooper pairs having total spin of zero which represents that cooper pair is a Bose particle. Such particles posses a remarkable property: if the temperature of the system falls below critical temperature they can all gather in lowest energy level. This process is called Bose condensation. All particles in condensate have same wave function. So according to the BCS theory phenomenon of superconductivity can be briefly described follows:

At $T<T_c$ there exists a condensate of Cooper pairs. This condensate is superfluid. It means that the dissipation free electric current is carried by the Cooper pairs i.e. the charge of an elementary current carrier is 2e. Bardeen, Cooper, and Schrieffer received the Nobel Prize in 1972 for the development of this theory [4].

1.6.4. Meissner Effect

A bulk superconductor in a weak magnetic field acts as a perfect diamagnet, with zero magnetic induction in the interior. When a specimen is placed in a magnetic field and the magnetic flux originally present is ejected from the specimen. This is called Meissner effect [13].

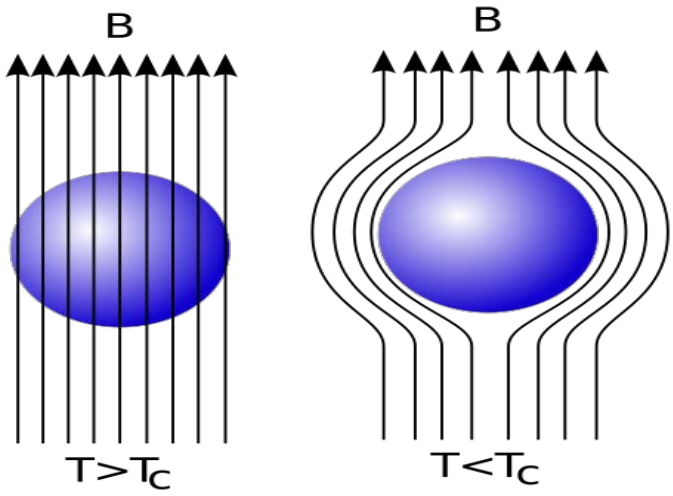

Fig. 1.8: Meissner effect (a)

In 1933, Walther Meissner and his student Robert Ochsenfeld discovered an important magnetic property of superconductors. They observed that a magnetic field lower than H_c was suddenly expelled by superconductor specimens on cooling below T_c [14]. In other words, the material becomes fully diamagnetic in the superconducting state. This was found to be an intrinsic property of superconductors. It has been widely used for the testing of the superconducting state. Due to the Meissner effect, if an external magnetic field is applied to a sample which is in the superconducting state, an electric current is produced near the surface of the sample, in such a way as to create a magnetic

field that exactly cancels the external magnetic field. The magnetic induction inside the substance is given by

$$B = \mu o\ (H + M) = \mu_o\ (1+ \chi)\ H \qquad (1.2)$$

Where H is external magnetic field, M is magnetization in the medium, and χ is the magnetic susceptibility. Since B=0 in the superconducting state so,

$$M = -H \qquad (1.3)$$

The magnetization M is equal and opposite of H. The medium is thus diamagnetic, the susceptibility is

$$\chi = -1 \qquad (1.4)$$

Such a condition is referred to as *perfect diamagnetism* [15].

1.6.5. Critical Magnetic Field (H_c):

Let us consider a superconductor at a temperature T<Tc in a magnetic field. As the magnetic field is increased to a certain critical value H_c, the superconducting state is destroyed. The critical field limits the amount of current that can flow in a superconductor. As soon as the field owing to the current exceeds H_c, the specimen reverts back to the normal state since it is no more free of the magnetic flux. The change of state, in fact, is also advantageous on energy consideration. The value of $H_c(T)$ determines the minimum strength of the magnetic field that destroys superconductivity at a temperature $T<T_c$. It is known as the critical field. The value decreases as T_c is approached from below T_c and finally drops to zero at T_c. On reducing the field below H_c, the specimen transforms back into the superconducting phase. The manner in which penetration occurs with increasing field strength depends in general on the geometry of the specimen. However, for the simplest geometry long, thin, cylindrically shaped samples with their axes parallel to applied field there are two clearly distinguishable kinds of behavior: [16]

1.6.6. Critical Current Density

Since there is no loss in electrical energy when superconductors carry electrical currents, relatively narrow wires made of superconducting materials can be used to carry huge currents. But there is a certain maximum current limit that these materials can carry, above which they become normal conductors. If too much current is pushed through a superconductor, it will revert back to a normal state even though it may be below its

transition temperature. The value of the critical current density (J_c) as a function of the temperature is shown in Fig.1.9. During J_c measurements it is observed that the colder you keep the superconductor the more current it can carry. For practical applications, J_c values in excess of 1000 A/mm^2 are preferred.

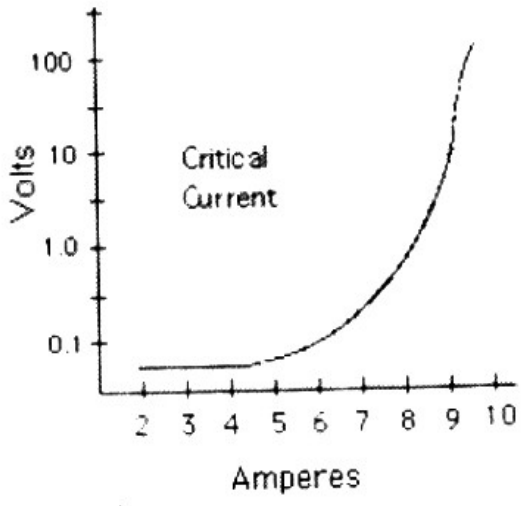

Fig. 1.9: I-V Characteristic of a superconductor.

1.6.7. Correlation of three Critical Values:

As we know that superconducting state is defined by three very important factors.

1. Critical Temperature (T_c)
2. Critical Magnetic Field (H_c)
3. Critical Current Density (J_c)

Each of these parameters is much dependent on the other two properties present. Maintaining of the superconducting state requires that the magnetic field and current density as well as the temperature remain below the critical values, all of which depend upon the material characteristics. The phase diagram of Fig.1.10 demonstrates the relationship between the three critical properties.

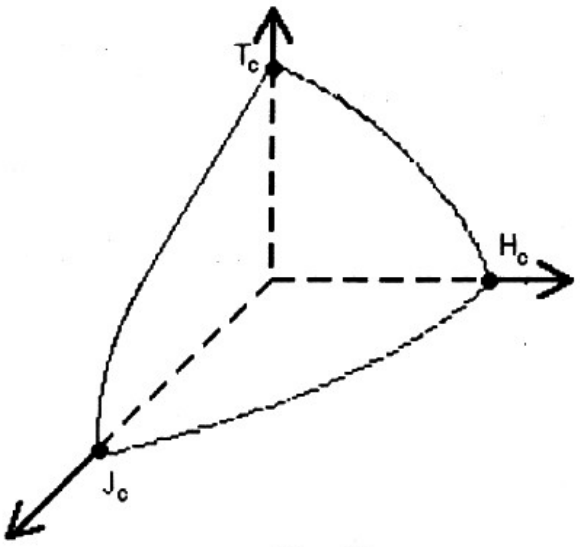

Fig. 1.10: Correlation between J_c, T_c, and H_c for a superconductor.

The highest values of J_c and H_c occur at 0K, while the highest value of T_c occurs when H and J are zero. When considering all three parameters, the plot represents a critical surface. From this surface and moving towards the origin, the material is superconducting. In the regions outside of this surface, the material is normal or in a mixed state. In the superconducting state when electrons form cooper pairs, they can share the same quantum wave function or energy state. This result in a lower energy state for the superconductors; the T_c and H_c are the values where it becomes favorable for the electron pair to break apart.

The current density larger than the critical value forces current to flow through normal conducting electrons of the material. This current flow through normal material of the mixed state is connected with motion of the magnetic field lines through pinning sites. For most practical applications, superconductor must be able to carry high current and withstand high magnetic fields without reverting to its normal state.

1.6.8. Perfect Diamagnet

If a conductor already had a steady magnetic field through it and was then cooled through the transition to a zero resistance state, becoming a perfect diamagnet, the magnetic field would be expected to stay the same as shown in Fig.1.11.

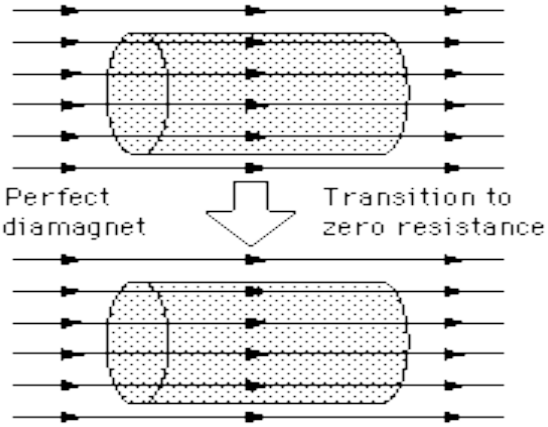

Fig. 1.11: perfect diamagnet

1.6.9. Perfect Diamagnetism

A conductor will oppose any change in externally applied magnetic field. Circulating currents will be induced to oppose the buildup of magnetic field in the conductor (Lenz's law) as shown in Fig.1.12. In a solid material, this is called diamagnetism, and a perfect conductor would be a perfect diamagnet. That is, induced currents in it would meet no resistance, so they would persist in whatever magnitude necessary to perfectly cancel the external field change. A superconductor is a perfect diamagnet, but there is more than this involved in Meissner effect.

1.6.10. Superconductor

The magnetic behavior of a superconductor is distinct from perfect diamagnetism. It will actively exclude any magnetic field present when it makes the phase change to the superconducting state as shown in Fig.1.13.

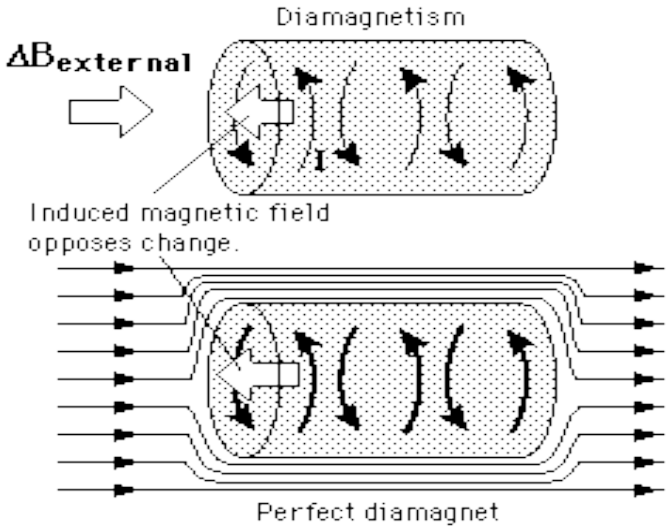

Fig. 1.12: Induced magnetic field in perfect diamagnet.

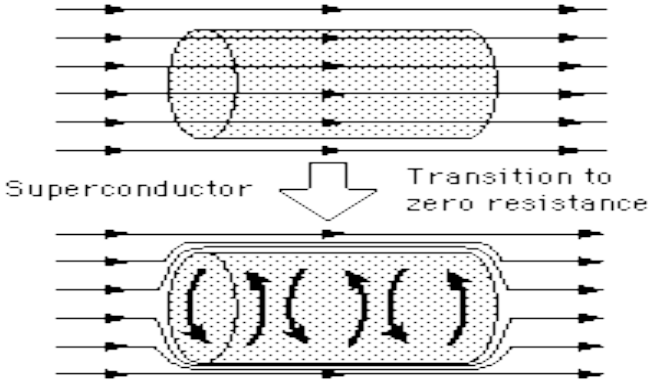

Fig. 1.13: Meissner effect (b)

1.6.11. London penetration depth (λ)

In 1935, Fritz and Heinz London theoretically explained the Meissner effect by positing two groups of electrons in a superconducting material, the superconducting electrons and the normal state electrons. They employed the Maxwell equations to develop a set of electrodynamics equations, called the *London equations* [17]. According to the London equations, the magnetic field exponentially falls off with increasing distance from the surface of a superconducting sample. The characteristic decay length is called the *London penetration depth* (λ).

1.6.12. Coherence Length

The maximum distance over which the states of paired electrons are correlated to produce superconductivity is called coherence length. The paired electrons (Cooper pairs) are not scattered because of their peculiar property of smoothly riding over the lattice imperfections without over exchanging energy with them. The concept of coherence is the idea that superconductivity is due to the mutual interaction and correlation of the behavior of electrons which extends over a considerable distance [1].

1.6.13. Energy gap

The energy difference between the free state of the electron (i.e. energy of individual electron in normal state) and the paired state (the energy of paired electron a case of superconducting state) appears as the energy gap of width 2Δ at the Fermi surface. The normal electron states are above the energy gap and the superconducting electron states are below the energy gap at the Fermi surface [18]. According to BCS theory intrinsic coherence length is related to the energy gap as

$$\xi \approx \hbar V_F / 2\Delta \qquad (1.5)$$

V_F is the Fermi velocity.

Energy gap is a function of temperature, since pairing is complete at 0K and is completely broken at a critical temperature.

$$2\Delta = 3.52 K_B T_c \qquad (1.6)$$

K_B is the Boltzman's constant

1.6.14. Specific heat

The specific heat of the normal metal is seen to be of the form,

$$C_n(T) = \gamma T + \beta T^3 \qquad (1.7)$$

The first term in the Eq. (1.8) is the specific heat of electrons in the metal and the second term is the contribution of the lattice vibrations at low temperatures. The specific heat of the superconductor shows a jump at T_c. Since the superconductivity affects electrons mainly, it is natural to assume that lattice vibration part remains unaffected, i.e., it has the same value βT^3 in the normal and superconducting state. On subtracting this, we notice

that the electronics specified heat C_{es} is not linear with temperature. It rather fits an exponential form

$$C_n(T) = A\exp(-\Delta/k_B T) \qquad (1.8)$$

This exponential form is an indication of the existence of a finite gap in the energy spectrum of electrons separating the ground from the excited state. The energy gap is believed to be a characteristic feature of the superconducting state which determines the thermal properties as well as high frequency electromagnetic response of all the superconductors

1.6.15. Isotope effect

The critical temperature of superconductors varies with isotopic mass. This observation was first made by Maxwell and others; the argument was that the isotopic mass can enter in the process of the formation of the superconducting phase of the electron states only through the electron - phonon interaction. The experimental of an isotope series can be summarized by the following relationship

$$M^a T_c = \text{constant} \qquad (1.9)$$

where 'a' is fitting constant.

1.6.16. Magnetic Levitation

Magnetic fields are actively excluded from superconductors (Meissner effect). If a small magnet is brought near a superconductor, it will be repelled because induced super currents will produce mirror images of each pole. If a small permanent magnet is placed above a superconductor, it can be levitated by this repulsive force. The black ceramic material in the illustrations is a sample of the yttrium based superconductor. By tapping with a sharp instrument, the suspended magnet can be caused to oscillate or rotate. This motion is found to be damped, and will come to rest in a few seconds

.

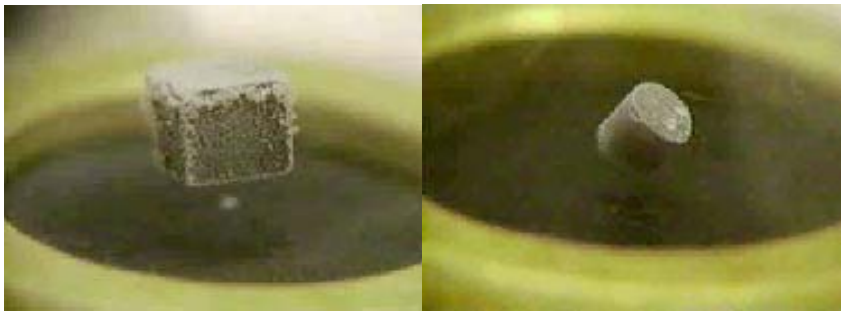

Fig. 1.14: Magnetic Levitation.

1.7. Tl Based High Temperature Superconductors

The thallium based Tl-Ba-Ca-Cu-O (TBCCO) superconductors discovered in 1988 by Sheng and Hermann [19-24] are the best among all other cuprates due to their high transition temperature, [$T_c(0)$], transport critical current densities, [J_c] and low microwave surface resistances, [R_s]. Since the discovery of superconductivity in this system, several new phases of $Tl_mBa_2Ca_{n-1}Cu_nO_{2n+2}$ (m=1, 2; n=1, 2, 3, 4, 5) have been prepared [25-28]. In two-layer thallium compounds, the $Tl_2Ba_2Cu_1O_6$, $Tl_2Ba_2Ca_1Cu_2O_8$, $Tl_2Ba_2Ca_2Cu_3O_{10}$, $Tl_2Ba_2Ca_3Cu_4O_{12}$, and $Tl_2Ba_2Ca_4Cu_5O_{14}$ are major phases, which can be simply represented as, Tl-2201, Tl-2212, Tl-2223, Tl-2234 and Tl-2245 with critical temperatures of 95, 118, 127, 112 and 105K, respectively. The maximum critical temperature of ~127 K is found in Tl-2223 superconductor [29, 30]. These materials exhibit tetragonal symmetry with I4/mmm space group. The structure of these compounds comprises copper provskite-like blocks with $nCuO_2$ (n = 1, 2, 3…) planes separated by two TlO layers. Each CaO layer is sandwiched between two CuO_2 planes and BaO layer between the CuO_2 plane and TlO layers. These compounds can be represented by a formula Tl-22(n-1)n, where n represents the number of CuO_2 planes. The oxygen coordination number of Tl, Cu, Ca and Ba in these compounds is 6, 4/5, 8 and 9 respectively. The c-axis length in these materials ranges from 23.248 Å for n =1 to 42.07 Å for n = 4 [31, 32]. The critical temperature increases up to 127 K with number of CuO_2 planes n from 1 to 3 and then decreases for higher number of CuO_2 planes in the unit cell of bilayer TlO compounds.

Since Tl-based superconductor materials have higher critical temperature, so much attention has been given to the synthesis of bulk and thin film samples of these

compounds, which can be used for electronic devices [33-42]. On the other hand, the monolayer Tl-based system includes $TlBa_2Ca_1Cu_2O_7$, $TlBa_2Ca_2Cu_3O_9$, $TlBa_2Ca_3Cu_4O_{11}$, and $TlBa_2Ca_4Cu_5O_{13}$ superconductor phases, which for brevity can be represented as Tl-1212, Tl-1223, Tl-1234 and Tl-1245 with critical temperatures 103, 123, 112 and 107 K respectively. The materials with double Tl-O layers have body centered tetragonal structure and single Tl-O layer compounds have primitive tetragonal structure. The family of thallium based superconductors with single Tl-O layer is comprised of Tl-1212, Tl-1223 and Tl-1234 compounds. These superconducting compounds are more promising because of their lower anisotropy, higher $T_c(0)$, higher critical current densities and irreversibility field H_{irr} as compared to their counterparts in double Tl-O layer superconductors family [43-51].

1.8. Applications of High Temperature Superconductors

1.8.1. Superconducting Transmission Lines

Since 10% to 15 % of generated electricity is dissipated in resistive losses in transmission lines, the prospect of zero loss superconducting transmission lines is appealing. In prototype superconducting transmission lines at Brookhanven National laboratory, 1000 MW of power can be transported within an enclosure of diameter 40 cm. This amounts to transporting the entire output of a large power plant on one enclosed transmission line. This could be a low voltage AC transmission lines on towers in the conventional systems. The superconductor used in these prototype applications is usually niobium-titanium, and liquid helium cooling is required. Current experiments with power applications of high-temperature superconductors focus on uses of BSCCO in tape forms and YBCO in thin film forms. Current densities above 10,000 amperes per square centimeter are considered necessary for practical power applications, and this threshold has been exceeded in several configurations.

1.8.2. Fault-Current Limiters

High fault-currents caused by lighting strikes are a troublesome and expensive nuisance in electric power grids. One of the near-term applications for high temperature superconductors may be the construction of fault-current limiters, which operate at 77K.

The need is to reduce the fault current to a fraction of its peak value in less than a cycle (1/60sec). A recently tested fault-current limiter can operate at 2.4 kV and carry a current of 2200 amperes. It was constructed from BSCCO material.

1.8.3. Superconducting Motors

Superconducting motors and generators could be made with a weight of about one tenth that of conventional devices for the same output. This is the appeal of making such devices for specialized applications. Motors and generators are already very efficient, so there is not the power savings associated with superconducting magnets. It may be possible to build very large capacity generators for power plants where structural strength considerations place limits on conventional generators. In 1995, the Navel Research Laboratory demonstrated a 167 hp motors with high-T_c superconducting coils made from Bi-2223. It was tested at 4.2K and at liquid neon temperature, 28K with 112 hp produced at the higher temperature.

1.8.4. Superconducting Maglev Trains

While it is not practical to lay down superconducting rails, it is possible to construct a superconducting system onboard a train to repel conventional rails below it. The train would have to be moving to create the repulsion, but once moving would be supported with very little friction. There would be resistive loss of energy in currents in the rails. Ohanian reports an engineering assessment that such superconducting trains would be much safer than conventional rail system at 200 km/h. A Japanese magnetically levitated train set a speed record of 321 mile/h in 1997 using superconducting magnets on board the train. The magnets induced currents in the rails below them, causing a repulsion, which suspends the train above the track.

1.8.5. Superconductors in NMR Imaging

Superconducting magnets find application in magnetic resonance imaging (MRI) of the human body. Besides requiring strong magnetic fields of the order of a Tesla, magnetic resonance imaging requires uniform fields and stability of extreme type over the time across the subject. Maintaining the magnet coils in the superconducting helps to achieve parts-per-million spatial uniformity over a space large enough to hold a person, and ppm/hour stability with time.

1.8.6. SQUID Magnetometer

The superconducting quantum interference device **(**SQUID) consists of two superconductors separated by thin insulating layers to form two parallel Josephson junctions. The device may be configured as a magnetometer to detect incredibly small magnetic fields small enough to measure the magnetic fields in living organisms. Squids have been used to measure the magnetic fields in mouse brains to test whether there might be enough magnetism to attribute their navigational ability to an internal compass. The great sensitivity of the SQUID devices is associated with measuring changes in magnetic field associated with one flux quantum [52]. One-flux quanta can be expressed as

$$\Phi_o = 2\pi h/2e \approx 2.0678\times10^{-15} \text{ tesla.m}^2$$

1.9. References

[1]. S.O.Pillai, Solid State Physics, 5th Edition, New Age International (p) Limited Publishers (2002).

[2]. S.O.Pillai, Solid State Physics, 5th Edition, New Age International (p) Limited Publishers,p: 400 (2002).

[3]. M. S. Vijaya, Materials Science, MC Graw-Gill Publishing Company Limited, P: 323,324 (2003).

[4]. V.V. Schmidt, the Physics of Superconductors, Nauka Publishers, Moskaue, p: 1(1982).

[5]. James. F. Annett, Superconductivity, Superfluids and Condensates, Oxford University Press, p: 58, 67 (2004).

[6]. James. F. Annett, Superconductivity, Superfluids and Condensates, Oxford University Press, p: 67 (2004).

[7]. V.V. Schmidt, the Physics of Superconductors, Nauka Publishers, Moskaue, p: 18, 19 (1982).

[8]. G. Bednorz and K. A. Muller, Z. phys. B64, p: 189 (1986).

[9]. M. K. Wu, Phy. Rev. Lett. 58, p: 908 (1987).

[10]. A. A. Abrikosov and L. P. Gor, Kov, Zh. Eksperim. i Teor. Fiz, 39, p: 1781 (1960).

[11]. Phillip Phillips, Advanced Solid State Physics

[12]. Charles Kittles, Introduction to Solid State Physics, 7th Edition.

[13]. Charles Kittles, Introduction to Solid State Physics, 7th Edition, p: 337

[14]. Meissner, W. and R. Ochsenfeld, Naturwissenschaften, , p: 787 (1933).

[15]. M. A. Omar, Elementary Solid State Physics, 3rd Edition, (2007)

[16]. J.P. Srivastava, Elements of Solid State Physics, 2nd Edition.

[17]. London. F and H. London, Proc. Roy. Soc. A 149, P: 71-88 (1935).

[18]. S.O.Pillai, Solid State Physics, 5th Edition, New Age International (p) Limited Publishers (2002).

[19]. Z. Z. Sheng and A. M. Hermann, Nature **332**, 55 (1988).

[20]. Z. Z. Sheng, A. M. Hermann, A. E. Ali, C. Almasan, J. Estrada, T. Datta, and R. J. Matson, Phys. Rev. Lett. **60**, 937 (1988).

[21]. Z. Z. Sheng, and A. M. Hermann, Nature **332**, 138 (1988).

[22]. G. Malandrino, D. S. Richeson, T. J. Marks, D. C. De Groot, J. L. Schindler, and C. R. Kannewurf, Appl. Phys. Lett. **58**, 182 (1991).

[23]. M. L. Chu, H. L. Chang, C. Wang, J. Y. Juang, T. M. Uen, and Y. S. Gou, Appl. Phys. Lett. **59**, 1123 (1991).

[24]. W. L. Oslon, M. M. Eddy, T. W. James, R. B. Hammond, G. Gruner, and L

[25]. M. Kikuchi, T. Kajitani, T. Suzuki, S. Nakajima, K. Hiraga, N. Kobayashi, H. Iwasaki, Y. Syono, and Y. Muto, Jpn. J. Appl. Phys. **28**, L382 (1989).

[26]. S. S. P. Parkin, V. Y. Lee, E. M. Engler, A. I. Nazzal, T. C. Huang, G. Gormau, R. Savoy, and R. Beyer, Phys. Rev. Lett. **60**, 2539 (1988).

[27]. I. K. Schuller, and J. D. Jorgensen, Mater. Res. Bull. **XIV**, 27 (1989).

[28]. A. W. Sleight, M. A. Subramanian, and C. C. Torardi, Mater. Res. Bull. **XIV**, 45 (1989).

[29]. C. Martin, C. Michel, A. Maignan, M. Hervieu, and B. Raveau, C. R. Acad. Sci. Ser.2, 307, 27 (1988).

[30]. C. Park, and R. L. Synder, J. Am. Ceram. Soc. **78**, 3171(1995).

[31]. J. B. Parise, J. Gopalkrishnan, M. A. Subramanian, and A. W. Sleight, J. Solid State Chem. **76**, 432 (1988).

[32]. Y. Tang, B. Lin, D. Zhou, W. Zhu, F. Chen, N. Li, K. Chen, and G. Lu, Mod. Phys. Lett. B **3**, 853 (1989).

[33]. D. S. Ginley, J. F. Kwak, R. P. Hellmer, R. J. Baughman, E. L. Venturini, M. A. Mitchell, and B. Morosin, Physica C **156**, 592 (1988).

[34]. W. L. Olson, M. M. Eddy, T. W. James, R. B. Hammond, G. Gruner, and L. Drabeck, Appl. Phys. Lett. **55**, 188 (1989).

[35]. W. Y. Lee, V. Y. Lee, J. Salem, T. C. Huang, R. Savoy, D. C. Bullock, and S. S. P. Parkin, Appl. Phys. Lett. **53**, 329 (1988).

[36]. D. S. Ginley, J. F. Kwak, R. P. Hellmer, R. J. Baughman, E. L. Venturini, and B. Morosin, Appl. Phys. Lett. **53**, 406 (1988).

[37]. K. K. Verma, G. D. Verma, R. S. Tiwari, and O. N. Srivastava, Jpn. J. Appl. Phys. **29**, L880 (1990).

[38]. W. Y. Lee, J. Salem, V. Lee, D. Deline, T. C. Huang, R. Savoy, J. Duran, and R. L. Sandstrom, Physica C **160**, 5117 (1989).

[39]. H. L. Chang, C. Wang, M. L. Chu, T. M. Uen, and Y. S. Gou, Jpn. J. Appl. Phys.

28, L631 (1989).

[40]. H. S. Koo, W. –M. Hurng, W. H. Lee, T. Y. Tseng, M. Chen, and J. R. Lo, Appl. Phys. Lett. **62**, 3354 (1993).

[41]. D. Thopart, J. Hejtmanek, D. Pelloquin, C. Martin, and A. Maignan, Physica C **336**, 143 (2000).

[42]. Z. Zhang, C-Chun Chen, C. M. Lieber, B. Morosin, D. S. Ginley, and E. L. Venturini, Phys. Rev. B **45**, 987 (1992).

[43]. A. Sundaresan, H. Asada, A. Crisan, J. C. Nie, H. Kito, A. Iyo, Y. Tanaka, M. Kusunoki, and S. Ohshima, IEEE Trans. Appl. Supercond. **13**, 2913 (2003).

[44]. J. Y. Juang, J. H. Horng, S. P. Chen, C. M. Fu, K. H. Wu, T. M. Uen, and Y. S. Gou, Appl. Phys. Lett. **60**, 885 (1995).

[45]. A. Sundaresan, H. Asada, A. Crisan, J. C. Nie, H. Kito, A. Iyo, T. Tanaka, M. Kusunoki, and S. Oshima, Physica C **388**, 473 (2003).

[46]. D. J. Miller, J. G. Hu, J. D. Hettinger, K. E. Gray, J. E. Tkaczyk, J. Deluca, P. L. Karas, J. A. Sutliff, and M. F. Garauskas, Appl. Phys. Lett. **63**, 556 (1993).

[47]. A. Iyo, Y. Ishiura, Y. Tanaka, P. Badica, K. Tokiwa, T. Watanabe, and H. Ihara, Physica C **370**, 205 (2002).

[48]. W. Mexner, J. Hoffmann, S. Heede, K. Heinemann, H. C. Freyhardt, F. Ladenberger, and E. Schwarzmann, Z. Phys. B **101**, 181 (1996).

[49]. D. N. Zheng, J. D. Johnson, A. R. Jones, A. M. Campbell, W. Y. Liang, T. Doi, M. Okada, and K. Higashyama, J. Appl. Phys. **77**, 5287 (1995).

[50]. R. T. Liu, S. L. Yan, L. Fang, and M. He, Supercond. Sci. Technol. **14**, 948 (2001).

[51]. R. S. Liu, D. N. Zheng, J. W. Loram, K. A. Mirza, A. M. Campbell, and P. P.

[52]. The Physics of Superconductors, An Introduction to Fundamental and Application, P.Muller, A.V Ustinov (Eds.) and V.V Schmidt.

Chapter 2

Literature Review

2.1. Literature Review

S Isber et al [1] prepared superconducting samples of type $TlBa_2Ca_2(Cu_{3-x}Co_x)O_{9-\delta}$ with ($0 \leq x \leq 0.6$) by a single-step solid-state reaction technique. The prepared samples were characterized by powder x-ray diffraction and the superconductivity of these samples was investigated by electrical resistivity and ac magnetic susceptibility measurements. The x-ray data indicated that the lattice parameters *a* and *c* were varied but the structure of Tl-1223 remains tetragonal with cobalt substitution up to x = 0.6. The transition temperature 'T_c', deduced from electrical resistivity and ac magnetic susceptibility measurements, was suppressed by substituting Co impurities at Cu sites. The suppression in T_c has been discussed using a Cooper pair-breaking mechanism due to the Abrikosov and Grokov model. There was no separation between the intergrain and dissipative intergrain transition in ac magnetic susceptibility measurements. These observations showed good electrical contacts between the superconducting grains. The effects of external magnetic field on the ac magnetic susceptibility as well as calculations of critical current density as a function of cobalt content and temperature were reported. The critical current density as well as reversibility field was decreased by increasing Co content. The critical exponent γ was found to be equal to 2, indicating that the intergrain junctions are of the SNS type.

R. Awad et al [2] prepared samples of $TlBa_2Ca_{2-x}Na_xCu_3O_{9-\delta}$; with $0 \leq x \leq 0.4$ using stoichiometric amounts of Tl_2O_3, BaO_2, CaO, Na_2O_2, and CuO by single step of solid state reaction technique. They investigated the effect of Na substitution at Ca sites on the lattice parameters, electrical resistivity, magnetic susceptibility and thermo-power coefficient. X-ray spectra indicated that the major phase present in the prepared samples is the Tl-1223 phase with very small amounts of impurities such as $BaCuO_2$ and Tl-1212 phases which are typical phases in samples prepared by solid-state reaction method. The lattice constants "a" and "c" were found to slightly increase with increasing Na-content. They observed a little increase in T_c as

x increases from 0 to 0.05 followed by suppression for x > 0.05. They suggested that as the preparation of their samples was carried out in closed tubes filled with air instead of vacuum tubes, so the un-doped sample, x =0, lies in the over-doped region. Na has a valance state of +1 and its substitution in Ca site would reduce the amount of oxygen in the preparation tube implying that the substitution of Ca by Na may have changed the un-doped sample from over-doped regime to optimum-doped at x=0.05 and then to the under-doped regime for x = 0.05. This observation was attributed to the fact that Na has converted the Tl-1223 phase from over-doped regime to under-doped regime which was in conformity with the thermo-power results, that found to change from negative (over-doped regime) to positive (under-doped regime). The inter-grain critical current density as function of Na has been also reported from ac magnetic susceptibility measurements. They observed that the critical current density at 0 K increases as x is increased from 0 to 0.05 and then it decreases in similar fashion to the transition temperature. The suppression in $J_c(0)$ at higher Na content is explained by the increase of the grain boundaries resistance and the reduction of the flux pinning inside the sample.

M Eder et al [3] investigated the effect of incorporating uranium into thallium-based superconducting samples. $(Tl_{0.6}Pb_{0.5})(Sr_{0.8}Ba_{0.2})_2Ca_2Cu_3U_xO_y$ samples were prepared by a wet chemical route followed by solid-state reactions. The x values of 0.005, 0.01 and 0.02 yielded almost the pure Tl-1223 phase with $T_{c(0)}$ values of 114 K. For x values of 0.08 and 0.2, considerable amounts of the Tl-1212 phase were found. They observed two-step transitions in the resistance–temperature curves and the transition temperature was dropped to 107 K and 103 K for x=0.08 and x=0.2, respectively. Energy dispersive X-ray analysis showed that uranium was incorporated into the superconducting crystallites. Concentrations of uranium above x = 0.2 did not result in superconducting material. X-ray diffraction indicated that small amounts of U ($x \leq 0.04$) did not affect the formation of the Tl-1223 phase. It was observed that for x values of 0.08 and 0.2, the content of the Tl-1212 phase became noticeable in the X-ray diffraction. The introduction of uranium into the tetragonal Tl-1223 phase led to a decrease in the *c*-axis, but did not affect the *a*-axis. The temperature dependences of the resistances yielded two-step transitions. Such two-step transitions indicated that the content of the Tl-1223

crystallites is too small to provide an electrical short cut through the sample. Precursors with x values above 0.4 did not result in any superconducting material, although peaks for the Tl-1223 and the Tl-1212 superconducting phases still appeared in the x-ray diffraction scans. They suggested that increase of the Tl-1212 phase with increasing uranium content may be due to the incorporation of U^{6+} into the Ca layers of the superconducting lattice.

Ren Yanru et al [4] studied the TlBaCaCuO superconductor having critical temperature in the range of 100K to 123K. The samples were prepared by wrapped method and open method. Structural analyses were carried out by scanning electron microscope (SEM) and X-ray diffraction. The resistive transitions of the samples were examined with a standard DC four probe method and diamagnetic transitions were measured by AC mutual inductance method. Infrared spectra were measured at room temperature. The SEM of the sample was found to be porous consisting of plane like grains with irregular shapes. Electron microprobe analysis carried on number of plate like grains showed that the sample consist of both 2212 and 2223 phases. The XRD of the sample showed the tetragonal structure with lattice parameter a=5.404Å and c=35.634Å corresponding to the 2223 phase. Both synthesizing method have produced samples having superconducting transition in the range of 100-123K. Most of the samples prepared with open method were having the T_c values around 95-105K except few samples having T_c up to 119K. It was suggested that the lower T_c might be due to the decomposition of Tl_2O_3 to Tl_2O and volatilization as dark brown smoke. It was found that the samples prepared from wrapped method have zero resistance in the range of 115-120K. The IR spectra of multiphase samples showed that Cu-O stretching vibrations peaked at P_1~590 cm^{-1} and P_2 ~530cm^{-1}, respectively. The wave number and the relative strength of the P_1 and P_2 peaks were found to be closely related to the composition and the crystal structure of the samples. The difference$\Delta P=P_1-P_2$ can be used as an indication of high T_c for oxide superconductors. It was concluded that the electron-like excitation at ~0.1eV and the phonon like feature at ~ 850 cm^{-1} might have played important role to the occurrence of high T_c.

N.M. Hamdan et al [5] studied the effect of fluorine on various superconducting and normal state properties of superconducting samples

$(Tl_{0.5}, Pb_{0.5})\ Sr_{1.6}Ba_{0.4}Ca_2Cu_3O_y$ through partial replacement of CuO by CuF_2 in the starting materials. They examined seven samples with nominal fluorine content x atom per formula unit $(0 \leq x \leq 3.6)$ by X -ray diffraction (XRD), scanning electron microscopy (SEM), resistivity and magnetization M(H) measurements. Fluorine addition has raised the onset transition temperature to 128K, and increased the critical current density to 300%, the value of the fluorine free sample. X-ray diffraction (XRD), scanning electron microscopy (SEM) and energy dispersive X-ray (EDX) results showed that the formation of the Tl-1223 phase was enhanced as fluorine was introduced, and the formation of large grains was observed. The presence of fluorine as a species of the structure of the Tl-1223 grains was revealed by EDX spot analysis. The c-axis of Tl-1223 decreased with increasing x, indicating that fluorine had replaced oxygen in the structure. The behavior of the normal state resistivity with temperature indicated that fluorine addition changed this material from over-doped to optimally doped, and upon further fluorine addition, it was changed to slightly under-doped state. It was observed that the width of the hysteresis loops ΔM has increased with increasing fluorine content up to 2.2 to 300% of its fluorine-free value, and ΔM become less field-dependent. This also suggested that fluorine has enhanced the pinning strength and affected the pinning mechanism. These improvements in the superconducting and transport properties along with structural changes suggested the entering of fluorine into the structure of the super-conducting Tl-1223 phase, and changing the density of charge carriers in the Cu–O planes.

S Mikusu et al [6] prepared the samples $TlBa_2Ca_2Cu_3O_y$ by solid state reaction. Samples were characterized by powder X-ray diffraction (XRD) and scanning electron microscope (SEM). The T_c of these samples was determined by measuring both the electrical resistivity and the DC magnetic susceptibility. The electrical resistivity was measured using the conventional four-probe method. The DC magnetic susceptibility was measured by a Quantum Design MPMS under the field cooling mode with a magnetic field of 5 Oe. The DC magnetization hysteresis loops were also measured using MPMS at temperatures ranging from 5 to 110K and fields up to 7T. They observed that maximum T_c values for Tl-system superconductors $TlBa_2Ca_2Cu_3O_y$ (Tl-1223) can be controlled by slightly varying the

starting composition. From the DC magnetization measurements, they estimated intra-grain critical current densities (J_c) and irreversibility fields (B_{irr}) of Tl-1223 samples with different maximum T_c values (~130K and 120K). These results were compared with those values for previously reported optimally doped Hg-1223. It was found that, in the B_{irr} -T curve at temperatures above 77K, B_{irr} values of the Tl-1223 samples with T_c~130K shows slightly higher values than that of the Tl-1223 samples with low T_c and Hg-1223 samples. However they observed that the B_{irr} values of their samples are still smaller than that of Y-123 at 77K. It was concluded that introduction of effective pinning centers seems to be necessary for the application at 77K.

A. I. Abou-Aly et al [7] synthesized $Tl_{1-x}In_xBa_2(Ca_{0.9}Y_{0.1})_2Cu_3O_{9-\delta}$ for x = 0.1, 0.2, 0.3 and 0.5 superconductors using stoichiometric amount of $Ba_2(Ca_{0.9}Y_{0.1})_2Cu_3O_{7+\delta}$ precursor, Tl_2O_3 and In_2O_3 in a tube furnace at 870°C. The samples were characterized using the X-ray powder diffraction and the scanning electron microscope (SEM) whereas the composition of these samples was determined by micro-probe analysis. The electrical resistance was measured by using a conventional four-probe technique. The X-ray diffraction patterns indicated that the lattice parameter of all samples are nearly similar, where *a* =3.862Å and c=15.902Å. The transition temperature T_c for as-synthesized (Tl, In)-1223 compound, determined from the electrical resistance measurements, varied from 122K for x= 0 to 100K for x= 0.6. These results showed that the addition of indium suppressed the transition temperature in contrary to the addition of Hg, Pb and Bi which increases the transition temperature. They concluded that this is due to the difference in the electronic configuration of In ($4d^{10}5s^25p^1$) compared to other 6s metal cations ($4f^{14}5d^{10}6s^2\ 6p^n$). It was observed that the transition temperature in (Tl, In)-1223 phase is strongly dependent on the argon annealing. They observed that transition width is increased by increasing the external magnetic fields and these fields do not affect the first stage of transition.

Nurul H. Ahmad et al [8] studied the effects of Cu substitution at Tl site in $Tl_{1-x}Cu_xSr_{1.6}Yb_{0.4}CaCu_2O_{7-\delta}$ (x = 0–0.5) ceramics and Mg substitution at Sr site in $Tl_{0.5}Pb_{0.5}Sr_{2-y}Mg_yCa_{0.8}Yb_{0.2}Cu_2O_{7-\delta}$ ceramics, respectively on superconducting and structural properties. Excess conductivity analyses based on Asmalazov–Larkin

(AL) theory revealed 2D–3D transition and showed Cu substitution affects the A_{3D} constant and increases c-axis coherence length, $\xi_c(0)$. FTIR analysis for $Tl_{1-x}Cu_xSr_{1.6}Yb_{0.4}CaCu_2O_{7-\delta}$ (x=0–0.5) showed CuO_2 planar oxygen mode observed around 578.7cm^{-1} in the x = 0 sample was softened to 570cm^{-1} with increased Cu substitution indicating enhanced coupling between CuO_2 planes. On the other hand, $Tl_{0.5}Pb_{0.5}Sr_{2-y}Mg_yCa_{0.8}Yb_{0.2}Cu_2O_{7-\delta}$ (y =0–1.0) showed increasing semiconductor like normal state behavior and gradual suppression of T_c with Mg. Excess conductivity analyses of $Tl_{0.5}Pb_{0.5}Sr_{2-y}Mg_yCa_{0.8}Yb_{0.2}Cu_2O_{7-\delta}$ (y = 0) showed exclusively 1D–2D transition behavior. FTIR analyses indicated the possible tilting of oxygen atoms in the CuO_2 plane as a result of unequal bond lengths of Pb–O_A–Cu(2) and Tl–O_A–Cu(2) and enhanced CuO_2 inter-plane coupling. Superconductivity in both series is suggested to be due to some form of interplay between the effect of increased inter-plane coupling on ξ_c (0) and hole's concentration in CuO_2 planes.

Najmul Hassan et al [9] studied $Cu_{0.5}Tl_{0.5}Ba_2Ca_{0.5}M_{1.5}Cu_{1.5}Ni_{1.5}O_{10-\delta}$ (M= Mg, Be) superconductor. The samples were prepared by solid-state reaction method. The structure and physical properties were investigated by powder X-ray diffraction (XRD), resistivity, ac-susceptibility and Fourier Transform Infrared absorption Spectroscopy (FTIR). The X-ray diffraction showed that c-axis length is decreased with substitution of Mg or Be at the calcium site, which was suggested by these authors to be arising from small ionic size of the doped atoms. Electrical resistivity and ac-susceptibility measurements showed that the T_c(R = 0) values increase for the sample with M=Mg and got even higher values for M= Be, as the level of doping increases from 0.0 to 1.5. It was most likely arising from the improved inter-plane coupling promoted by more electronegative atoms of Mg and Be substituted at the Ca sites. In FTIR absorption measurements, the phonon modes related to apical oxygen atoms shifted towards lower wave number confirming that inter-plane coupling has improved. The increase in (T_c) magnitude of diamagnetism, as suggested by these authors, to be arising from the lowering in the anisotropy and increase in the coherence length of the final compound. They found that after post annealing, the magnitude of diamagnetic signal is enhanced for un-doped sample whereas it is suppressed for Mg and Be-doped samples. The

optimization of the carriers in the conducting plane is most likely reason for such behavior.

S. K. Agarwal et al [10] synthesized $CuBa_2Ca_3Cu_4O_{12-\delta}$ (Cu-1234) superconductors with 5%, 10%, 20%, and 33% Mg doping at the Ca sites in gold capsules under 3.5 GPa pressure and at about 1000°C temperature using a cubic anvil-type high-pressure machine . The samples were characterized through X-ray diffractometry, resistivity, dc susceptibility, and Hall effects measurements. Both *a*- and *c*-axis lattice parameters were found to decrease with Mg incorporation. Holes concentration n_H as determined through Hall measurements was found to decreases from 0.5 to 0.34 per CuO_2 layer for the highest doped sample. The superconducting anisotropy γ was determined by the ratio of upper critical field measurements (through magnetization in H // ab and H // c) in the *c*-axis aligned samples and was found to be least among such families of HTSC's. Such a situation of low superconducting anisotropy might be due to the Mg doping in the charge reservoir blocks that causes hole concentration to lower down which in turn decreased the spacing among the inter-superconducting $Ca_3Cu_4O_8$ block, causing the c parameter to reduced, eventually reducing the anisotropy in these materials.

P. Kameli et al [11] studied the effect of Mg substitution in place of Ca on the inter-granular properties of $Bi_{1.66}Pb_{0.34}Sr_2Ca_{2-x}Mg_xCu_3O_y$ (x = 0, 0.2 and 0.4) samples using the AC susceptibility technique. The samples were prepared by conventional solid state reaction method. They observed that Mg substitution in place of Ca reduces the inter-granular coupling of Bi-2223 system. The temperature dependence of the AC susceptibility near the transition temperature (T_c) has been done employing Bean's Critical State Model. The observed variation of inter-granular critical current densities (J_c) with temperature indicated that this critical current density decreases by increasing the amount of Mg. It was investigated that the higher electro-negativity of Mg in the unit cell promotes more intake of oxygen in the material, and the grain boundaries are in more over-doped regime. These over-doped regions caused the inter-granular coupling to reduce and increases weak link behavior of Mg doped samples. Post-annealing in oxygen improved the weak link network at grain boundaries that caused inter-granular critical current density to decrease.

R. Awad et al [12] prepared superconductor samples of the type $Tl_2Ba_2Ca_2Cu_{3-x}Zn_xO_{10-\delta}$ with x ranging from 0 to 0.6 by a solid-state reaction technique. The samples were characterized by using X-ray powder diffraction, scanning electron microscope (SEM) and EDX. The variation transition temperature versus Zn-content showed a suppression in its value and this suppression was attributed to the reduction of oxygen-content when Cu ions is replaced by Zn ions. They investigated that there is no separation between the intergrain and the dissipative intra-grain transition in the AC-magnetic susceptibility. This observation indicated good electrical contacts between the superconducting grains. It was observed that critical current density as well as the reversibility field increases as the Zn content increases till x = 0.1 and then decreases. The critical exponent n, determined from critical current density, was found to be equal to 2, indicating that the intergrain junctions are of the SNS type. The values of the exponent q, determined from irreversibility field, are close to 4, indicating a two dimensional pancake of Tl-2223 phase.

F. Foong et al [13] successfully fabricated thin films with mostly $(Hg, Tl)_1Ba_2Ca_2Cu_3O_{8+\delta}$ [(Hg, Tl)-1223] phase by radio frequency magnetron sputtering of precursor films and post-annealing method. Superconducting films with more then 80% (Hg, Tl)-1223 phase was determined by X- ray diffraction patterns. They observed that doping of a small amount of thallium in the film is helpful to the formation of the three-layer CuO_2 compound. It was observed that these films have a highly oriented structure with the *c*-axis perpendicular to the surface of the film, and the grains are connected very well, thus showing a low resistivity of the normal state. Resistivity measurements showed that the films after annealing at 300°C for 1h in O_2 have the superconducting transition temperature of T_c(onset)=133K and T_c(zero)=127K. Scanning electron micrographs of the film revealed plate-like micrometer-size grains coalesce to cover the substrate surface.

Nawazish A. Khan et al [14] prepared superconducting samples of the type $Cu_{0.5}Tl_{0.5}Ba_2Ca_{2-y}Mg_yCu_3O_{10-\delta}$ (y=0, 0.5, 1.0, and 1.5) at normal pressure using the simple solid state reaction method. The prepared samples were characterized by powder X- ray diffraction. The superconductivity of these samples was investigated by electrical resistivity and a.c magnetic susceptibility. The phonon modes of the

samples were identified by Fourier transform infrared (FTIR) absorption measurements. They investigated that material has tetragonal structure and its zero resistivity critical temperature increases with the increase of Mg concentration. The inter-plane coupling was enhanced with the increased Mg concentration; this was manifested in the decrease of c-axis length. The softening of apical oxygen modes provided another evidence of improved inter-plane coupling. The improved inter-plane coupling in their studies was found to enhance the critical current density by two orders of magnitude.

X. S. Wu et al [15] studied $La_{1.85}St_{0.15}Cu_{1-y}Mg_yO_4$ superconductor with $0.00 \leq y \leq 0.30$. The samples were prepared using solid state reaction method. The resistivity of each sample at room temperature was measured by standard four probe method and it was observed that the relation between resistivity and doped Mg content at room temperature was linear for $y \leq 0.10$ and non linear for $y \geq 0.1$, suggesting that impurity scattering mechanism is valid only in the low doping level ($y \leq 0.10$) for Mg doped LSCO. No phase transition was detected by X-ray diffraction (XRD) measurements. All samples were found to have tetragonal symmetry with the space group I4/mmm. The bond distance between two apical oxygen atoms in the CuO_6 octahedra was found to increase with y as $y \leq 0.10$ and decreases with the y as $y \geq 0.1$. It was concluded that structural variation due to Mg doping may vary the carrier distribution, which affects the superconductivity and other physical properties.

A. Iyo et al [16] studied the high pressure synthesis of $TlBa_2Ca_{n-1}Cu_nO_y$ (n=3 and n=4) superconductors. They studied X-ray diffraction, composition analysis and susceptibility measurements of the samples. It was observed in their study that there are a lot of conditions which can improve the transition temperature of Tl-1223 superconductor. The higher pressure condition was found to be very effective to improve critical transition temperature. The inadvertent inclusion of carbon, being incorporated in the samples from the starting compound, was also studied. They observed that there was no definite information on position and quantity of carbon in the lattice of Tl-1223 system. Residual carbon would enter into thallium site which reduces hole's concentration in CuO_2 planes and disturb the formation of ideal composition. The lower Tl contents were also found to be

effective in enhancing the T_c of Tl-1234 system. They also found that lower thallium contents are effective to increase T_c due to suppression of substitution of Tl for Ba and Ca sites. They found in their study that maximum transition temperature for $TlBa_2Ca_{n-1}Cu_nO_y$ is around 133.5K for n=3 and 127K for n=4 in this system. These authors found that transition temperature of Tl-1223 and Tl-1234 system is comparable with those of Hg-1223 system. Hg-1223 system has Tc >130K because Hg did not substitute for Ba and Ca sites while in Tl-1223; Tl partially substitutes the Ba and Ca sites. They found that substitution of Tl at Ba and Ca sites is significantly suppressed under high pressure with low residual carbon concentration. They found that thallium content, synthesis temperature and residual carbon concentration play a significant role in enhancing the transition temperature and overall superconducting properties of the samples. In order to suppress the substitution of Tl, samples must be prepared under high pressure using precursor with low residual carbon concentration in the starting compounds.

M. Roumie et al [17] prepared $TlBa_2Ca_{2-x}Sc_xCu_3O_{9-x}$ superconductor ($0 \leq x \leq 0.6$) by solid state reaction technique. They determined the satoichiometery of the samples by combining particle induced X-ray emission (PIXE) with Rutherford backscattering spectrometry (RBS). However, the oxygen content was obtained by using non-Rutherford backscattering cross-section at 3 MeV proton beam. Furthermore, the prepared samples were also characterized using X-ray powder diffraction (XRD) and electrical resistivity measurements. The elemental composition obtained from PIXE of Ba, Ca, Sc and Cu was nearly close to the starting values, while thallium composition was found to be lowered then starting composition value because thallium is a very volatile. During the preparation some of the thallium may be evaporated and some of it may be deposited on the silver wrap. The Ca content was decreased when Sc content was increasing except for the particular sample of Sc-0.1. The Sc/Ca ratio showed an increasing trend as Sc-content is increased. The oxygen stoichiometry obtained by non-Rutherford back scattering was very close to nominal value. Their X-ray diffraction data indicated that the partial substitution of Ca^{2+} by Sc^{3+} ions does not affect the tetragonal structure of Tl-1223 superconducting phase whereas the lattice parameter c contracts with the increase of Sc-content. The superconducting transition

temperatures (T_c), determined from electrical resistivity is suppressed as Sc-content increases. Cooper pair breaking was suggested to be one of the possible reasons that suppress T_c and it was also suggested that the hole-filling mechanism plays an important role for the suppression of T_c.

Nawazish A. Khan et al [18] synthesized $Cu_{0.5}Tl_{0.5}Ba_2Ca_{2-y}Mg_yCu_3O_{10-\delta}$ (y = 0, 0.05, 0.1, 0.2, 0.4, 0.6, 0.8, 1.0, 1.5, 2.0) superconductor at the atmospheric pressure by the solid state reaction method. The prepared samples were characterized by powder X-ray diffraction and the superconductivity of these samples was investigated by electrical resistivity and ac magnetic susceptibility. Oxygen-related phonon modes of the material were determined by FTIR absorption measurements. It was found that the Mg doped material grows in tetragonal structure and follows P4/mmm symmetry with a & *c*-axes lengths of 3.894 Å & 15.091 Å for y = 1.5. The axes lengths were found to decrease with the increase of Mg content in the unit cell, which shows that anisotropy of the material decreases. The zero resistivity critical temperature was found to increase to 98K with Mg concentration of y = 0.6, but saturates to 97K with further enhancement of Mg to y = 0.8, 1.0, and 1.5. The critical current density and the quantity of diamagnetism in the samples with Mg contents were higher than in the samples without Mg. The apical oxygen mode of the type Tl-OA-Cu (2) was softened to 459 cm^{-1} with the increased concentration of Mg (y = 2) in the unit cell. They suggested that the possible reason for the softening of this apical oxygen mode is better inter-plane coordination. The more electronegative Mg possibly shifted the electronic charge cloud of planar Cu(2) atoms more towards Mg atoms; the bond lengths between CuO2 planes is decreased, while the bond lengths of apical oxygen modes slightly increases.

L Raffott et al [19] studied the superconducting properties of $YBa_2(Cu_{1-x}Mg_x)_3 O_{7-\delta}$ ($0 \leq x \leq 0.1$) and $La_{1.85}Sr_{0.15}(Cu_{1-x}Mg_x)O_4$ ($0 \leq x \leq 0.07$). The samples were prepared by solid state reaction. Mg solubility limit less than about 2.5% was suggested for the YBCO structure, in contrast to previous determinations, while in the case of LASCO up to x = 7% no impurity phase was observed-in XRD experiments. These authors observed a contraction of the crystallographic unit cell along the c-axis for both systems and attributed to a

reduction in the local Jahn-Teller distortion of the oxygen octahedron around Cu^{2+}. It was observed in both systems that an increase of the dopant content induces a contraction of the crystallographic c-axis and a reduction of the critical temperature T_c, with effects very similar to those observed in Zn-doped samples. An onset temperature of 79K was found for YBCO at the maximum Mg solubility ($x \approx 0.025$). In LASCO superconductivity was suppressed at $x = 0.03$**.** Their results supported the hypothesis that the detrimental effects on superconductivity of all non-magnetic dopants are similar, and are linked to the formation of a net magnetic moment in the CuO_2 plane. An estimation of the inter-granular shielding current density J_s(T, U**)** was also presented. It was observed that Mg substitution affects the temperature dependence of J_s but it does not change the variation induced by the application of an external DC magnetic field.

G. Subramanyam et al [20] prepared nearly single phase $Tl_2Ba_2Ca_1Cu_2O_8$ (2212) and $(Tl_{0.5}Pb_{0.5})Sr_{2-x}Ba_xCa_2Cu_3O_9$) (1223) superconductors. They also identified the processing conditions to synthesize nearly single phase $Tl_2Ba_2Ca_1Cu_2O_8$ (2212) and $(Tl_{0.5}Pb_{0.5})Sr_{2-x}Ba_xCa_2Cu_3O_9$) (1223) superconductors. The samples were characterized by powder X- ray diffraction (XRD). Magnetization measurements were taken using either a vibrating sample magnetometer (VSM) or ac susceptibility measurements. They observed that the growth of single phase (2212) superconductor can be achieved in two step heat treatment process. They also found that growth of single phase 1223 superconductor is possible only with finite Ba content of $x \geq 0.4$. The highest T_c(onset) of 117K was achieved at $x = 0.75$ with superconducting volume fraction over 50%. The optimum processing conditions for the final heat treatment were 870ºC for 11 min inside the Pt crucible, with 50% excess Tl_2O_3 and PbO. They suggested that the present results obtained are significant for the processing of thin films of $(Tl_{0.5}Pb_{0.5})\ Sr_{1.25}\ Ba_{0.75}Ca_2Cu_3O_x$ 1223 superconductor.

2.2. References

[1]. S Isber, R Awad, A. IAbou-Aly, M Tabbal and J M Kaouar, Supercond. Sci. Technol. **18**, 311 (2005).

[2]. R. Awad, A. I. Abou-Aly, S. Isber and W. Malaeb, Journal of Physics: Conference Series **43**, 474 (2006).

[3]. M Eder and G Gritzner, Supercond. Sci. Technol. **13**, 1302 (2000).

[4]. Ren Yanru, Liu Hanpeng, Lin Mingzhu, Tu Qingyun, Sang Lihua, Lin Zhenjin and Meng Xianren, Physica C **156,** 799(1998).

[5]. N.M. Hamdan, Kh.A. Ziq, A.S. Al-Harthi, Physica C **314**, 125(1999).

[6]. S Mikusua, G Watanabea, K Tokiwaa, Y Tanakab, A Iyob, and T Watanabea, Journal of Physics: Conference Series **150**, 052161 (2009).

[7]. A. I. Abou- Aly, I. H. Ibrahim, R. Awad, Journal of Material Science **35**, 2893 (2000).

[8]. Nurul H. Ahmad, Nawazish A. Khan, A.K. Yahya, Journal of Alloys and Compounds **492**, 473 (2010).

[9]. Najmul Hassan, Nawazish A. Khan, Materials Chemistry and Physics **112**,412 (2008).

[10]. S. K. Agarwal, A. Iyo, K. Tokiwa, Y. Tanaka, K. Tanaka, M. Tokumoto, N. Terada, T. Saya, M. Umeda, and H. Ihara, Physical Review B. Volume **58**, number 14(1998).

[11]. P. Kameli , H. Salamati, I. Abdolhosseini, Journal of Alloys and Compounds **458**, 61(2008).

[12]. R. Awad , A.I. Abou-Aly , I.H. Ibrahim , M. El-Korek , S. Isber , A. Faraj, Journal of Alloys and Compounds **460**, 500(2008).

[13]. F. Foong, B. Bedard, Q. L. Xu,a) and S. H. Liou, Appl. Phys. Lett. **68,** 1153(1996)

[14]. Nawazish A. Khana, and A. A. Khurram, Applied Physics Letters **86**, 152502 (2005).

[15]. X.S. Wu, Z.Q. Mao, J. Lin, W.M Chen, X. Jin, Xu, Y. H. Zhang, F. M. Pan, S.S. Jiang, Physica C **282-287,** 787 (1997).

[16]. A. Iayo, Y. Aizawa, Y. Tanaka, M. Tokiwa, T. Watanabe and H. Ihara, Physica C

357, 324(2001).

[17]. M. Roumie´, R. Awad, I.H. Ibrahim, A. Zein, K. Zahraman and B. Nsouli, Nuclear Instruments and Methods in Physics Research B **266**, 133 (2008).

[18]. Nawazish A. Khan · A.A. Khurram · Mushtaq Ahmed, J Supercond Nov Magn **20**, 343 (2007).

[19]. L Raffott, R Caciuffoi, D Rinaldit and F Liccit, Supercond. Sci. Technol. **8**, 409 (1995).

[20]. G. Subramanyam, Z. Ju, M. Fahmy, P. M. Shand, M. Zhang and P. Boolchand, Applied Superconductivity Vol. **4**, No. 12, 591 (1996).

Chapter 3

Experimental Techniques

3.1. Synthesis of Tl-based high T_c superconductive oxides

Chemical purity of the starting material is still a topical issue for a reproducible preparation of cuprate high temperature superconductors (HTS). The use of chemicals with a purity of 99.99% and better is mandatory but still not sufficient. During the preparation procedure, the formation of even a small amount of liquid has to be carefully avoided since this may corrode the substrate or crucible and may thus introduce impurities into the sample. Some of these reaction products have turned out to be well suited as materials for corrosion resistant crucibles for the preparation of cuprate HTS. The plethora of preparation degrees of freedom, the inherent tendency towards in-homogeneities and defects, in combination with the very short superconductor coherence length of the order of the dimensions of the crystallographic unit cell did not allow easy progress in the preparation of these materials [1].

The ability to synthesize powders of high phase purity is essential to many basic studies and practical applications of high T_c superconductors. From the J_c (critical current density) point of view, the presence of impurity phases among superconductive grains impedes the transport of the electrical current, resulting in a low J_c has been thought to increase the flux pinning, the preparation processes in general employ single phase superconductive powders as starting material and only subsequently, by following a well defined heating procedure, dies one generate the desired secondary phases in a controlled manner.

One of the problems with the high T_c related materials is that they are mechanically hard. Experimentally, the materials are very difficult to work with. They are brittle transition metal oxides that are highly anisotropic. Making reliable electrical contacts to them can be difficult. It has now become clear that high purity single crystals are essential in order to obtain reliable, repeatable measurements. Their surfaces are also complicated: when they cleave, they do so between interstitial layers, and so tunneling experiments are never directly into the CuO plane [1].

Like the other high T_c superconductors oxides, the Tl based superconductive oxides have most commonly been prepared by the solid state reaction method. Subsequently, methods have been developed to avoid the use of off-stoichiometry starting compositions, and many successful results have been reported [2-7]. Basically these methods synthesize the desired superconductive phase either in a single step or through a series of calcinations steps with well defined intermediate compounds formed after each calcinations. Until now, with proper selection of calcinations conditions, Tl based superconductive powders of high phase purity could be synthesized in short calcinations times without resorting to complicated wet processes [8].

3.2. Sample preparation

The $Tl(Ba_{2-x}Mg_x)(Ca_{2-y}Be_y)Cu_3O_{10-\delta}$ (y=0,1; x=0, 0.25, 0.5, 0.75, 1.0, 1.25, 1.50, 1.75) samples were prepared by the solid state reaction method accomplished in two stages. At the first stage $(Ba_{2-x}Mg_x)Ca_{2-y}Be_y)Cu_3O_{10-\delta}$ (y=0,1; x=0, 0.25, 0.5, 0.75, 1.0, 1.25, 1.50, 1.75) precursor material was prepared, by thoroughly mixing $Ba(NO_3)_2$, $Ca(NO_3)_2$, MgO/BeO and Cu(CN) in a quartz mortar and pestle in appropriate ratios. The mixed material was fired twice at 860^{o}C in a quartz boat for 24 hours and furnace cooled to room temperature. At the second stage, the precursor material was ground for about an hour and mixed with Tl_2O_3 to give $Tl(Ba_{2-x}Mg_x)Ca_{2-y}Be_y)Cu_3O_{10-\delta}$ (y=0,1; x=0, 0.25, 0.5, 0.75, 1.0, 1.25, 1.50, 1.75) as final reactants composition. Thallium mixed material was palletized under 3.8 tons/cm^2 and the pellets were enclosed in a gold capsule. Gold capsule containing pellets was annealed for about 10 minutes at 860^{o}C followed by quenching to room temperature.

3.2.1. Post-annealing of the samples

In oxide superconductors oxygen concentration in the unit cell plays a vital role; as it can modify the distribution of the carriers in various bands of compound. The electronic distribution ultimately controls the mechanism of superconductivity. Oxygen intercalation in the unit cell of oxide superconductor has a temperature window between 400-650^{o}C. Therefore, we have carried out post-annealing of $Tl(Ba_{2-x}Mg_x)(Ca_{2-y}Be_y)Cu_3O_{10-\delta}$ (y=0,1; x=0, 0.25, 0.5, 0.75, 1.0, 1.25, 1.50, 1.75)

superconductors at 550^{o}C for such oxygen intercalation. This is done by loading the samples into a preheated tubular furnace at 550^{o}C followed by furnace cooling the samples to room temperature after the heat treatment.

3.3. Characterization

The samples were characterized by the following techniques:

- X-ray diffraction
- Resistivity measurements
- AC susceptibility measurements
- Fourier Transform Infrared (FTIR) Spectroscopy

In this section a brief theoretical background and the description of the experimental setup for above mentioned characterization techniques will be given.

3.3.1. X- ray Diffraction

XRD (X-ray diffraction) analysis gives us the information about the crystal structure of the material. This technique is used to know whether the intended sample has the crystalline structure or not and also to know the lattice cell parameters. The most important aspect in materials science is the study of crystal structure of material. The crystal structure determination is an important parameter. In the beginning years of the field of materials science it was assumed that the solids are made of atoms, which are periodically arranged, but there were no experimental evidences of this thought. The discovery of X-ray made it possible to probe the material for their structure determination. The wavelength of X-rays (0.5Å-2.5Å) is comparable to the spacing between the atomic planes in solids. The X-rays, which originate from the K shell transitions, are used for the diffraction analysis because these are shorter wavelength as compared to the one coming from L or M shell transition. The commonly used target materials in X-ray tubes are Cu and Mo. These two target material produce X-rays with wavelengths 1.54Å and 0.8Å, respectively [9-10]. An incident X-ray beam on a material penetrates into it and the intensity in the direction of the reflected beam is determined by the periodicity of the atomic planes in the crystalline solid. The consideration of such an X-ray beam of wavelength ‘λ’ incident to a crystalline material at an angle ‘θ’ and diffracted also at the same angle is shown

in Fig.3.1. The inter-planer spacing of the material is equal to d. These rays will interfere constructively when the path difference between the rays is an integer multiple of the wavelength used. The path difference is

$AB + BC = n\lambda$

$AB = d\sin\theta$ and $BC = d\sin\theta$

$2d\sin\theta = n\lambda, \qquad n=0, 1, 2 \ldots\ldots \qquad (3.1)$

Where n is the order of diffraction. The above diffraction rule was given by W. L. Bragg and is known as Bragg's law. Only the X-rays that satisfied this law will give the diffraction pattern.

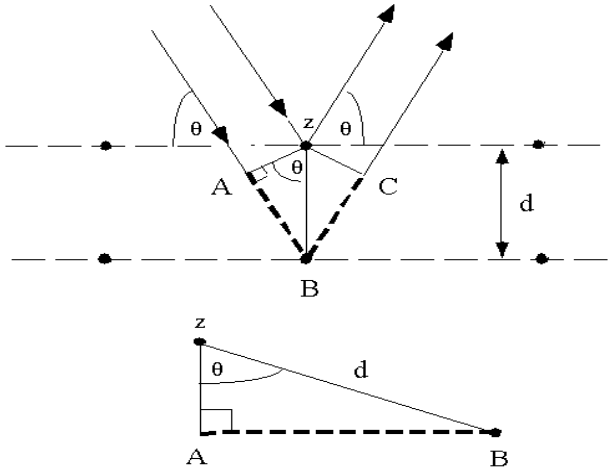

Fig. 3.1: Diffraction of X-rays from crystal planes.

The X-ray diffraction technique is also used to identify whether a material is a crystalline or amorphous. In crystalline solid many sharp crystalline peaks are observed due to periodic arrangement of atoms, but in the amorphous material there is no periodic structure and only one or two broad diffraction bands are observed. Through this technique we can also determine the size of the unit cell i.e. lattice parameters, atomic position and degree of crystallinity. X-ray diffraction studies of the crystal structure with different orientation of the planes take place by adopting one of the following methods.

3.3.1.1. Laue's Method

In the Laue's Technique a single crystal is held stationary and a beam of radiation is incident on it at a fixed angle θ, i.e. θ is fixed while wavelength λ is

varied. These different wavelengths select the appropriate reflecting planes out of the numerous present in the crystal such that the Bragg's condition is satisfied.

3.3.1.2. Rotating crystal method

In rotating crystal method a single crystal is held in the path of the monochromatic radiations and is rotated about an axis, λ is fixed while θ is varied. Different sets of parallel atomic planes are exposed to incident radiation for different values of θ and reflection takes place for those planes for which d and θ satisfied the Bragg's law.

3.3.1.3. Powdered diffraction method

In powder method a sample in the powdered form is placed in the path of monochromatic X-rays, i.e., λ is fixed while both θ and is vary. Thus a number of small crystallites with different orientations are exposed to X-rays. The reflections take place for those values of d, θ and λ which satisfied the Bragg's law. Superconducting sample is polycrystalline and the tiny crystals are randomly oriented so powder diffraction method is usually employed. A powder pattern is therefore, a reasonably complete display of the diffraction effects from a compound. The procedure to analyze the powder pattern of an unknown compound consists of measuring the diffraction angles, calculating the spacing of the reflecting planes and then deducing the dimensions of the unit cell. The schematic diagram of an X-ray diffractometer is shown in Figure. 3.2. Once the scattered peaks data is obtain then the data is analyzed for the determination of the crystal structure. The process proceeds in stages. The first step is to compare the location of the peaks or rings with those produced by the various known crystal structures and effort is made to identify the crystal structure. Next step is refinement procedure; varying locations of atoms and intensities of the species best fitting data is obtained. In our work we used computer software "Check cell" which when provided with peak data, identified the crystal structure and also provide lattice parameters.

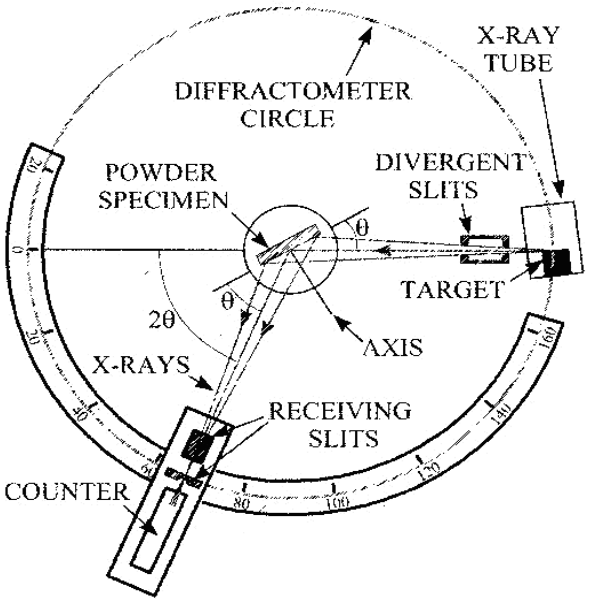

Fig. 3.2: Diffractometer

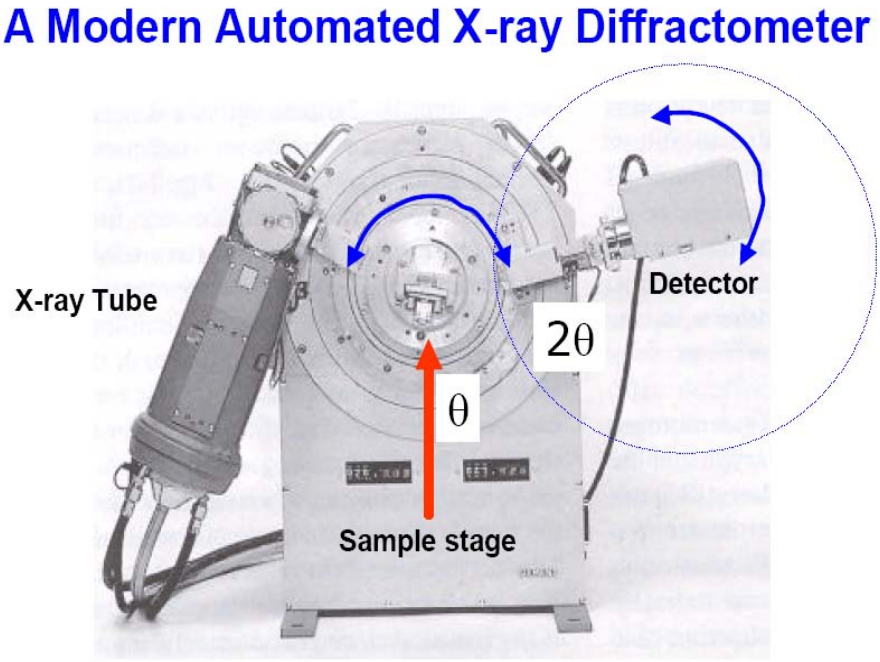

Fig. 3.3: A modern automated X-ray diffractometer.

3.3.2. Four probe method for resistivity

Ohm-meter measurements are normally made with just a two-point measurement method (one probe on each of the two resistor leads). However, when measuring very small resistances, in the milli- or micro-ohm range, the two-point method is not satisfactory because test contact resistance becomes a significant factor.

The lead resistance, due to long lead length, will affect the measurement results. The four-point resistance measurement method eliminates lead resistance or contact resistance [11].

One of the most striking features about the cuprate superconductors is the behavior of the resistivity of the normal state that is found above the transition temperature of the optimally doped materials. Before we look at the resistivity of the high T_c compounds, it will be instructive to first review the properties of the resistance of normal metals. In normal metals, the resistance takes on the form

$$\rho = \rho_{res} + AT^2 + \rho_{ph} \tag{3.2}$$

ρ_{res} is a temperature independent resistivity due to impurity scattering. The T^2 term arises due to electron-electron scattering. At a temperatures T, the density of final states will include scattering off of the empty quasi-particle states found within kT of the Fermi surface [12, 13]. This leads to the T^2 dependence, which we expect to see in systems with strong electron-electron scattering. The last term is the phonon contribution.

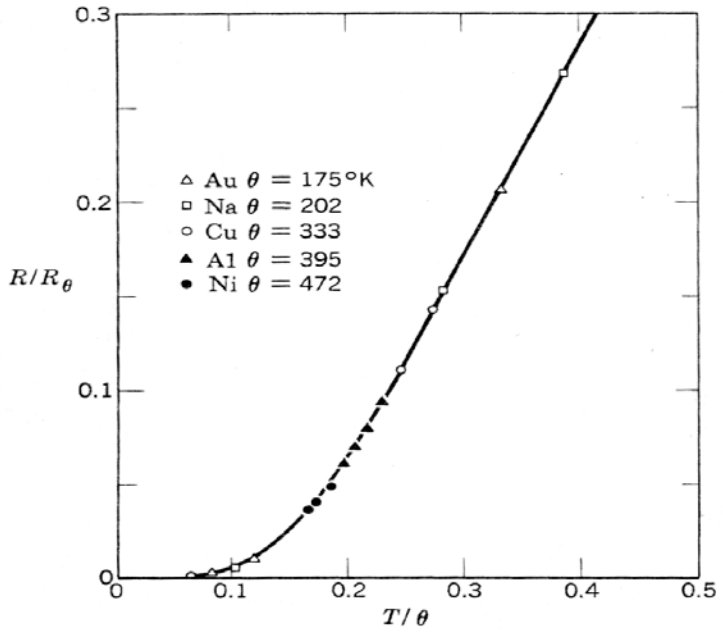

Fig. 3.4: The phonon contribution to the resistivity in normal metals. μ is the Debye temperature**.**

The temperature dependence of the phonon contribution is shown is Fig. 3.4**.** For $T < \mu_D$, there is a contribution $\rho_{ph} \alpha T^5$. The strong suppression at low temperatures is due to the low thermal occupation of the phonon modes and the fact that at low temperatures, phonon scattering is strongly peaked in the forward direction due to the presence of the Fermi surface. For temperatures $T > \mu_D$, the contribution is $\rho_{ph} \alpha T$, since the thermal occupation of the phonon modes is linear in T at high temperatures. Generally, it is found that non linear behavior begins around $T \alpha 0.3 \mu_D$, and becomes sub linear [14].

The resistance of any substance can be measured by using Ohm's law. The Ohm's law states that potential across a conductor is directly proportional to the current flowing through the conductor provided the temperature remains the same. So we can measure the resistance of a conductor if we can measure the current through it and potential across it, by using R = V/I

Where V is the voltage across the conductor, 'I' is the current flowing through the circuit and R is the resistance offered by the conductor to the moving electrons that constitute the current. Experiments have shown that the resistance of the conductor also depends upon the geometry of the conductor along with the temperature. The geometry independent measure of resistance is given by resistivity (ρ). If 'L' is the length of a certain conductor and 'A' is the area of cross section of it, then we can write that

$$R \quad \alpha \quad \frac{L}{A}$$

$$\Rightarrow \qquad R = \rho \frac{L}{A}$$

The resistivity of a material depends upon the temperature as discussed earlier. So the temperature dependent resistivity in terms of Ohm's law can be written as

$$\rho (T) = \frac{A}{L} R$$

$$\rho (T) = \frac{A}{L} \frac{V}{I} \qquad (3.3)$$

The SI unit of the resistivity is Ω-m. Resistivity of the superconducting materials is measured using the four-probe method. This method is used for measurements of resistivity in metals, semiconductors and superconductors around the world. Fig.3.5 shows the experimental arrangement for four-probe method. The wire contacts with samples were made by silver paste on the surface. The outer leads were used to supply current and the resulting voltage drop was measured across the middle contacts. A homemade cryostat is used for cooling the samples down to 77 K. The temperature of the samples is measured by copper-constantan thermocouple. These measurements were done using high resolution P-2000/E Kiethley multimetres.

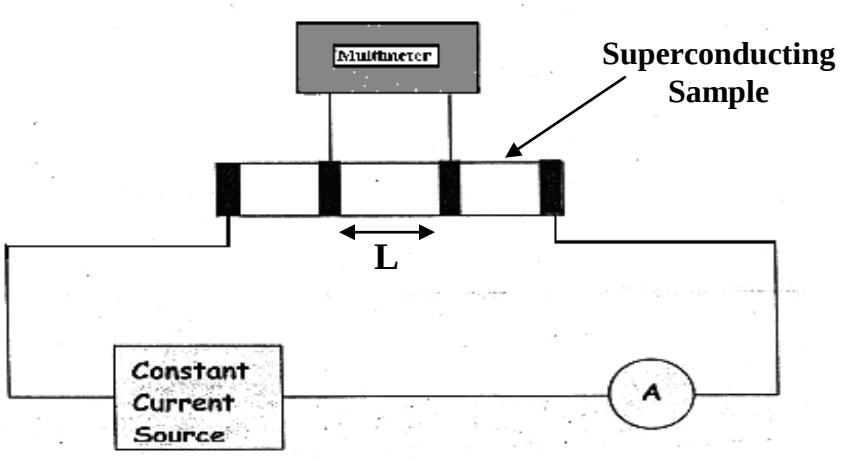

Fig. 3.5: Arrangement for resistivity measurements.

3.3.3. AC susceptibility

As superconductors have magnetic properties as interesting as their electrical properties, so a study of the magnetic properties is a key pre-requisite for characterization of any superconductor sample. Apart from other magnetic properties, diamagnetic behavior of a superconductor to applied magnetic field is very essential test of existence of superconductivity. AC susceptibility study not only provides the better measurement of T_c (critical temperature) but also other information like

magnitude of diamagnetism in the sample and weak link behavior of the samples. Therefore, we carried out the AC susceptibility studies of our samples.

In measuring AC magnetic susceptibility measurements one come across complex magnetic susceptibility. Actually in a periodically varying magnetic field of frequency ω susceptibility has in general two parts χ' and χ''; χ' is the part of χ in phase with applied magnetic field H where as χ'' is the part of χ out of phase with H by 90^0. The real part often called diamagnetic susceptibility and is equal to the derivative dM/dH, where as the imaginary part is related to the energy or hysteresis losses due to the magnetic field cycling [15]. We can represent χ' and χ'' with the diagram in time domain as shown in following Figure.3.6. The real and imaginary parts of ac susceptibility $(\chi' + i\chi'')$ represent two complimentary aspects of magnetization and diamagnetic transition in polycrystalline (granular) superconductors.

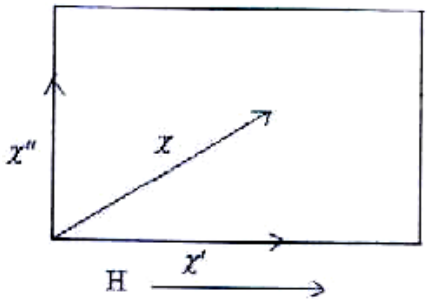

Fig. 3.6: Phase diagram of ac- susceptibility and applied ac field H in time Domain.

3.3.3.1. AC susceptibility measurement setup

AC susceptibility is generally measured by using inductive coils coupled to lock-in amplifier. A schematic diagram of ac susceptibility apparatus is shown in Figure 3.7.

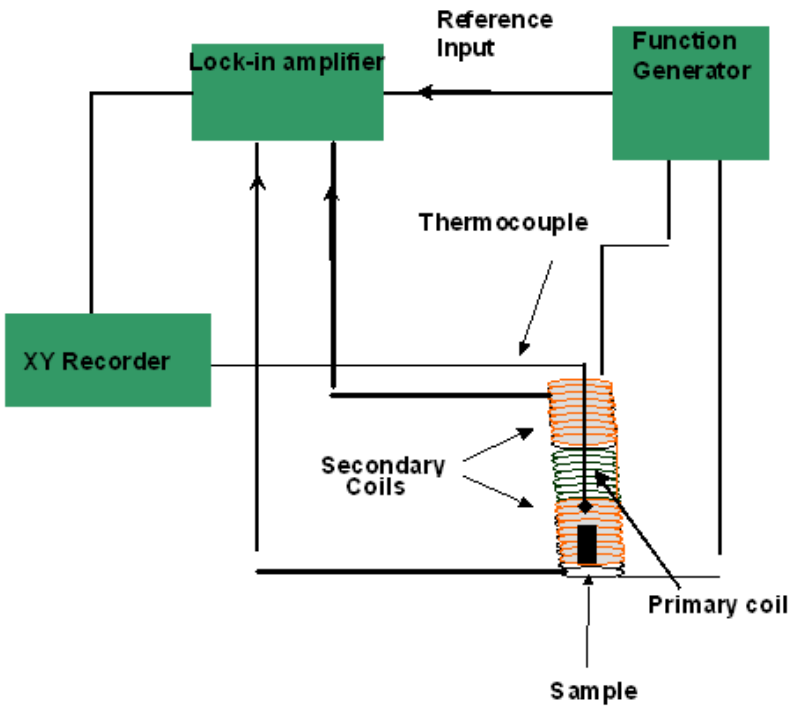

Fig. 3.7: Experimental setup for AC susceptibility measurements.

The measurements of the ac-susceptibility rely on the change in the mutual inductance of a set of two similar but oppositely wound coils. First of all an AC signal of 1volt and frequency of 270 Hz is given to the primary coil of the susceptometer and the signal from the secondary coil is fed to preamplifier. The weak signal is amplified and sent to lock-in amplifier. From here signal is displayed with the reference. This display on the lock-in amplifier gives the susceptibility measurements, which is plotted against the temperature and then these graphs are read to find out the magnitude of the susceptibility of sample. Experimentally, the susceptometer operates as a modified bridge network; a primary coil produces a small field directly proportional to the derivative of the magnetization of the sample, and the resulting induced emf in the secondary (pick-up) coil wound around the sample, which is analyzed as mention above.

3.3.4. Infrared Spectroscopy

Infrared (IR) spectroscopy is one of the most common spectroscopic techniques used by organic and inorganic chemists. Simply, it is the absorption measurement of different IR frequencies by a sample positioned in the path of an IR

beam. Infrared radiation spans a section of the electromagnetic spectrum having wave numbers from roughly 13,000 to 10 cm^{-1}, or wavelengths from 0.78 to 1000 μm. It is bound by the red end of the visible region at high frequencies and the microwave region at low frequencies. IR absorption positions are generally presented as either wave numbers (cm^{-1}) or wavelengths (λ). Wave number defines the number of waves per unit length. Thus, wave numbers are directly proportional to frequency, as well as the energy of the IR absorption. The wave number unit (cm^{-1}, reciprocal centimeter) is more commonly used in modern IR instruments that are linear in the cm^{-1} scale. In the contrast, wavelengths are inversely proportional to frequencies and their associated energy. At present, the recommended unit of wavelength is μm (micrometers). Wave numbers and wavelengths can be interconverted using the following equation:

$$\upsilon\ (cm^{-1}) = [1 / \lambda(\text{in } \mu m)] * 10^4 \qquad (3.4)$$

IR absorption information is generally presented in the form of a spectrum with wavelength or wave number as the x-axis and absorption intensity or percent transmittance on the y-axis. Transmittance, T, is the ratio of radiant power transmitted by the sample (I) to the radiant power incident on the sample (I_0). Absorbance (A) is the logarithm to the base 10 of the reciprocal of the transmittance (T).

$$A = \log_{10}(1/T) = -\log_{10}T = -\log_{10}I/I_0 \qquad (3.5)$$

The transmittance spectra provide better contrast between intensities of strong and weak bands because transmittance ranges from 0 to 100% T whereas absorbance ranges from infinity to zero.

3.3.4.1. Theory of Infrared Absorption

At temperatures above absolute zero, all the atoms in molecules are in continuous vibration with respect to each other. When the frequency of a specific vibration is equal to the frequency of the IR radiation directed on the molecule, the molecule absorbs the radiation. Each atom has three degrees of freedom, corresponding to motions along any of the three Cartesian coordinate axes (x, y, z). A polyatomic molecule of n atoms has 3n total degrees of freedom. However, 3 degrees of freedom are required to describe translation, the motion of the entire molecule through space. Additionally, 3 degrees of freedom correspond to rotation of the entire

molecule. Therefore, the remaining 3n – 6 degrees of freedom are true, fundamental vibrations for nonlinear molecules. Linear molecules possess 3n–5 fundamental vibrational modes because only 2 degrees of freedom are sufficient to describe rotation. Among the 3n–6 or 3n–5 fundamental vibrations (also known as normal modes of vibration), those that produce a net change in the dipole moment may result in an IR activity and those that give polarizability changes may give rise to Raman activity. Naturally, some vibrations can be both IR- and Raman-active.

The total number of observed absorption bands is generally different from the total number of fundamental vibrations. It is reduced because some modes are not IR active and a single frequency can cause more than one mode of motion to occur. Conversely, additional bands are generated by the appearance of overtones (integral multiples of the fundamental absorption frequencies), combinations of fundamental frequencies, difference of fundamental frequencies, coupling interactions of two fundamental absorption frequencies, and coupling interactions between fundamental vibrations and overtones or combination bands. The intensities of overtone, combination, and difference bands are less than those of the fundamental bands. The combination and blending of all the factors thus create a unique IR spectrum for each compound.

The major types of molecular vibrations are stretching and bending. Infrared radiation is absorbed and the associated energy is converted into these types of motions. The absorption involves discrete, quantized energy levels. However, the individual vibrational motion is usually accompanied by other rotational motions. These combinations lead to the absorption bands, not the discrete lines, commonly observed in the mid IR region.

3.3.4.2. Spectrometer Components

There are three basic spectrometer components in an FT system: radiation source, interferometer, and detector. A simplified optical layout of a typical FTIR spectrometer is illustrated in Figure.3.8. However, the source is more often water-cooled in FTIR instruments to provide better power and stability.

The most commonly used interferometer is a Michelson interferometer. It consists of three active components: a moving mirror, a fixed mirror, and a beam-splitter. The two mirrors are perpendicular to each other. The beam-splitter is a semi-

reflecting device and is often made by depositing a thin film of germanium onto a flat KBr substrate. Radiation from the broadband IR source is collimated and directed into the interferometer, and impinges on the beam-splitter. At the beam-splitter, half the IR beam is transmitted to the fixed mirror and the remaining half is reflected to the moving mirror. After the divided beams are reflected from the two mirrors, they are recombined at the beam-splitter. Due to changes in the relative position of the moving mirror to the fixed mirror, an interference pattern is generated. The resulting beam then passes through the sample and is eventually focused on the detector.

For an easier explanation, the detector response for a single-frequency component from the IR source is first considered. This simulates an idealized situation where the source is monochromatic, such as a laser source. As previously described, differences in the optical paths between the two split beams are created by varying the relative position of moving mirror to the fixed mirror. If the two arms of the interferometer are of equal length, the two split beams travel through the exact same path length. The two beams are totally in phase with each other; thus, they interfere constructively and lead to a maximum in the detector response. This position of the moving mirror is called the point of zero path difference (ZPD). When the moving mirror travels in either direction by the distance $\lambda/4$, the optical path (beam splitter–mirror–beam splitter) is changed by 2 ($\lambda/4$), or $\lambda/2$. The two beams are 180° out of phase with each other, and thus interfere destructively. As the moving mirror travels another $\lambda/4$, the optical path difference is now 2 ($\lambda/2$), or λ. The two beams are again in phase with each other and result in another constructive interference.

When the mirror is moved at a constant velocity, the intensity of radiation reaching the detector varies in a sinusoidal manner to produce the interferogram output. The interferogram is the record of the interference signal. It is actually a time domain spectrum and records the detector response changes versus time within the mirror scan. If the sample happens to absorb at this frequency, the amplitude of the sinusoidal wave is reduced by an amount proportional to the amount of sample in the beam.

The interferogram contains information over the entire IR region to which the detector has responded. A mathematical operation known as Fourier transformation

converts the interferogram (a time domain spectrum displaying intensity versus time within the mirror scan) to the final IR spectrum, which is the familiar frequency domain spectrum showing intensity versus frequency. This also explains how the term Fourier transform infrared spectrometry is created. The greatest amplitude occurs at the point of zero path difference (ZPD) [16].

3.3.4.3. Procedure

A typical operating procedure is described as follows:

- A background spectrum is first obtained by collecting an interferogram (raw data), followed by processing the data by Fourier transform conversion. This is a response curve of the spectrometer and takes account of the combined performance of source, interferometer, and detector. The background spectrum also includes the contribution from any ambient water (two irregular groups of lines at about 3600 cm^{-1} and about 1600 cm^{-1}) and carbon dioxide (doublet at 2360 cm^{-1} and sharp spike at 667 cm^{-1}) present in the optical bench.
- Next, a single-beam sample spectrum is collected. It contains absorption bands from the sample and the background (air or solvent).
- The ratio of the single-beam sample spectrum against the single beam background spectrum results in a “double-beam” spectrum of the sample.

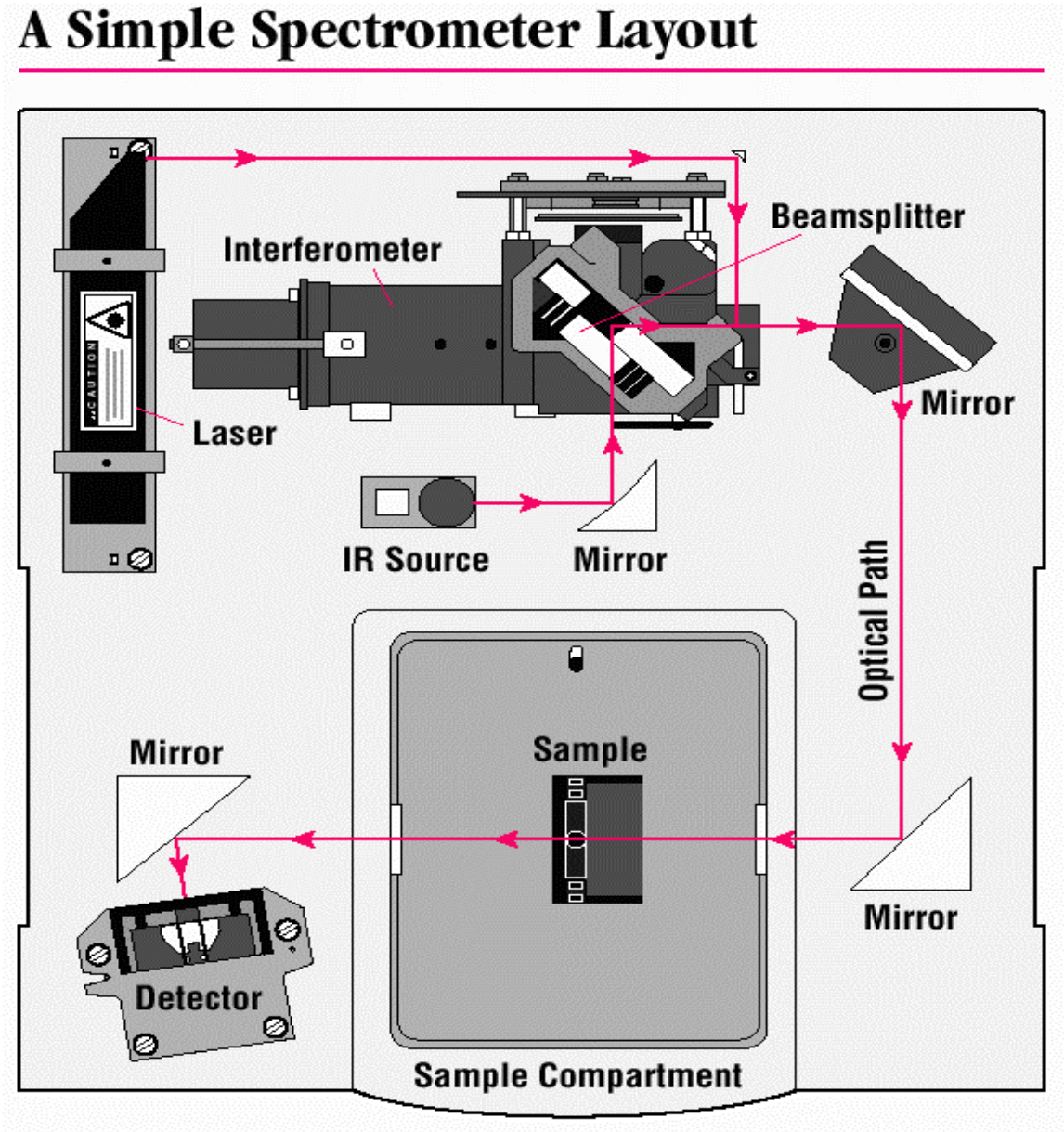

Figure 3.8: Simplified optical layout of a typical FTIR spectrometer.

Almost any solid, liquid or gas sample can be analyzed. Many sampling accessories are available. Solids 50 to 200 mg are desirable, but 10 μg ground with transparent matrix (such as KBr) is the minimum for qualitative determinations. Little or no preparation is required; may have to grind solid into KBr matrix. Estimated time to obtain spectrum from a routine sample varies from 1 to 10 min depending on

the type of instrument and the resolution required. Most samples can be prepared for infrared (IR) analysis in 1 to 5 minutes approximately [16].

To reduce the strong background absorption from water and carbon dioxide in the atmosphere, the optical bench is usually purged with an inert gas or with dry, carbon dioxide-scrubbed air (from a commercial purge gas generator). Spectrometer alignment, which includes optimization of the beam splitter angle, is recommended as part of a periodic maintenance or when a sample accessory is changed.

Copper oxide superconductors exhibit the highest critical temperature found so far. Since their discovery in 1986, the microscopic mechanism at the origin of their superconductivity is still unexplained [17]. While it is well established that in conventional superconductors the coupling between electrons and phonons (collective vibrations) leads to charge carrier pairing, and therefore superconductivity, the role of this coupling in copper-oxide superconducting compounds is still the subject of intense research efforts. There is a strong coupling between the lattice vibrations and the charge carriers, as the conduction in the copper oxide superconductors takes place by charge hopping along the Cu-O bond in the CuO_2 planes. Within this framework, the optical phonon anomaly is expected to be ubiquitous, and therefore should also be observed in electron-doped copper oxide superconductors [18].

3.4. References

[1]. Allen M. Hermann, Thallium-Based High-Temperature Superconductors, Marcel Dekker, Inc. p 41 (1994)

[2]. C. C. Torardi et al, Science 240, 631 (1988)

[3]. N. L. Wu et al, Mater. Lett. 7, 169 (1988)

[4]. N. L. Wu et al, Jpn. J. Appl. Phys. 28, L1349 (1989)

[5]. N. L. Wu et al, Physica C 161, 302 (1989)

[6]. E. Ruckenstein and C. T. Cheung, J. Mater. Res**.** 4, 1116 (1989)

[7]. E. Ruckenstein and S. Narain, Mater. Lett**.** 8, 421 (1989)

[8]. N. P. Ong, R. J. Cava, Science 305, 52 (2004)

[9]. B. D. Cullity, Element of X-ray Diffraction, second edition, (Addision-Wesely Publishing company, Inc. London 1977.

[10]. M. Ali Omer, Elementary Solid State Physics, First Edition, Edition Wesely Publishing Company (1974)

[11]. N. Ashcroft, N. Mermin 1976 Solid State Physics (Orlando, FL: Saunders) 31pp346.

[12]. P. Nozieres 1964 Theory of Interacting Fermi Systems (New York, NY: Benjamin) pp92

[13]. C. Kittel 1976 Introduction to Solid State Physics (New York, NY: Wiley)

[14]. M. Okada, Supercond. Sci. Technol. 13, 29 (2000)

[15]. A. G. Mamalis and D. E. Manolakos, "Processing of High-Temperature Superconductors at High Strain Rates", Technomic Publishing Company, Lancaster, Pennsylvania, 2000

[16]. Handbook of Instrumental Techniques for Analytical Chemistry Chapter 15 C.-P. Sherman Hsu, Ph.D. Separation Sciences Research and Product Development Mallinckrodt, Inc. Mallinckrodt Baker Division 247

[17]. J. Orenstein and A. J. Millis, Science 288, 468 (2000)

[18]. L. Pintschovius et al., Physica B 185, 156 (1993)

Chapter 4

Results and Discussion

4.1. Introduction

The an-isotropy in low dimensional superconductors is defined as $\gamma = \rho_c/\rho_{ab} = H_{c\perp}/H_{c||} = \lambda_c/\lambda_{ab} = \xi_{ab}/\xi_c$ and the superconducting properties critically depend on lower values of it [1, 2]. In these low dimensional superconductors, there is an $MBa_2O_{4-\delta}$ (M=Tl, Bi, Cu, Hg, etc) charge reservoir layer and n CuO_2 conducting planes [3, 4]. In various superconducting compounds the charge reservoir layers are insulating, partial metallic or completely metallic. The final superconducting properties of a compound critically depend on the composition and the thickness of the charge reservoir layers. The intrinsic reason for higher anisotropy in these compounds originates from the impeded motion along the c-axis of the charge carriers since these carriers during their transport have to tunnel metallic/semi-metallic Josephson barriers which imparts additional resistivity to the final compounds. In previous studies we have decreased the an-isotropy of $TlBa_2Ca_2Cu_3O_{10-\delta}$ and $Cu_{0.5}Tl_{0.5}Ba_2Ca_2Cu_3O_{10-\delta}$ ($Cu_{0.5}Tl_{0.5}$-1223) superconductors by doping Be and Mg at the Ca sites in the unit cell [5, 6]. These smaller sized and higher electronegativity doped atoms (Be and Mg) have been found to increase the inter-plane coupling. In the present studies, we have decreased the thickness of the charge reservoir layer by doped Mg at the Ba sites in $TlBa_2Ca_2Cu_3O_{10-\delta}$ superconductors. In another batch of the samples we have also doped fixed amount of Be =1 at the Ca sites and then decreased the thickness of charge reservoir layer by doping Mg at the Ba sites. In these experiments, it is expected that the efficiency of the charge transfer mechanism of $TlBa_2O_{4-\delta}$ charge reservoir layer will be significantly enhanced. It is also expected that oxygen concentration in the final compound will be disrupted with the doping of Mg and Be. We have tried to adjust the optimum concentration of it by carrying out the post-annealing of the samples in oxygen atmosphere. The intercalation of O_δ oxygen atoms of the charge reservoir layer would control the carriers flow to the conducting planes employing higher electro-negativity of it [7]. Concentration of oxygen in the unit cell of

the final compound influences the phonon modes of oxygen atoms in the unit cell will be determined by FTIR absorption measurements [8].

In $TlBa_2Ca_2Cu_3O_{10-\delta}$ superconductors the three oxygen CuO_2 planes are not equivalent i.e. the outer planes (OP) are over-doped with carriers whereas the inner planes are under-doped with the carriers [2, 3]. The reason for the outer CuO_2 planes to be over-doped with the carriers is its immediate presence in the neighborhood of the charge reservoir layer whereas the inner planes are far away from the charge reservoir layer. The smaller density of the carrier in the IP promotes anti-ferromagnetic alignment of magnetic moments existing at the $3d^9$ Cu-sites in the CuO_2 planes. The Cu atoms in the CuO_2 planes accomplish their minimize energy through the anti-ferromagnetic alignment of their spins [9, 10]. These anti-ferromagnetism aligned inner-planes IP suppress the superconducting properties of the final compound [11, 12]. We have replenished this deficiency by doping Be at the Ca sites that is expected to increase the inter-CuO_2-plane coupling and the uniform distribution of the carriers in the IP and OP planes [13].

4.2. Results and Discussion

4.2.1. As-Prepared $Tl(Ba_{2-x}Mg_x)\ Ca_{2-y}\ Be_yCu_3O_{10-\delta}$ (y=0; x=0, 0.25, 0.5, 0.75, 1.0, 1.25, 1.50) samples.

4.2.1(a) Resistivity and AC-Susceptibility

The measurements of resistivity versus temperature of $Tl(Ba_{2-x}Mg_x)Ca_{2-y}\ Be_yCu_3O_{10-\delta}$ (y=0; x=0, 0.25, 0.5, 0.75, 1.0, 1.25, 1.50) samples are shown in Fig.4.1

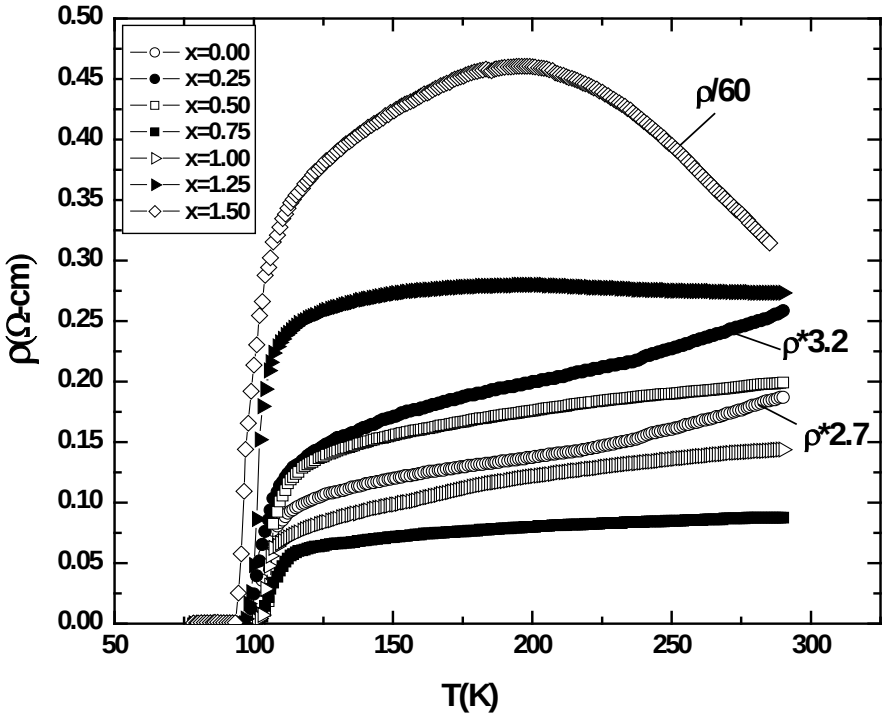

Fig. 4.1: Resistivity versus temperature measurements of as-prepared Tl $(Ba_{2-x}Mg_x)$ $(Ca_{2-y}Be_y)Cu_3O_{10-\delta}$ (y=0; x=0.0, 0.25, 0.5, 0.75, 1.0, 1.25, 1.5) samples.

Except for the samples with Mg-doping of 1.25, 1.5, most of the samples have metallic variations of resistivity from room temperature down to onset of superconductivity. These samples have shown room temperature resistivity from 0.069 to 0.273Ω-cm for the samples with Mg-doping of x=0, 0.25, 0.5, 0.75, 1.0, 1.25 and about 18.87Ω-cm for the sample with Mg-doping of 1.5.

These samples have shown onset of superconductivity around 107, 109, 112, 113, 109, 105K and zero resistivity critical temperature around 100, 98, 101, 102, 100, 96K, respectively, which are plotted as a function of Mg-doping concentration in figures 4.2 and 4.3.

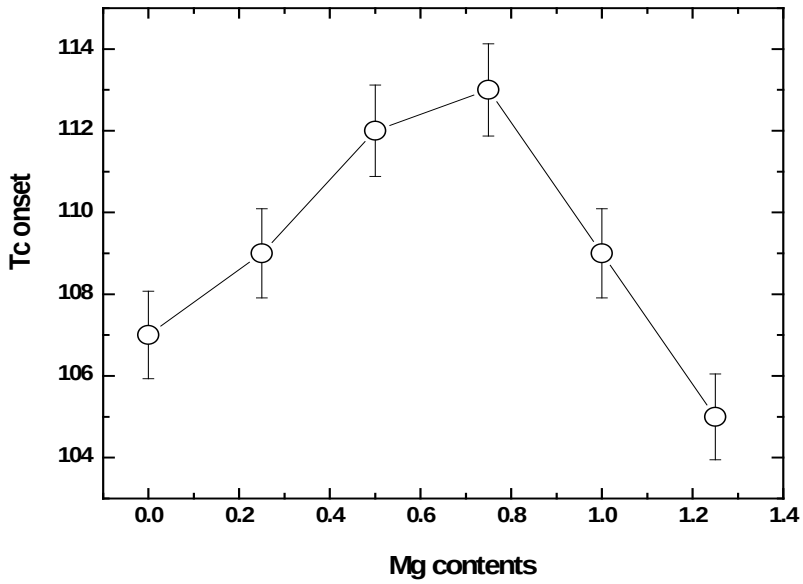

Fig. 4.2: Tc onset versus Mg contents measurements of as-prepared Tl $(Ba_{2-x}Mg_x)(Ca_{2-y}Be_y)Cu_3O_{10-\delta}$ (y=0; x=0.0, 0.25, 0.5, 0.75, 1.0, 1.25) samples.

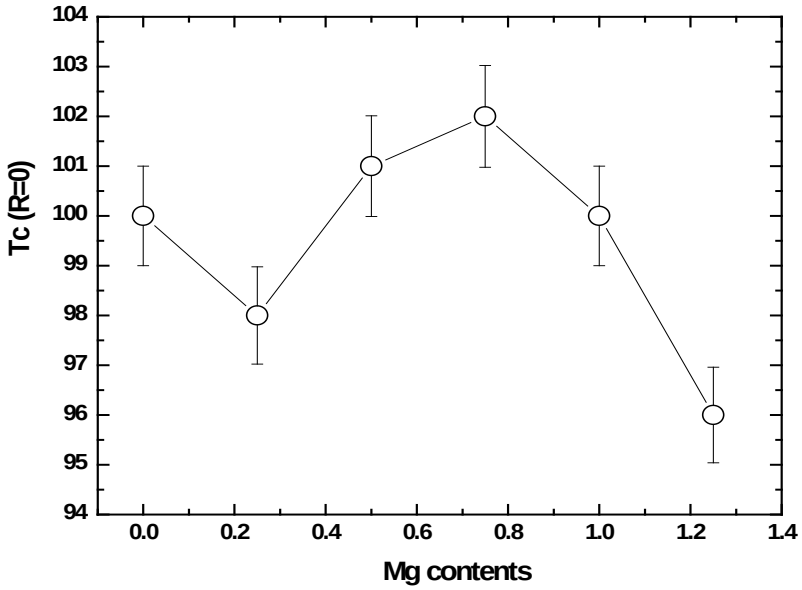

Fig. 4.3: Tc (R=0) versus Mg contents measurement of as-prepared $Tl(Ba_{2-x}Mg_x)(Ca_{2-y}Be_y)Cu_3O_{10-\delta}$ (y=0; x=0.0, 0.25, 0.5, 0.75, 1.0, 1.25) samples.

Ac-susceptibility measurements of $Tl(Ba_{2-x}Mg_x)(Ca_{2-y}Be_y)Cu_3O_{10-\delta}$ (y=0; x=0, 0.25, 0.5, 0.75, 1.0, 1.25) samples are shown in Fig.4.4

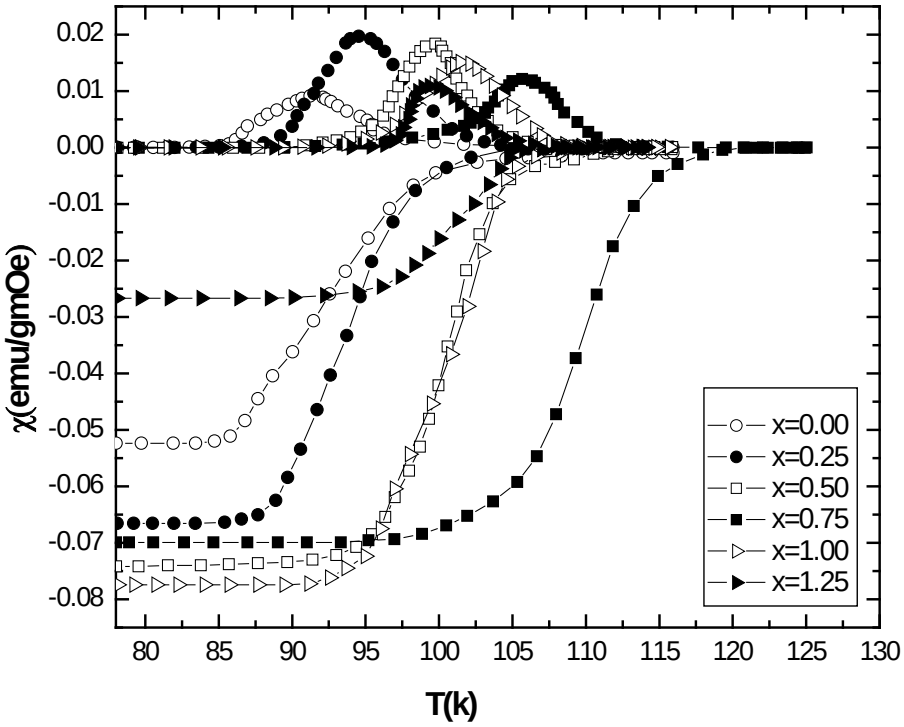

Fig. 4.4: The ac-susceptibility versus temperature measurements of as-prepared $Tl(Ba_{2-x}Mg_x)(Ca_{2-y}Be_y)Cu_3O_{10-\delta}$ (y=0; x=0.0, 0.25, 0.5, 0.75, 1.0, 1.25) samples.

The onset superconductivity except in the samples with Mg-doping of x=0.25, 1.25, is increased with the doping of Mg. Moreover, the magnitude of diamagnetism, except for Mg-doping of x=1.25, is increased with doping of Mg. The magnitude of diamagnetism as a function of increased Mg doping concentration is shown in Fig. 4.5.

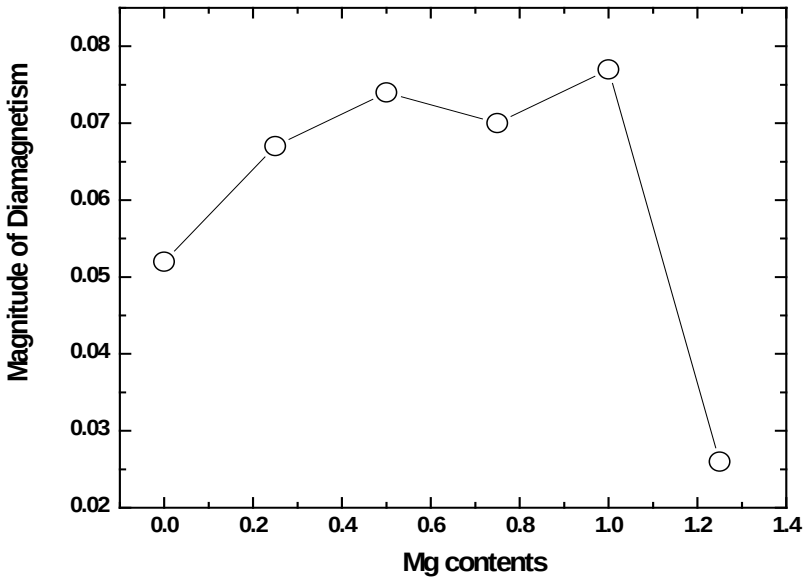

Fig. 4.5: Magnitude of diamagnetism versus Mg contents measurements of as- prepared $Tl(Ba_{2-x}Mg_x)(Ca_{2-y}Be_y)Cu_3O_{10-\delta}$ (y=0; x=0.0, 0.25, 0.5, 0.75, 1.0, 1.25) samples.

These samples have shown onset of superconductivity around 110, 106, 112, 120, 111 and 105K. It is most likely that the decreased thickness of the charge reservoir layers facilitate the easy charge reservoir layer possible promoting the enhancement in the density of the charge carriers in the conducting CuO_2 planes thereby increasing the magnitude of the superconductivity in Mg-doped compound.

4.2.1(b). X-ray diffraction and Infrared spectroscopy

X-ray diffraction scans of $Tl(Ba_{2-x}Mg_x)(Ca_{2-y}Be_y)Cu_3O_{10-\delta}$ (y=0; x=0, 0.25, 0.5, 0.75, 1.0, 1.25, 1.50) samples are shown in Fig.4.6(a, b). Most of the diffraction lines in these samples are fitted to the orthorhombic structure following PMMM space group. The c-axes length decreases up to Mg-doping of x=0.75 in $Tl(Ba_{2-x}Mg_x)Ca_2Cu_3O_{10-\delta}$ samples whereas it increases for Mg-doping beyond this doping level.

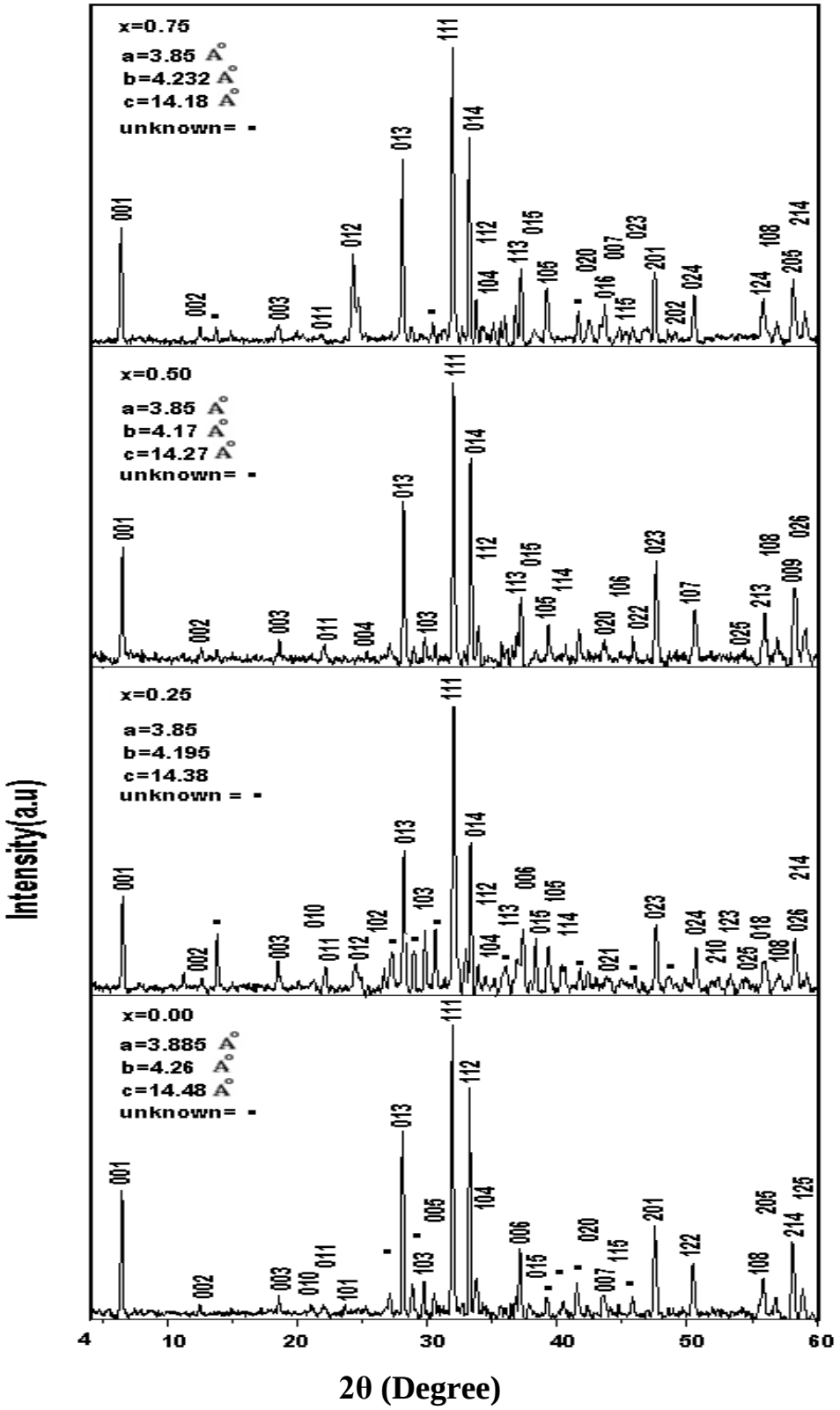

Fig. 4.6(a): X-ray Diffraction scans of $Tl(Ba_{2-x}Mg_x)(Ca_{2-y}Be_y)Cu_3O_{10-\delta}$ (y=0; x=0.0, 0.25, 0.5, 0.75) samples.

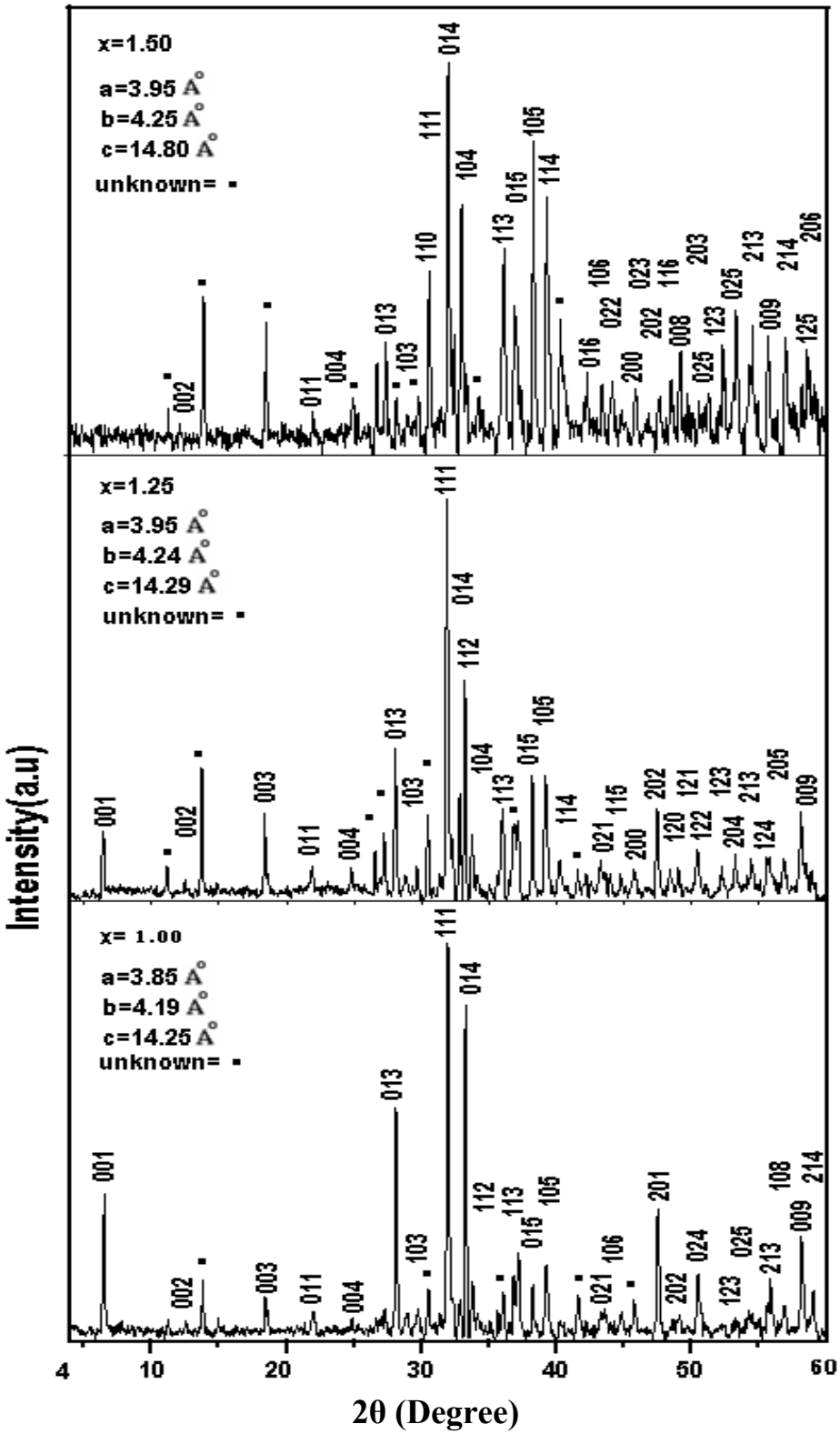

Fig. 4.6(b): X-ray Diffraction scans $Tl(Ba_{2-x}Mg_x)(Ca_{2-y}Be_y)Cu_3O_{10-\delta}$ (y=0; x=1.0, 1.25, 1.5) samples.

The FTIR absorption measurements of $Tl(Ba_{2-x}Mg_x)(Ca_{2-y}Be_y)Cu_3O_{10-\delta}$(y=0; x=0, 0.25, 0.5, 0.75, 1.0, 1.25, 1.50) samples are shown in Fig.4.7. In $Cu_{0.5}Tl_{0.5}Ba_2Ca_2Cu_3O_{10-\delta}$ samples, the modes of vibrations related to apical oxygen atoms are observed around 400-540cm^{-1}, due to CuO_2 planar oxygen atoms around 540-600cm^{-1} and that of O_δ atoms of $Cu_{0.5}Tl_{0.5}Ba_2O_{4-\delta}$ charge reservoir layer around 660-700cm^{-1} . In Mg un-doped $TlBa_2Ca_2Cu_3O_{10-\delta}$ samples single apical oxygen mode of the type Tl-O_A-Cu(2) is expected to be observed around 490cm^{-1}. In Mg free $TlBa_2Ca_2Cu_3O_{10-\delta}$ samples the apical oxygen mode of the type Tl-O_A-Cu(2) is observed around 473cm^{-1}. The CuO_2 planar oxygen mode is observed around 603cm^{-1} and O_δ mode of oxygen atoms of $TlBa_2O_{4-\delta}$ charge reservoir layer is peaked around 669-668cm^{-1}. The apical oxygen mode of the type Tl-O_A-Cu(2) for the Mg-doping of x=0.25, 0.5, 0.75, 1.0, 1.5 is observed around 472, 472, 472, 472, 473 and 473cm^{-1}, respectively. The CuO_2 planar oxygen mode in $Tl(Ba_{2-x}Mg_x)(Ca_{2-y}Be_y)Cu_3O_{10-\delta}$ (y=0; x=0, 0.25, 0.5, 0.75, 1.0, 1.25, 1.50) samples is observed around 605, 604, 613, 617, 616, 617cm^{-1}, respectively. Since the outer-planar oxygen (OP) atoms are connected with the $TlBa_2O_{4-\delta}$ charge reservoir layer, the doped Mg atoms suppress the thickness of the charge reservoir layer that would induce a decrease in the bond distances of outer planar oxygen atoms, consequently resulting into hardening of planar oxygen atoms.

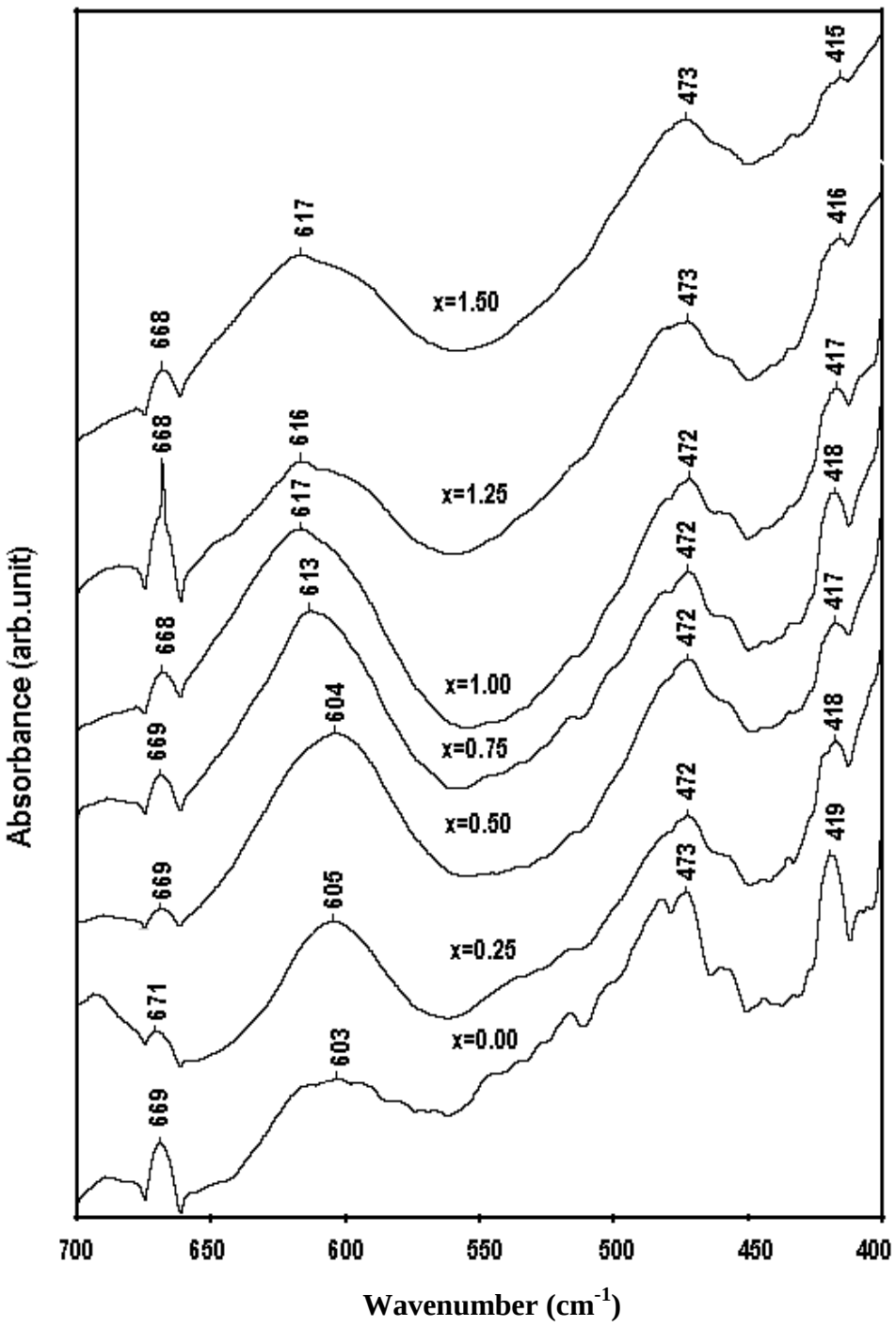

Fig. 4.7: The FTIR absorption spectra of as-prepared Tl $(Ba_{2-x}Mg_x)$ $(Ca_{2-y}Be_y)$ $Cu_3O_{10-\delta}$ (y=0; x=0.0, 0.25, 0.5, 0.75, 1.0, 1.25, 1.5) samples.

4.2.2. Oxygen post-annealed $Tl(Ba_{2-x}Mg_x)(Ca_{2-y}Be_y)Cu_3O_{10-\delta}$ (y=0 ; x=0, 0.25, 0.5, 0.75, 1.0, 1.25, 1.50) samples

4.2.2(a). Resistivity and AC-Susceptibility

The resistivity measurements of oxygen post-annealed $Tl(Ba_{2-x}Mg_x)(Ca_{2-y}Be_y)Cu_3O_{10-\delta}$ (y=0; x=0, 0.25, 0.5, 0.75, 1.0, 1.25, 1.50) samples are shown in Fig.4.8.

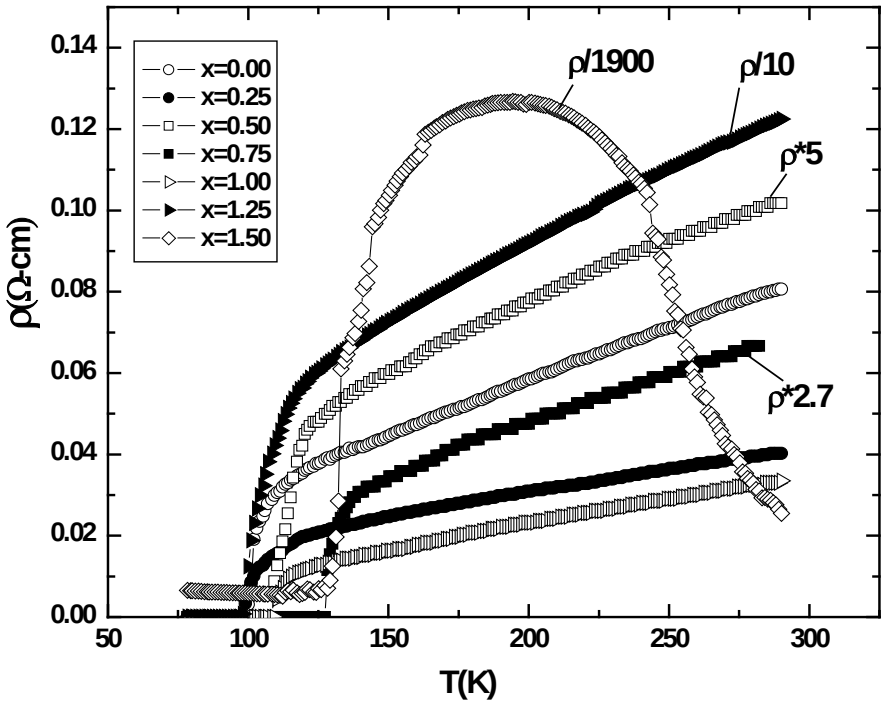

Fig. 4.8: Resistivity versus temperature measurements of Oxygen post annealed Tl $(Ba_{2-x}Mg_x)(Ca_{2-y}Be_y)Cu_3O_{10-\delta}$ (y=0; x=0.0, 0.25, 0.5, 0.75, 1.0, 1.25, 1.5) samples.

All the samples, except for the sample with x=1.5, have shown metallic variation of the resistivity from room temperature down to onset of superconductivity. These oxygen post-annealed samples have shown room temperature resistivity from 0.080 to 1.22Ω-cm for the samples with Mg-doping of x=0, 0.25, 0.5, 0.75, 1.0, 1.25 and about

48.48Ω-cm for the sample with Mg-doping of 1.5. These samples have shown onset of superconductivity around 105, 107, 120, 133, 114, 110K and zero resistivity critical temperature around 99, 98, 108, 127, 109, 97K, respectively, which are plotted as a function of Mg-doping concentration in figures 4.9 and 4.10.

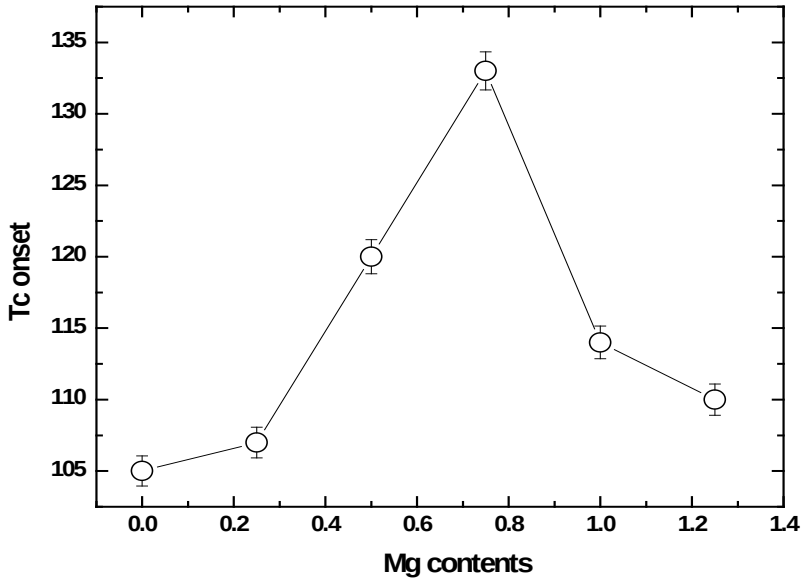

Fig. 4.9: Tc onset versus Mg contents measurements of Oxygen post annealed $Tl(Ba_{2-x}Mg_x)(Ca_{2-y}Be_y)Cu_3O_{10-\delta}$ (y=0; x=0.0, 0.25, 0.5, 0.75, 1.0, 1.25) samples.

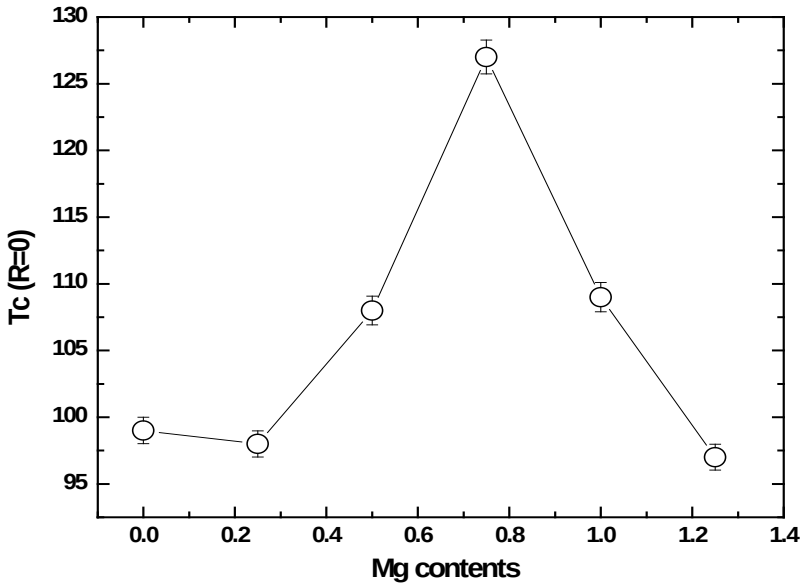

Fig. 4.10: Tc(R=0) versus Mg contents measurements of Oxygen post annealed $Tl(Ba_{2-x}Mg_x)(Ca_{2-y}Be_y)Cu_3O_{10-\delta}$ (y=0; x=0.0, 0.25, 0.5, 0.75, 1.0, 1.25) samples.

The onset temperature of superconductivity increases with Mg-doping and T_c(R=0) increases for moderate doping of Mg i.e 0.5, 0.75, 1.0.

The ac-susceptibility measurements of $Tl(Ba_{2-x}Mg_x)(Ca_{2-y}Be_y)\ Cu_3O_{10-\delta}$ (y=0;x=0, 0.25, 0.5, 0.75,1.0,1.25,1.50) samples are shown in Fig. 4.11.

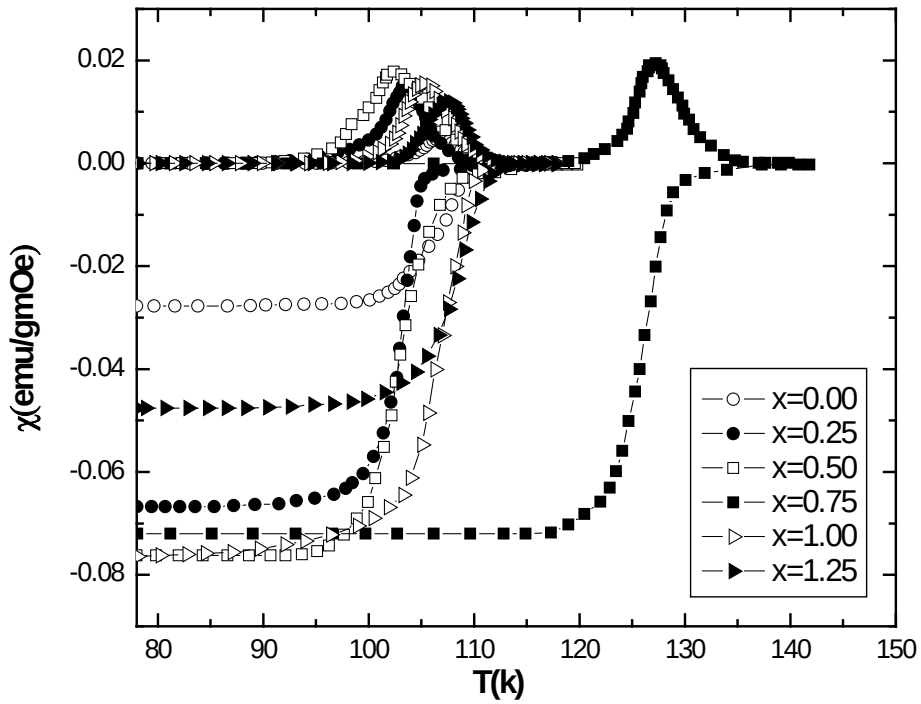

Fig. 4.11: The ac-susceptibility versus temperature measurements of Oxygen post annealed $Tl(Ba_{2-x}Mg_x)(Ca_{2-y}Be_y)Cu_3O_{10-\delta}$ (y=0; x=0.0, 0.25, 0.5, 0.75, 1.0, 1.25) samples.

These samples have shown onset of superconductivity around 113, 111, 115, 137, 114, 112K for the Mg-doping of x=0, 0.25, 0.5, 0.75, 1.0, 1.25 in $Tl(Ba_{2-x}Mg_x)Ca_{2-y}Be_yCu3O10_{-\delta}$ (y=0) superconductivity. The magnitude of diamagnetism increased with the doping of Mg. The magnitude of diamagnetism as a function of increased Mg doping concentration is shown in figure 4.12.

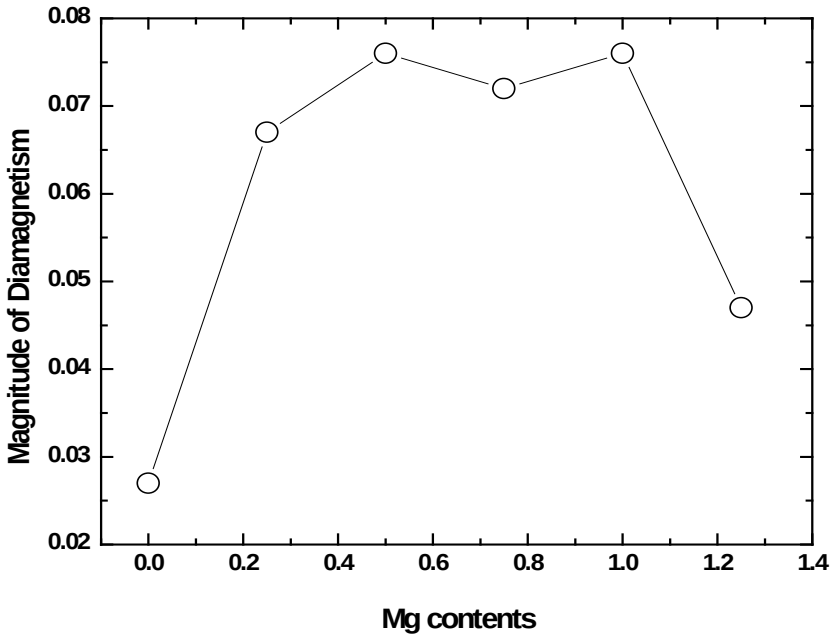

Fig. 4.12: Magnitude of diamagnetism versus Mg contents measurements of Oxygen post annealed $Tl(Ba_{2-x}Mg_x)(Ca_{2-y}Be_y)Cu_3O_{10-\delta}$ (y=0;x=0.0, 0.25, 0.5, 0.75, 1.0, 1.25) samples.

It is most likely that the decreased thickness of the charge reservoir layers facilitates the easy charge reservoir layer possible promoting the enhancement in the density of the charge carriers in the conducting CuO_2 planes thereby increasing the magnitude of the superconductivity in Mg-doped compound.

4.2.2(b). Infrared spectroscopy

The FTIR absorption measurements of oxygen post-annealed $Tl(Ba_{2-x}Mg_x)(Ca_{2-y}Be_y)Cu_3O_{10-\delta}$ (y=0; x=0, 0.25, 0.5, 0.75, 1.0, 1.25, 1.50) samples are shown in Fig. 4.13. The CuO_2 planar oxygen mode is observed around 580cm^{-1} and O_δ mode of oxygen atoms of $TlBa_2O_{4-\delta}$ charge reservoir layer is peaked around 690cm^{-1}. The intensity of O_δ mode of the charge reservoir layer decreases. The decrease in the intensity of O_δ mode of oxygen atoms of $TlBa_2O_{4-\delta}$ charge reservoir layer around 690cm^{-1} manifested that oxygen contents decrease with increased Mg-doping. The CuO_2 planar oxygen mode is

systematically hardened with increased Mg-doping and is observed around 578, 581, 589, 595, 596, and 597 cm^{-1} for x=0, 0.25, 0.5, 0.75, 1.0, 1.25, respectively.

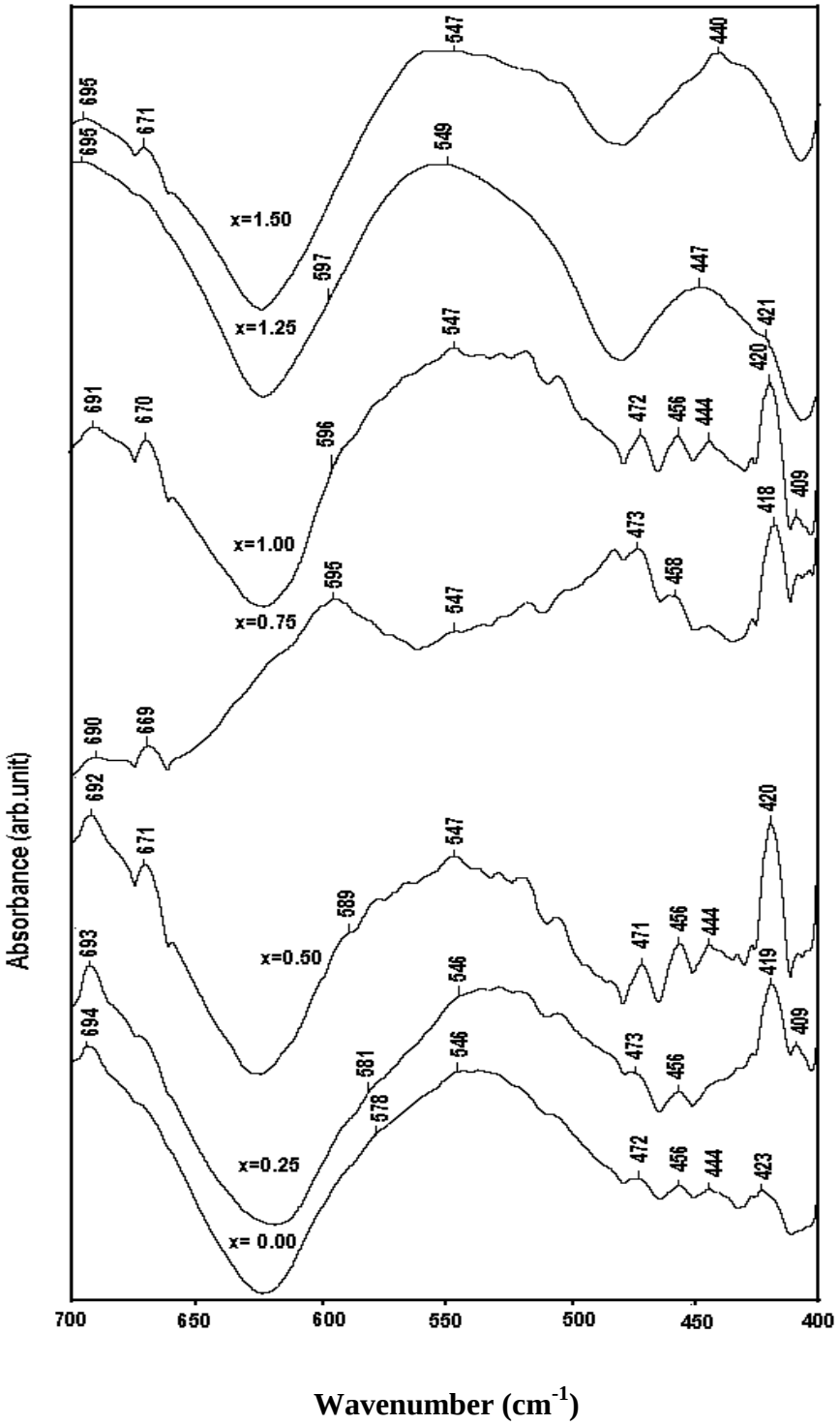

Fig. 4.13: The FTIR absorption spectra of Oxygen post annealed $Tl(Ba_{2-x}Mg_x)(Ca_{2-y}Be_y)Cu_3O_{10-\delta}$ (y=0; x=0.0, 0.25, 0.5, 0.75, 1.0, 1.25, 1.5) samples.

4.2.3. As-Prepared $Tl(Ba_{2-x}Mg_x)(Ca_1Be_1)Cu_3O_{10-\delta}$ (x=0, 0.25, 0.5, 0.75, 1.0, 1.25, 1.50, 1.75) samples.

4.2.3(a). Resistivity and AC-Susceptibility

The resistivity versus temperature measurements of $Tl(Ba_{2-x}Mg_x)(Ca_1Be_1)Cu_3O_{10-\delta}$ (x=0, 0.25, 0.5, 0.75, 1.0, 1.25, 1.50, 1.75) samples are shown in Fig. 4.14.

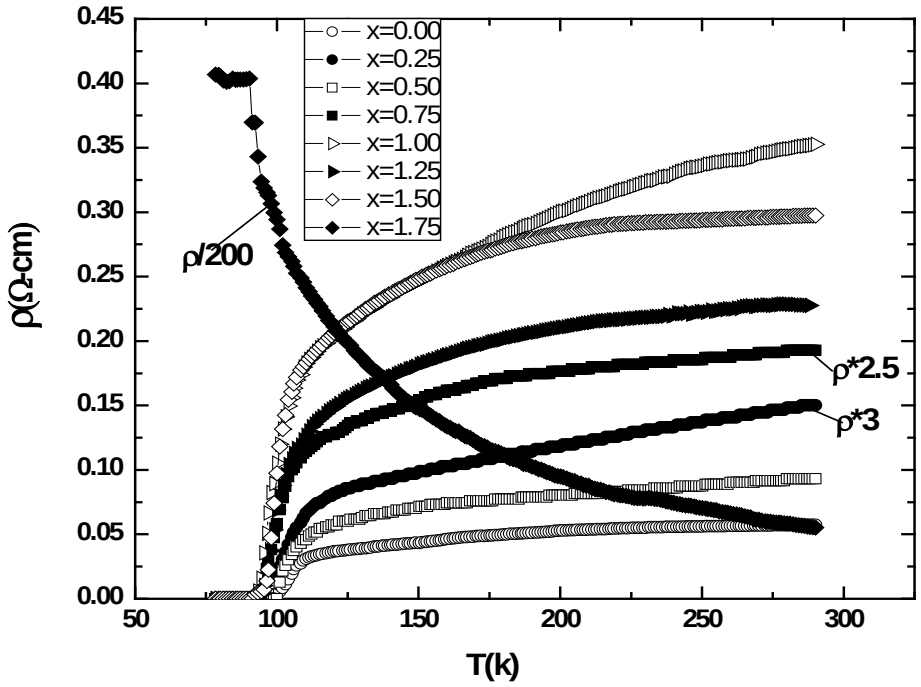

Fig. 4.14: Resistivity versus temperature measurements of as-prepared Tl $(Ba_{2-x}Mg_x)$ $(Ca_1Be_1)Cu_3O_{10-\delta}$ (x=0.0, 0.25, 0.5, 0.75, 1.0, 1.25, 1.5, 1.75) samples.

Except for the sample with highest Mg-doping of x=1.75, all the samples have shown metallic variation of the resistivity from room temperature down to onset of superconductivity. The room temperature resistivity of these samples varies between 0.057 to 0.297Ω-cm; sample with x=1.75 Mg-doping has shown semiconducting behavior all the way down to 77K. $Tl(Ba_{2-x}Mg_x)(Ca_1Be_1)Cu_3O_{10-\delta}$ (x=0, 0.25, 0.5, 0.75, 1.0, 1.25, 1.50) samples have onset of superconductivity around 110, 111, 112, 107, 106, 107, 106K and zero resistivity critical temperature around 97, 99, 100, 94, 92, 93, 91K, respectively, which are plotted as a function of Mg-doping concentration in figures 4.15 and 4.16.

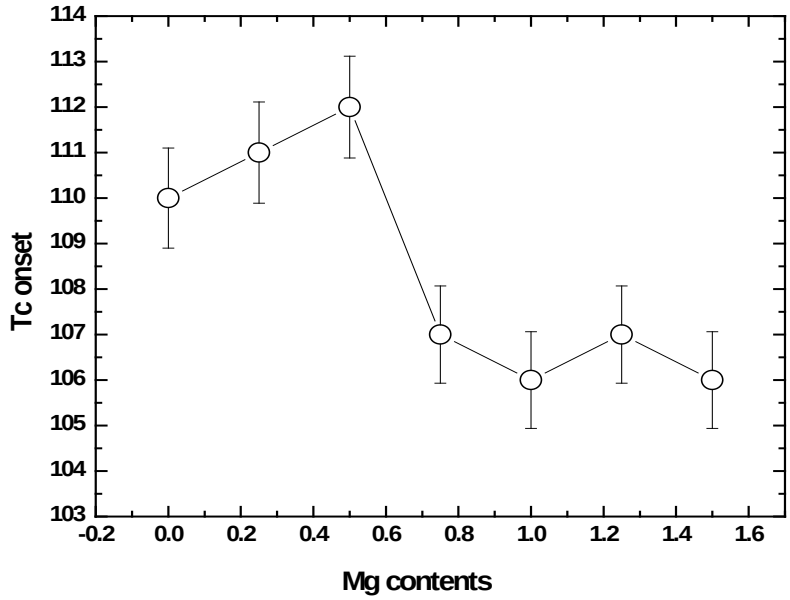

Fig. 4.15: Tc onset versus Mg contents measurements of as-prepared $Tl(Ba_{2-x}Mg_x)(Ca_1Be_1)Cu_3O_{10-\delta}$ (x=0.0, 0.25, 0.5, 0.75, 1.0, 1.25, 1.5) samples.

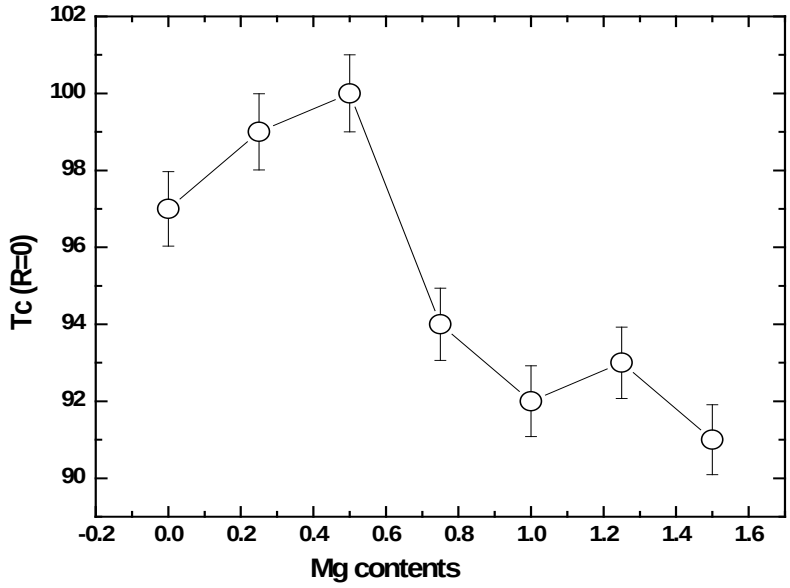

Fig. 4.16: Tc(R=0) versus Mg contents measurements of as-prepared $Tl(Ba_{2-x}Mg_x)(Ca_1Be_1)Cu_3O_{10-\delta}$ (x=0.0, 0.25, 0.5, 0.75, 1.0, 1.25, 1.5)

samples.

The ac-susceptibility measurements of $Tl(Ba_{2-x}Mg_x)(Ca_1Be_1)Cu_3O_{10-\delta}$ (x=0, 0.25, 0.5, 0.75, 1.0, 1.25, 1.50) samples are shown in Fig. 4.17.

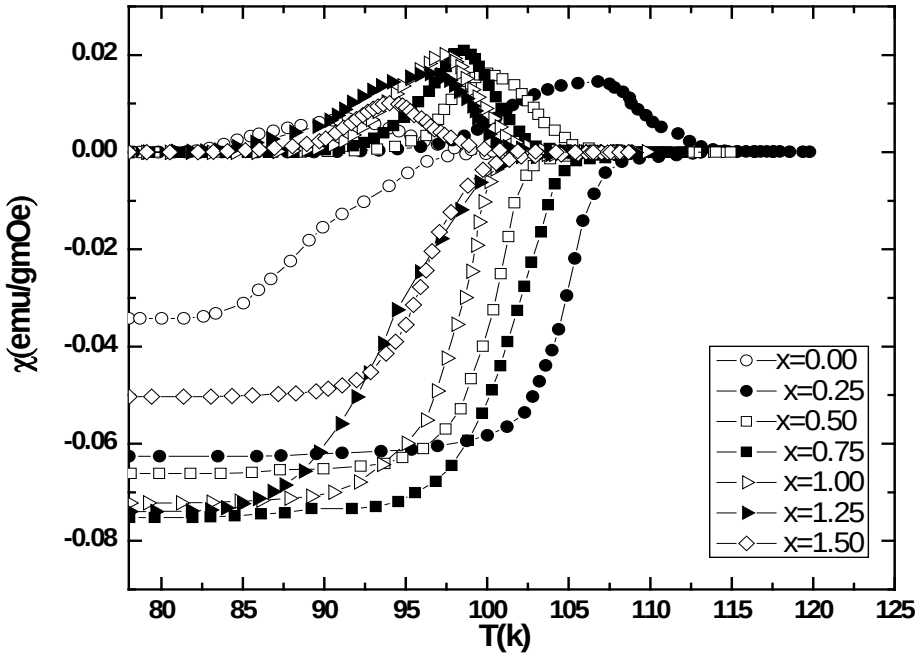

Fig. 4.17: The ac-susceptibility versus temperature measurements of as-prepared $Tl(Ba_{2-x}Mg_x)(Ca_1Be_1)Cu_3O_{10-\delta}$ (x=0.0, 0.25, 0.5, 0.75, 1.0, 1.25, 1.5) samples.

All Mg doped samples have shown increase in magnitude of diamagnetism and the onset temperature of superconductivity. The magnitude of diamagnetism as a function of increased Mg doping concentration is shown in figure 4.18.

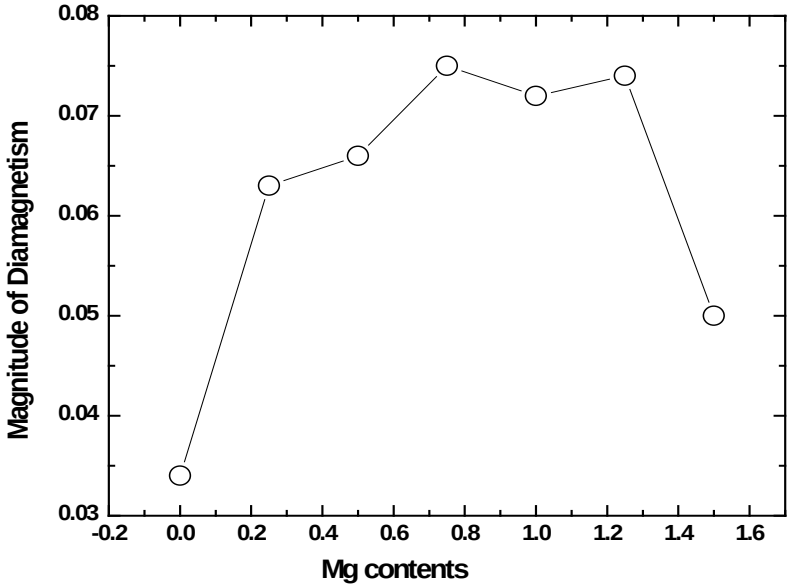

Fig. 4.18: Magnitude of diamagnetism versus Mg contents measurements of as- prepared $Tl(Ba_{x-2}\,Mg_x)(\,Ca_1Be_1\,)\,Cu_3O_{\,10-\delta}$ (x=0.0, 0.25, 0.5, 0.75, 1.0, 1.25, 1.5) Samples.

These samples have shown T_c(onset) around 102, 114, 108, 109, 106, 105, 106K in $Tl(Ba_{2-x}Mg_x)(Ca_1Be_1)Cu_3O_{10-\delta}$ (x=0, 0.25, 0.5, 0.75, 1.0, 1.25, 1.50), respectively. The increase in the magnitude of diamagnetism can be viewed in terms of decreased thickness of the charge reservoir layer. This plausible explanation of it is due to the fact that Be-doped samples have better inter-plane coupling that induces uniform carriers distribution in the inner oxygen (IP) and outer oxygen CuO_2 (OP) planes that consequently results into increased superconductivity parameters.

4.2.3(b). X-ray diffraction and Infrared spectroscopy

X-ray diffraction scans of $Tl(Ba_{2-x}Mg_x)(Ca_1Be_1)Cu_3O_{10-\delta}$ (x=0, 0.25, 0.5, 0.75, 1.0, 1.25, 1.50, 1.75) samples are shown in Fig. 4.19 (a,b).

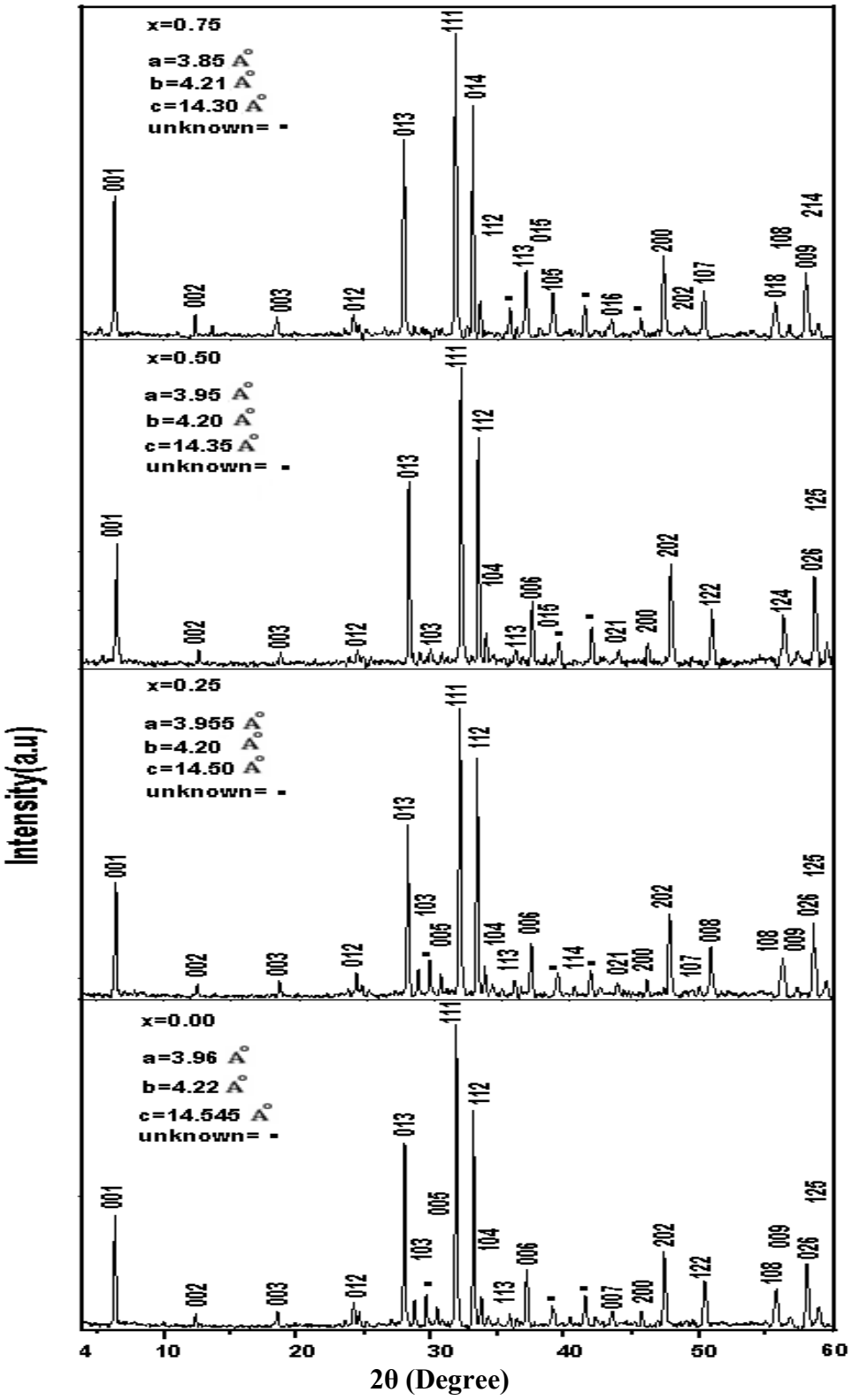

Fig. 4.19(a): X-ray Diffraction scans $Tl(Ba_{2-x}Mg_x)(Ca_1Be_1)Cu_3O_{10-\delta}$ (x=0.0, 0.25, 0.5, 0.75) samples.

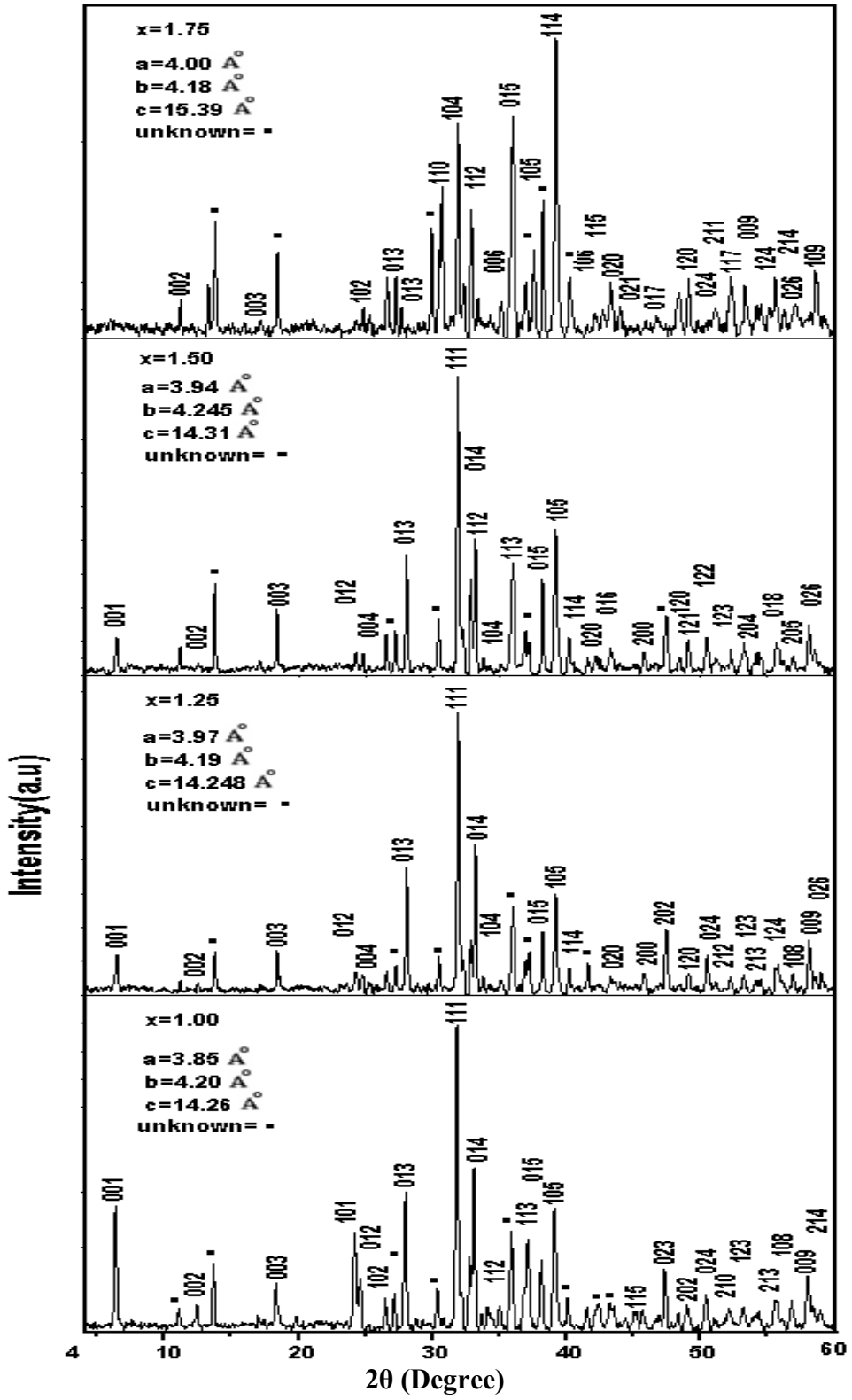

Fig. 4.19(b): X-ray Diffraction scans $Tl(Ba_{2-x}Mg_x)(Ca_1Be_1)Cu_3O_{10-\delta}$ (x=1.0, 1.25, 1.5, 1.75) samples.

Most of the diffraction lines in these samples are fitted to the orthorhombic structure following PMMM space group. The c-axes length decreases up to Mg-doping x=1.25 and then increases for Mg-doping of x=1.5, 1.75, respectively.

The FTIR absorption measurements of $Tl(Ba_{2-x}Mg_x)(Ca_1Be_1)Cu_3O_{10-\delta}$ (x=0, 0.25, 0.5, 0.75, 1.0, 1.25, 1.50, 1.75) samples are shown in Fig.4.20. In Mg un-doped $TlBa_2(Ca_1Be_1)Cu_3O_{10-\delta}$ samples, the apical oxygen mode of the type $Tl\text{-}O_A\text{-}Cu(2)$ is observed around 475cm^{-1} and the CuO_2 planar oxygen mode is observed around 595cm^{-1}. The CuO_2 planar oxygen mode is systematically hardened in $Tl(Ba_{2-x}Mg_x)(Ca_1Be_1)Cu_3O_{10-\delta}$ (x=0.25, 0.5, 0.75, 1.0, 1.25, 1.50) with increased Mg-doping and is observed around 602, 603, 617, 620, 628cm^{-1}, respectively. The hardening of planar oxygen modes provides intrinsic microscopic evidence of suppression of thickness of the charge reservoir layer that induces a decrease in the bond distances of outer planar oxygen atoms. This CuO_2 planar mode, however, vanishes at such higher wavenumber sites in the samples with Mg-doping of x=1.75; this modes has been observed around 580cm^{-1} in such samples, as shown in Fig.4.20.

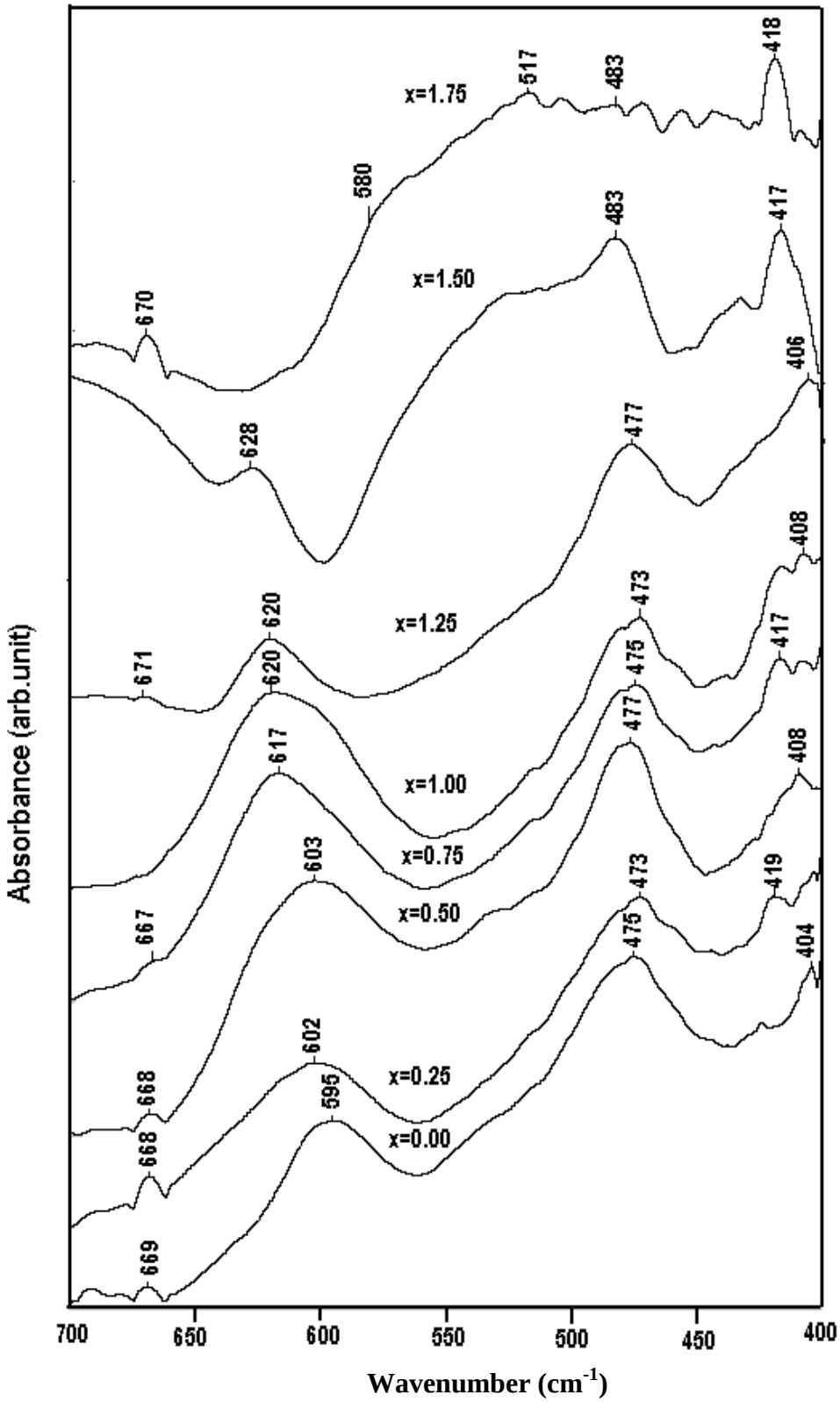

Fig 4.20: The FTIR absorption spectra of as-prepared $Tl(Ba_{2-x}Mg_x)(Ca_1Be_1)Cu_3O_{10-\delta}$ (x=0.0, 0.25, 0.5, 0.75, 1.0, 1.25, 1.5, 1.75) samples.

4.2.4. Oxygen post-annealed $Tl(Ba_{2-x}Mg_x)(Ca_1Be_1)Cu_3O_{10-\delta}$ (x=0, 0.25, 0.5, 0.75, 1.0, 1.25, 1.50, 1.75) samples

4.2.4(a). Resistivity and AC-Susceptibility

The resistivity measurements of oxygen post-annealed $Tl(Ba_{2-x}Mg_x)(Ca_1Be_1)Cu_3O_{10-\delta}$ (x=0, 0.25, 0.5, 0.75, 1.0, 1.25, 1.50, 1.75) samples are shown in Fig.4.21.

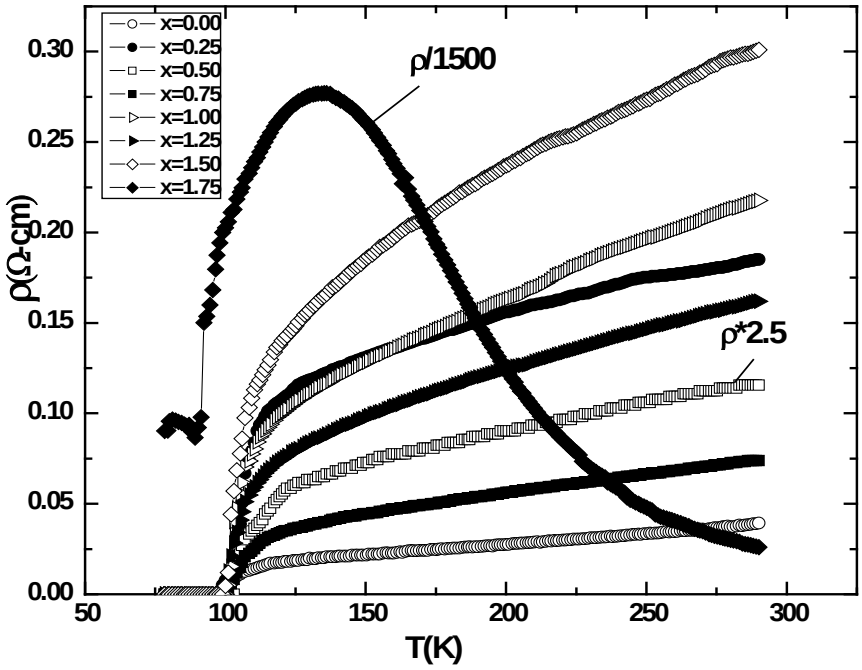

Fig. 4.21: Resistivity versus temperature measurements of Oxygen post annealed $Tl(Ba_{2-x}Mg_x)(Ca_1Be_1)Cu_3O_{10-\delta}$ (x=0.0, 0.25, 0.5, 0.75, 1.0, 1.25, 1.5, 1.75) samples.

Except in the sample with Mg doping of x=1.75, a metallic variations of resistivity from room temperature down to onset of superconductivity is typical feature in all the samples. The room temperature resistivity in oxygen post-annealed samples is found to vary from 0.039 to 0.3Ω-cm. In ρ(Ω-cm) versus temperature measurements these samples have shown onset of superconductivity around 109, 112, 116, 114, 112, 111, 110K and T_c(R=0) around 100, 98, 103, 101, 100, 99, 99K, respectively, which are plotted as a function of Mg-doping concentration in figures 4.22 and 4.23.

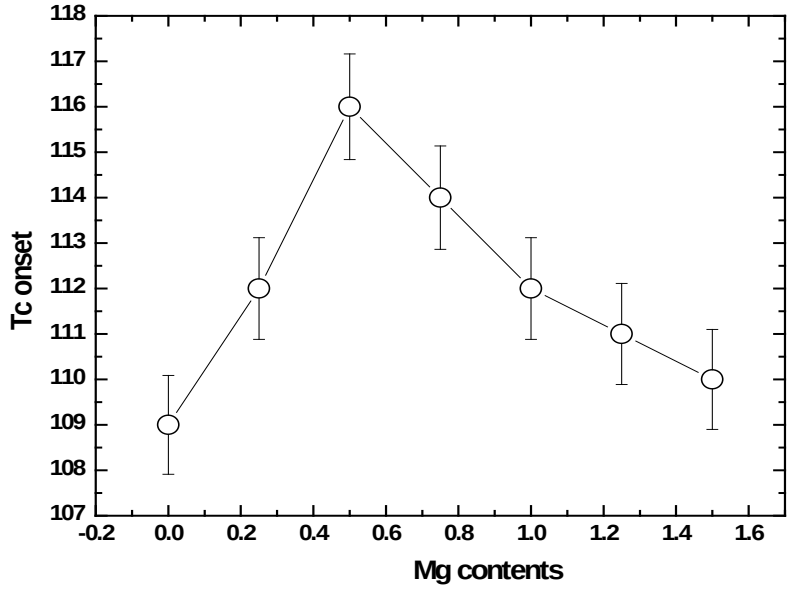

Fig. 4.22: Tc onset versus Mg contents measurements of Oxygen post annealed Tl $(Ba_{2-x}Mg_x)$ $(Ca_1Be_1)Cu_3O_{10-\delta}$ (x=0.0, 0.25, 0.5, 0.75, 1.0, 1.25, 1.5) samples.

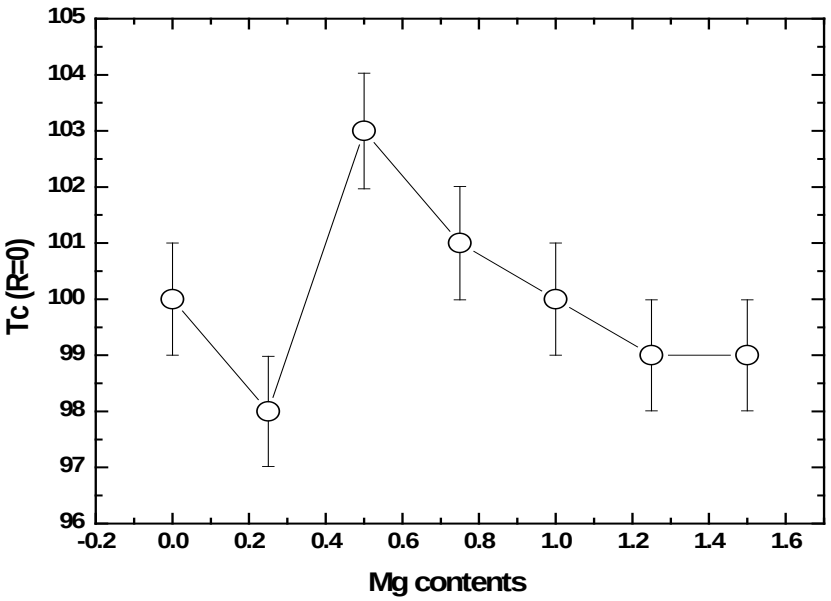

Fig. 4.23: Tc (R=0) versus Mg contents measurements of Oxygen post annealed Tl $(Ba_{2-x}Mg_x)$ (Ca_1Be_1) $Cu_3O_{10-\delta}$ (x=0.0, 0.25, 0.5, 0.75, 1.0, 1.25, 1.5) Samples.

Ac-susceptibility measurements of Tl $(Ba_{2-x}Mg_x)$ (Ca_1Be_1) $Cu_3O_{10-\delta}$ (x=0, 0.25, 0.5, 0.75, 1.0, 1.25, 1.50, 1.75) samples are shown in Fig.4.24.

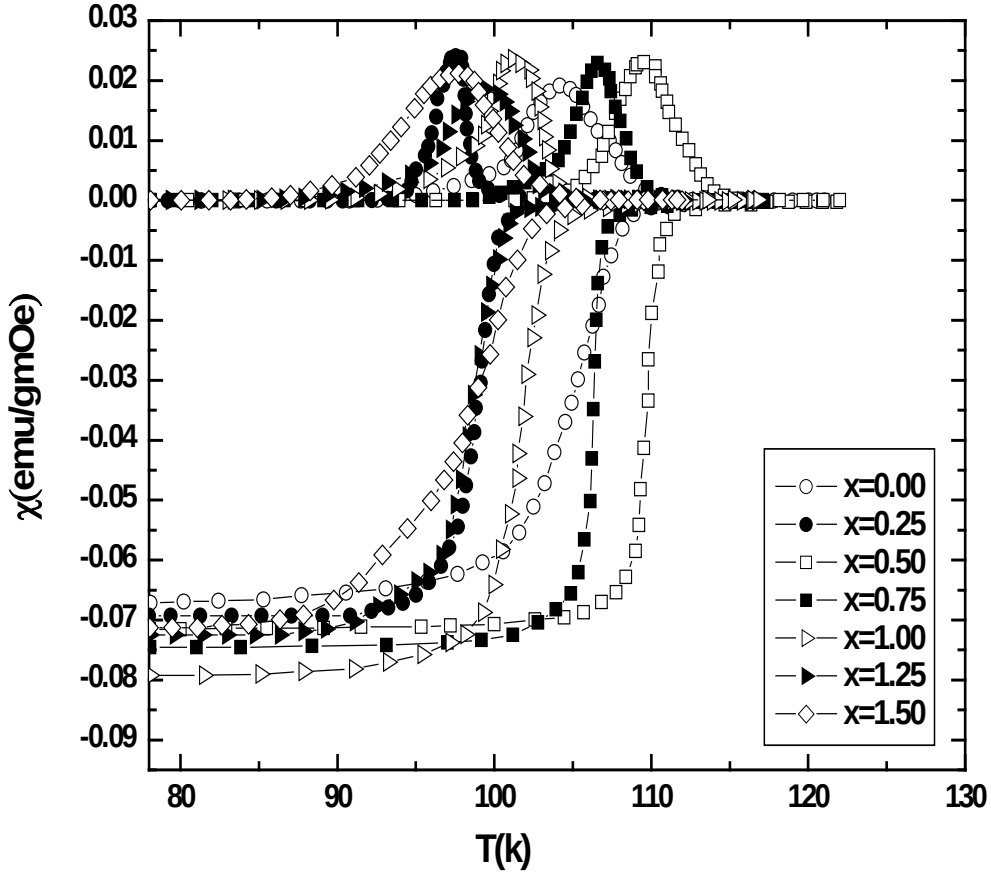

Fig. 4.24. The ac-susceptibility versus temperature measurements of Oxygen post annealed $Tl(Ba_{2-x}Mg_x)(Ca_1Be_1)Cu_3O_{10-\delta}$ (x=0.0, 0.25, 0.5, 0.75, 1.0, 1.25, 1.5) samples.

The magnitude of the superconductivity in all these samples increases with the doping of Mg. The magnitude of diamagnetism as a function of increased Mg doping concentration is shown in Fig. 4.25. These samples have shown onset of superconductivity around 112, 104, 117, 113, 111, 107 and 106K, respectively.

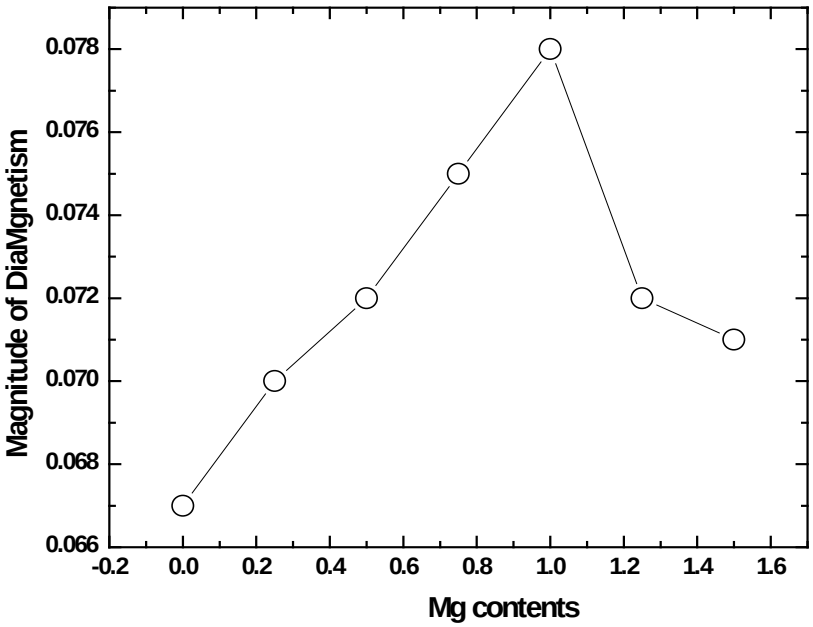

.

Fig. 4.25: Magnitude of diamagnetism versus Mg contents measurements of Oxygen post annealed $Tl(Ba_{2-x}Mg_x)(Ca_1Be_1)Cu_3O_{10-\delta}$ (x=0.0, 0.25, 0.5, 0.75, 1.0, 1.25, 1.5) samples.

4.2.4(b). Infrared spectroscopy

The FTIR absorption measurements of oxygen post-annealed $Tl(Ba_{2-x}Mg_x)(Ca_1Be_1)Cu_3O_{10-\delta}$ (x=0, 0.25, 0.5, 0.75, 1.0, 1.25, 1.50, 1.75) samples are shown in Fig.4.26. In Mg free $TlBa_2(Ca_1Be_1)Cu_3O_{10-\delta}$ samples the apical oxygen mode of the type Tl-O_A-Cu(2) is observed around 450cm^{-1}. The CuO_2 planar oxygen mode is observed around 575cm^{-1} and O_δ mode of oxygen atoms of $TlBa_2O_{4-\delta}$ charge reservoir layer is peaked around 668-693cm^{-1}. The intensity of O_δ mode of the charge reservoir layer increases after post-annealing in oxygen. The apical oxygen mode of the type Tl-O_A-Cu(2) is for the Mg-doping of x=0.25, 0.5, 0.75, 1.0, 1.5, 1.75 is observed around 455, 448, 448, 456, 455, 455 and 456cm^{-1}, respectively. The CuO_2 planar oxygen mode in $Tl(Ba_{2-x}Mg_x)(Ca_1Be_1)Cu_3O_{10-\delta}$ (x=0.25, 0.5, 0.75, 1.0, 1.25, 1.50) samples is observed around 570, 573, 576, 580, 583, 585 and 587cm^{-1}, respectively.

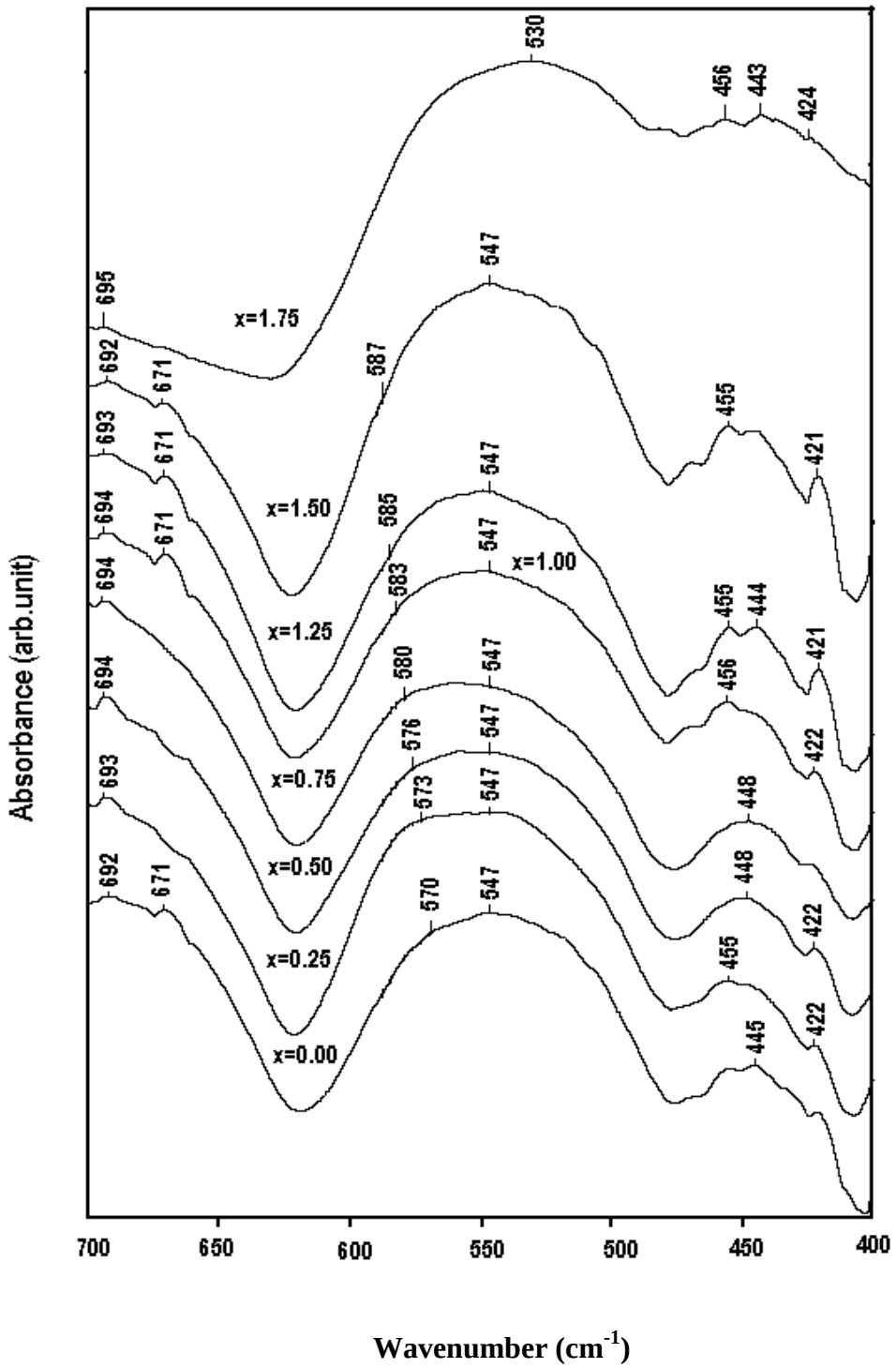

Fig. 4.26: The FTIR absorption spectra of Oxygen post annealed Tl $(Ba_{2-x}Mg_x)$ (Ca_1Be_1) $Cu_3O_{10-\delta}$ (x=0.0, 0.25, 0.5, 0.75, 1.0, 1.25, 1.5, 1.75) samples.

4.3. Conclusions

We have synthesized Mg doped $Tl(Ba_{2-x}Mg_x)(Ca_{2-y}Be_y)Cu_3O_{10-\delta}$ (y=0; x=0. 0.25, 0.5, 0.75, 1.0, 1.25, 1.5)and $Tl(Ba_{2-x}Mg_x)(Ca_1Be_1)Cu_3O_{10-\delta}$ (x=0, 0.25, 0.5, 0.75, 1.0, 1.25, 1.50, 1.75) superconductors at normal pressure and studied their superconducting properties. Mg-doped samples have shown orthorhombic crystal structure following PMMM space group. In Mg-doped samples a decrease in the c-axes length is observed for $Tl(Ba_{2-x}Mg_x)(Ca_{2-y}Be_y)Cu_3O_{10-\delta}$ (y=0; x=0, 0.25, 0.5, 0.75) and $Tl(Ba_{2-x}Mg_x)(Ca_1Be_1)Cu_3O_{10-\delta}$ (x=0, 0.25, 0.5, 0.75, 1.0, 1.25) samples. $Tl(Ba_{2-x}Mg_x)(Ca_{2-y}Be_y)Cu_3O_{10-\delta}$ (y=0; x=0, 0.25, 0.5, 0.75, 1.0, 1.25) have shown T_c(R=0) around 100, 98, 101, 102, 100, 96K and these samples post-annealed in oxygen atmosphere have shown T_c(R=0) at 99, 98, 108, 127, 109, 97K, respectively. Be-doped as-prepared $Tl(Ba_{2-x}Mg_x)(Ca_1Be_1)Cu_3O_{10-\delta}$ (x=0.25, 0.5, 0.75, 1.0, 1.25, 1.50) samples have shown T_c(R=0) at 97, 99, 100, 94, 92, 93, 91K and these samples post-annealed in oxygen atmosphere have shown T_c(R=0) at 100, 98, 103, 101, 100, 99, 99K, respectively. The magnitude of the superconductivity after Mg-doping is improved in $Tl(Ba_{2-x}Mg_x)(Ca_{2-y}Be_y)Cu_3O_{10-\delta}$ (y=0; x=0.25, 0.5, 0.75, 1.0, 1.25) and $Tl(Ba_{2-x}Mg_x)(Ca_1Be_1)Cu_3O_{10-\delta}$ (x=0.25, 0.5, 0.75, 1.0, 1.25, 1.50) samples. The phonon modes related to the different oxygen atoms in the unit cell have evidenced the incorporation of Mg at the Ba sites. It is observed from the FTIR absorption measurements that that phonon modes related to CuO_2 planar oxygen atoms are hardened with the doping of Mg at the Ba sites. Since the thickness of charge reservoir layer decreases, that would induce suppression in the bond distances of oxygen atoms in the outer CuO_2 planes as well, consequently resulting into a hardening of the planar oxygen modes. These studies have shown that a decreased thickness of charge reservoir layer makes the transfer mechanism more efficient that promotes the increase in the magnitude of superconductivity.

4.4. References

[1]. H. Ihara, Advances in Superconductivity VII, 255 (1995); Proceedings of the 7th International symposium on superconductivity (ISS'94) Kitakyushu, Japan.

[2]. H. Ihara, A. Iyo, K. Tanaka, K. Tokiwa, K. Ishida, N. Terada, M. Tokumoto, Y. Sekita, T. Tsukamoto, T. Watanabe and M. Umeda Physica C 282, (1997) 1973.

[3]. H. kotegawa, Y. Tokunaga, K. Ishida, G.-q. Zheng, Y. Kitaoka, K. Asayama, H. Kito, A. Iyo, H. Ihara, K. Tanaka, K. Tokiwa, T. Watanabe journal of physics and chemistry of solids 62, 171 (2001)

[4]. Fahim Ashraf, Nawazish A Khan, Muhammad Mumtaz, J. Supercond. Nov. Magn. 21, 279 (2008).

[5]. Nawazish. A. Khan and Shahid Nawaz, IEEE Trans. Appl. Supercond. 16, 2 (2006).

[6]. Nawazish A. Khan, G. Husnain, and K. Sabeeh, J. Phys. Chem. Solids 67, 1841 (2006).

[7]. Nawazish A. Khan and A.A. Khurram, Appl. Phys. Lett. 86, 152502 (2005).

[8]. Nawazish A. Khan, A.A. Khurram and M. Mazhar**,** Physica C 407, 23 (2004).

[9]. Nawazish A Khan and Najam-ul-Hassan, Materials Chemistry and Physics 105, 298 (2007).

[10]. Mumtaz and Nawazish A. Khan, Physica B 404, 3973 (2009).

[11]. Nawazish A. Khan and Najmul Hassan, Physica C 466, 106(2007).

[12]. Najmul Hassan and Nawazish A. Khan Journal of Alloys and Compounds 464, 550 (2008)**.**

[13]. Najmul Hassan and Nawazish A. Khan, Materials Chemistry and Physics 112, 412 (2008).